CHARACTERISATION AND SUBSTITUTION KINETICS OF CHROMIUM(III) - N-(CARBAMOYLMETHYL)-IMINODIACETATO COMPLEXES

A thesis submitted to meet the requirements for the degree of

MAGISTER SCIENTIAE

in the

Department of Chemistry

Faculty of Natural and Agricultural Sciences

at the

University of the Free State

by

Nicoline Cloete

Promotors

Dr. H.G. Visser

Prof. W. Purcell

Dankbetuigings

Hiermee wens ek my opregte dank en waardering te betuig aan:

My hemelse Vader en God, U lig is my leiding en inspirasie.
"Net by God vind ek rus, want op Hom vertrou ek." – Psalm 62:6.

My ouers, Hennie en Elize Cloete, vir al die ondersteuning en onvoorwaardelike liefde, ek voel trots om te kan sê ek is julle dogter. Ek het julle baie lief.

Shaun Cronjé, dankie dat jy nog altyd in my geglo het, jy spoor my aan om altyd my beste te gee.

My promotor, Deon Visser, vir jou geduld, moeite en ondersteuning. My respek vir jou as mens en chemikus het elke dag gegroei.

My mede-promotor, Prof. Purcell, u insig en oog vir detail word oneindig baie waardeer.

My twee broers, Henk en Deon, asook hul gesinne vir die belangstelling en aanmoediging.

Al my vriende, julle humor, waagmoed en algehele passie vir die lewe inpireer my om elke dag voluit te leef.

Al die personeel en studente by Departement Chemie vir julle wonderlike bydrae.
Die UVS en NRF vir finansiële steun.

Table of contents

List of abbreviations

acac	= pentane-2,3-dione
H_2ada	= N-(carbamoylmethyl)iminodiacetic acid
H_2apda	= N-(2-carboxyethyl)iminodiacetic acid
Bipy	= 2,2-bipiridine
H_2cida	= N-(o-carboxyphenyl)iminodiacetic acid
EBT	= Eriochrome Black T
H_2edda	= ethylenediaminediacetic acid
H_4edta	= ethylenediaminetetra-acetic acid
en	= ethylenediamine
gly	= glycine
GTF	= glucose tolerance factor
Ida	= iminodiacetic acid
Im	= imidazole
IR	= infrared
k_{obs}	= observed rate constant
lda	= (S)-leucine-N,N-diacetate
NMR	= nuclear magnetic resonance
H_3nta	= nitrilotriacetic acid
picH	= picolinic acid
pda	= (S)-phenylalanine-N,N-diacetate
phen	= *o*-phenantroline
pn	= 1,2-diaminopropane
TPPS	= *meso*-tetra(*p*-sulphonatophenyl)porphyrin
$trdta^{4-}$	= trimethylenediaminetetra-acetate

List of figures:

Chapter 1

Chapter 2

Chapter 3

List of figures

Chapter 4

Chapter 5

List of tables:

Chapter 3

Chapter 4

Chapter 5

List of schemes:

Chapter 2

Chapter 3

Chapter 4

Chapter 5

1 Aim of the study

The relevancy and aims of this study is discussed in this chapter. The history and significance of the complexes are discussed in the first part of this chapter while the specific aims of this study are discussed in the second part of this chapter.

1.1 Introduction

1.1.1 Chromium chemistry - history

Chromium was first isolated and identified in 1798 by the French chemist, Vauquelin. He named it chromium, derived from the Greek word *chroma*, meaning colour, because of the wide variety of brilliant colours displayed by its compounds. It is of no wonder then that one of the first applications of chromium was in the dying industry. One of the most important applications of chromium, namely its use as an alloying element, was developed during the nineteenth century. Its first application was in 1874 with the building of the famous East Bridge across the river in Mississippi. Today, the applications of chromium compounds are too numerous to mention, from uses in ceramics, electronics, catalysts, dyes and corrosion inhibitors to uses as fungicides in the agricultural industry (Westbrook, 1979:54 and Hartford, 1979:82).

Chromium salts and complexes are most commonly used in dyestuffs for polyamide fibers and leather because of their kinetic inertness and the stability of these complexes toward acid. The practical applications and popularity of these metal complexes stems principally from their very high light fastness which is

attributed to the protection of the azo group of the dye by the metal ion against attack by, for example, singlet oxygen (Gordon & Gregory, 1983).

The substitution reactions of octahedral chromium(III) complexes have been under investigation for many years. The reason for this is that a great variety of reactions with these complexes are slow enough to be followed by conventional means (Purcell & Kotz, 1985:710), which is illustrated by the large number of publications and review articles on the substitution reactions of these metal complexes (Hay, 1984:1 and Moore, 1984).

1.1.2 The significance of a Cr(III)-ada complex

Complexes of Cr(III) containing ligands that simulate binding sites found on protein chains have many applications and are of significant scientific value. According to Cooper *et al.* (1984:23) the glucose tolerance factor (GTF), a fraction isolated from brewer's yeast which displays biological activity in a number of assay systems, may have an important role to play in glucose metabolism. This has led to several studies on this subject (Toepfer, *et al.*, 1977:162, Mertz, 1975:129 and Haylock *et al.*, 1983:105). Other examples include the construction of molecular recognition models for enzyme-substrate complex formation through weak non-covalent interactions (Jitsukawa *et al.*, 1994:249), as well as many biomedical applications such as the removal of toxic metal ions from the human body by chelating agents like penicillamine (Helis *et al.*, 1977:3309 and Santos *et al.*, 1992:1687).

In this study the selected model complex is a novel chromium(III) complex with N-carbamoylmethyl-iminodiacetic acid (H_2ada). The bonding modes of the very similar nitriloacetic acid (H_3nta) have been of great interest for many years and N-carbamoylmethyl-iminodiacetic acid (H_2ada) (**Figure 1.1**) is a close analogue. The two multidentate ligands differ with respect to one another in that H_2ada has a primary amido group in the place of one of the acetate groups as in the case of

H_3nta. The ada^{2-} chelating agent has been widely used in 'biological buffers' of pH 6.0-7.2 and this tripod-type ligand functions as a tetradentate ligand in most metal chelation compounds and their structures are well characterised in both their zwitterionic and chelated forms (Bugella-Altamirano and co-workers, 2000:2463 and Sivak and co-workers, 1995:1057).

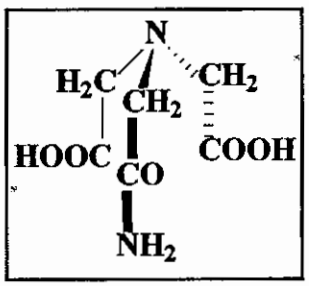

Figure 1.1: N-Carbamoylmethyl-iminodiacetic acid (H_2ada).

Substitution reactions at chromium(III) centers are normally slow, but the rate of substitution can be significantly enhanced by having Schiff-base, porphyrin chelates or $edta^{4-}$ and related ligands (such as nta^{3-}) which are coordinated to the metal centre (Leipoldt & Meyer, 1987:1631 and Beswick *et al.*, 1996:991). It is believed that these ligands donate extra electron density to the inert central chromium(III) ion, thereby changing its properties which allow the complex to react more like the labile chromium(II) ion complex.

The above factor, as well as the fact that fully coordinated ada^{2-} and nta^{3-} leave two *cis* positions available on the metal centre, make these kinds of complexes suitable biological models which allow the investigation of the substitution of these two aqua ligands (Visser *et al.*, 1994:1051 and Bhattacharyya & Banerjee., 1997:849).

1.2 Aim of this study

Chromium(III) complexes with N-carbamoylmethyl-iminodiacetic acid (H_2ada) have not been investigated until now. Structural studies on other metal ion-ada

complexes are also noticeably limited and no kinetic studies on any of these metal ion-ada complexes have been published.

The synthesis, characterisation and reactions of the chromium(III)-ada complex are crucially important to investigate ada^{2-} chelates of metal ions and specifically metal(III) cations.

The aim of this study was to:

a) Synthesize a suitable Cr(III)-ada complex that can be used as a biological model in future studies.
b) Characterise the complex with IR, UV/VIS and single-crystal X-ray crystallography so that it can be used as starting material in kinetic studies.
c) Determine the bonding mode of the ada^{2-} ligand to Cr(III)-ada complex.
d) Investigate the ring strain in the Cr(III)-ada complex.
e) Investigate the solution behaviour and reactivity of this complex.

2 Literature study

In this chapter...

The synthesis and characterisation of metal complexes with N-carbamoylmethyl-iminodiacetic acid (H_2ada) and similar ligands are discussed in the first part of this chapter. The second part focuses on the substitution reactions of similar types of complexes. The shortcomings and possible future contributions are discussed at the end of this chapter.

2.1 Introduction

N-Carbamoylmethyl-iminodiacetic acid (H_2ada) is widely used in biological buffers of pH 6.0-7.4 and is also a well known chelating agent that acts as a tetradentate ligand under most circumstances. H_2ada was for example used to extract labile Ca(II) from certain enzymes with concomitant loss of enzyme activity. It is however surprising to find that kinetic studies on metal-ada complexes are yet to be published. The rest of this chapter will concentrate on the different studies of metal-ada and similar tripod complexes. Examples of these tripod-type ligands are shown in **Figure 2.1.**

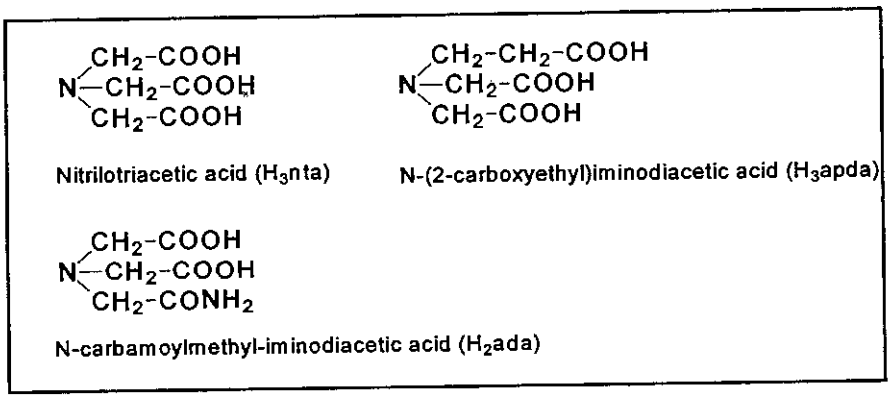

Figure 2.1: Tripod-type ligands.

2.2 Synthesis, characterisation and reactions of metal-N-carbamoylmethyl-iminodiacetato complexes.

2.2.1 Synthesis and characterisation

Metal-ada complexes

The coordination chemistry of the ada^{2-} ligand was first investigated by Schwarzenbach *et al.* (1955:1147). They studied the coordination tendency of ada^{2-} with a large number of metal(II) cations (M = Mg^{2+}, Ca^{2+}, Sr^{2+}, Ba^{2+}, Mn^{2+}, Fe^{2+}, Co^{2+}, Ni^{2+}, Cu^{2+}, Zn^{2+}, Cd^{2+}, Pb^{2+}, Hg^{2+}). They established by means of stability constants that the ada^{2-} ligand forms a third chelate ring when the iminodiacetato anion combines with the metal centre. This type of coordination was found to considerably increase the stability of the metal complexes. They also found that the carbonamide group preferably coordinates by its oxygen atom rather than by its nitrogen atom.

The complex formation constants of Co(II) and Zn(II) with ada^{2-} were also reported by Lance *et al.* (1981:L1) during their study of unusual metal ion deprotonation reactions. Their study not only confirmed the numerical stability constants obtained in the first study, but also reported an unusual Zn(II) induced amide deprotonation reaction.

The NMR and IR data obtained from this study was explained as indicating i) deprotonation of the amide group, ii) a change in stereochemistry (**Scheme 2.1**) iii) as well as an exchange reaction (**Scheme 2.2**). These results can be explained by the fact that deprotonated amide groups are powerful σ-donors and induce stereochemical changes in Ni(II) chelates (octahedral to square planar) and spin change in Co(II) (high to low). Weak σ-donors (H_2O, Cl^-) yield octahedral Zn(II) complexes in aqueous solution while strong σ-donors (CN^-) often yield tetrahedral Zn(II) complexes (Advanced Inorganic Chemistry, Edited by F.Cotton and G.Wilkinson (1966, p 662)).

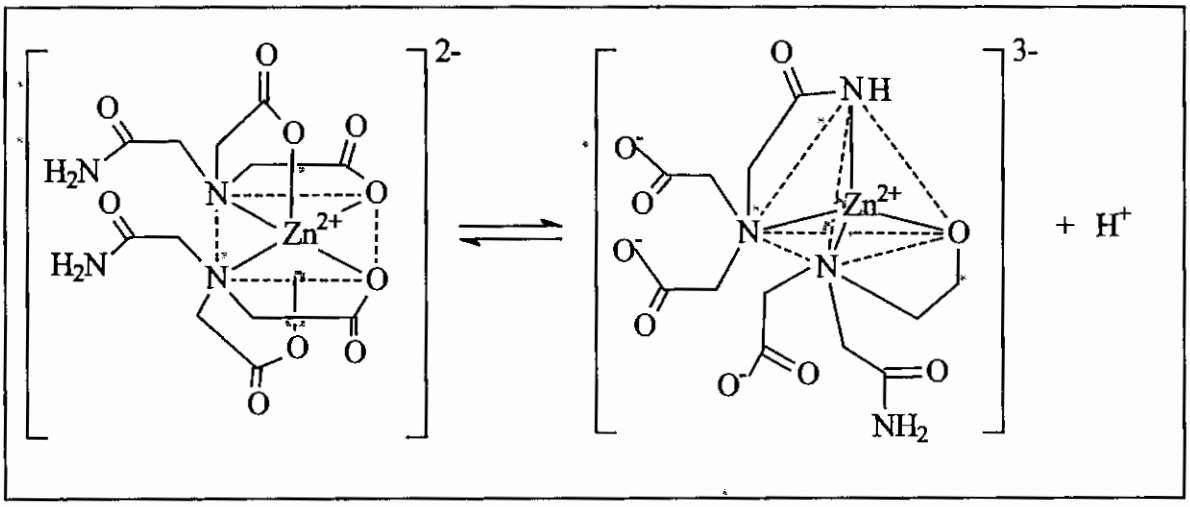

Scheme 2.1: Stereochemical change upon amide deprotonation of $[Zn(\eta^3\text{-ada})_2]^{2-}$.

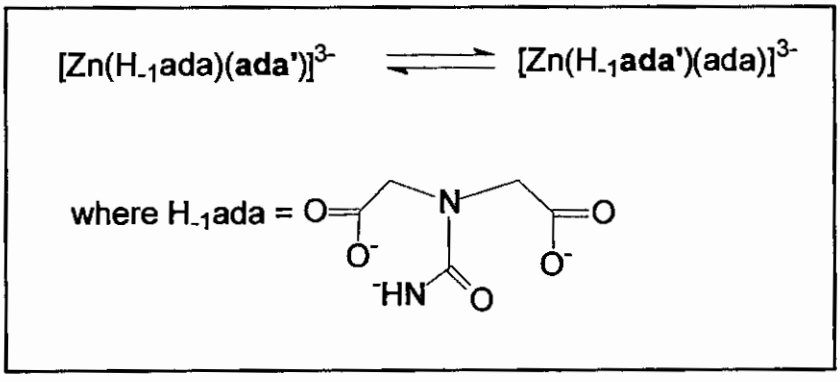

Scheme 2.2: Exchange reaction of $[Zn(\eta^2\text{-ada})_2]^{3-}$.

Lance *et al.* (1983:492) extended their study on the coordination behaviour of ada^{2-} by introducing a number of different metal(II) cations into the investigation. Ca(II) and Mg(II) were found to form 1:1 metal(II):ada^{2-} complexes, while Mn(II), Cu(II), Ni(II), Zn(II) and Co(II) all formed 1:2 metal(II):ada^{2-} complexes at or below physiological pH levels. The most likely structures for $[M(\eta^4\text{-ada})]$ and $[M(\eta^3\text{-ada})_2]^{2-}$ (M = metal(II)-ions) were found to be as depicted in **Figure 2.2**. These structures are based on various spectral data as well as the fact that COO^- is a better donor group compared to the amido carbonyl group.

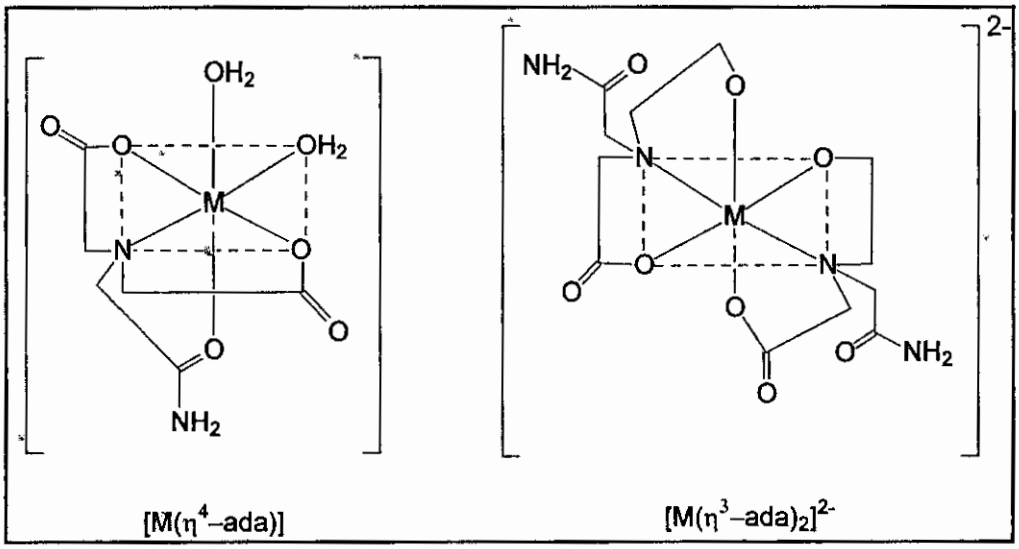

Figure 2.2: Possible structures of $[M(\eta^4\text{-ada})]$ and $[M(\eta^3\text{-ada})_2]^{2-}$.

In another study done by Parr *et al.* (1983:L11) it was found that ada^{2-} amide deprotonation occurred in alkaline solution. They established with visible spectra data as well as ESR data that the bis(N-2-acetamidoiminodiacetato)copper(II) chelate, $[Cu(\eta^3\text{-ada})_2]^{2-}$, undergoes a loss of one of the ada^{2-} ligands upon amide deprotonation. Interestingly it was found that the deprotonated amide group is responsible for new bond formation with the metal ion and the subsequent displacement of the other ada^{2-} ligand. It was understandably surprising to find the breaking of Cu(II)-oxygen bonds during this intra substitution reactions since these bonds are usually quite strong and render the complex relatively inert. (see **Scheme 2.3**).

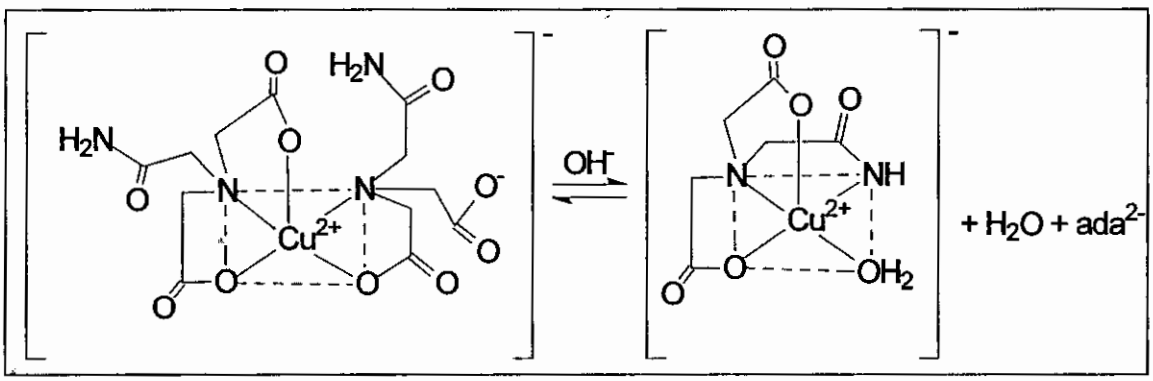

Scheme 2.3: Loss of ada^{2-} ligand upon amide deprotonation in $[Cu(\eta^3\text{-ada})_2]^-$.

The first known structure determination with coordinated ada^{2-} was reported by Sivak and co-workers (1995:1057) during a study in which they characterised a new vanadium(V) monoperoxo-ada, $[VO(O_2)(\eta^4\text{-ada})]^-$, complex. It was found that the ion had a coordination number of seven with bond formation with oxo, η^2-peroxo and tetradentately bonded ada^{2-} ligand. The structure determination clearly indicated that the ada^{2-} ligand bonds to the metal ion centre *via* one nitrogen and three oxygen atoms. The glycinate and one glycinamide ring are formed during this coordination process (see **Figure 2.3**).

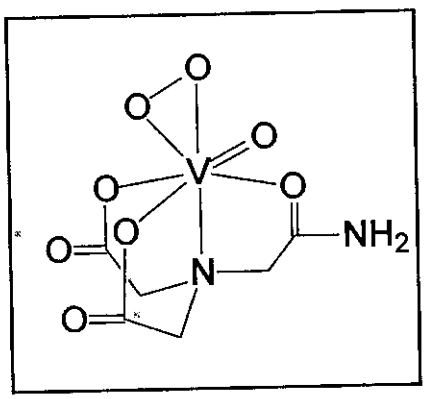

Figure 2.3: The $[VO(O_2)(\eta^4\text{-ada})]^-$ anion.

The next series of crystallographic studies on metal(II)-ada complexes were all reported by Bugella-Altamirano and co-workers, the first of which was the novel mixed ligand complex, $[Cu(\eta^4\text{-ada})(Im)]$ (Bugella-Altamirano and co-workers, 1999:3333). Results obtained from this crystal structure determination indicate that the ada^{2-} ligand acts as a tetradentate ligand in this polymeric complex.

Bugella-Altamirano and co-workers (2000:2463) were also the first to report the crystal structure of H_2ada, in spite of the fact that this chelating agent has been commercially available for many years. During their study they found that the crystal consists of a hydrogen bonded network of molecules where all polar N-H and O-H bonds are involved in these interactions. They also determined the pK_a values for H_2ada (I = 0.1 (KNO_3) and 25°C) as 1.59, 2.31 and 8.98 for the dissociation of the H_2ada, $Hada^-$ and ada^{2-} species respectively. The pK_a = 8.98

corresponds to the acid dissociation of the ada^{2-} amide group. Consequently it was assumed by Bugella-Altamirano and co-workers (2000:2463) that the protonated species exists as a zwitterion in solution. The crystal structure results also indicated that the molecule exists as a dipolar ion in solid state, which represents the asymmetric unit of the cell, see **Figure 2.4**.

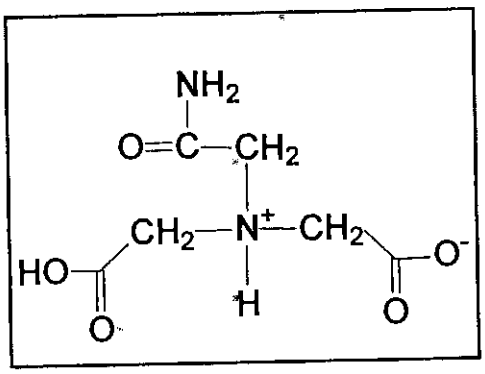

Figure 2.4: The zwitterionic acid H_2ada.

The next contribution by Bugella-Altamirano and co-workers (2000:2463) on the solid state study of metal(II)-ada complexes was the characterisation of the novel $[Ni(\eta^4\text{-ada})(H_2O)_2]\cdot 1.5H_2O$ complex. The two *cis*-aqua ligands in the octahedral complex gave a possibility for further studies on mixed ligand complexes. This possibility was explored by the same team of researchers, with the synthesis of the $[M(\eta^4\text{-ada})(Im)(H_2O)]\cdot 1.5H_2O$ (M = Co/Ni) complexes. It was concluded that the N(Im)-donor atom prefers to occupy the *trans*-position to the M-N(ada) bond (see **Figure 2.5**).

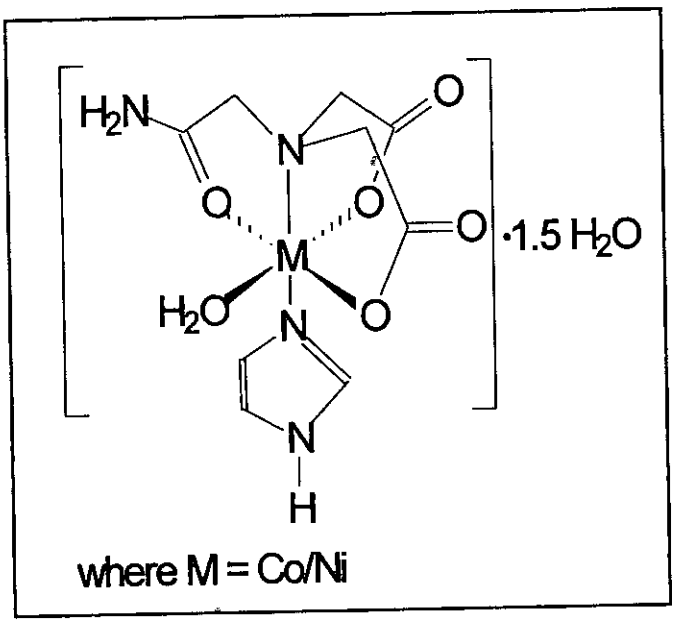

Figure 2.5: Structure of $[M(\eta^4\text{-ada})(Im)(H_2O)]\cdot 1.5H_2O$ (M = Co/Ni).

An unexpected tridentate coordination of the ada^{2-} ligand was reported by Bugella-Altamirano and co-workers (2002:727) for the $[Ni(\eta^3\text{-ada})(bipy)(H_2O)]\cdot 4H_2O]$ complex. The N-(2-amidomethyl) group of the ada^{2-} ligand remained uncoordinated in this mixed ligand complex, see **Figure 2.6**. This is in contrast to all other known structures of metal-ada chelates in which ada^{2-} acts as a tetradentate ligand. Another interesting aspect of this study is the fact that the 2,2'-bipy ligand chelates the Ni(II) atom, but that these two atoms bond *cis* with respect to the Ni-N(amino ada^{2-}) bond.

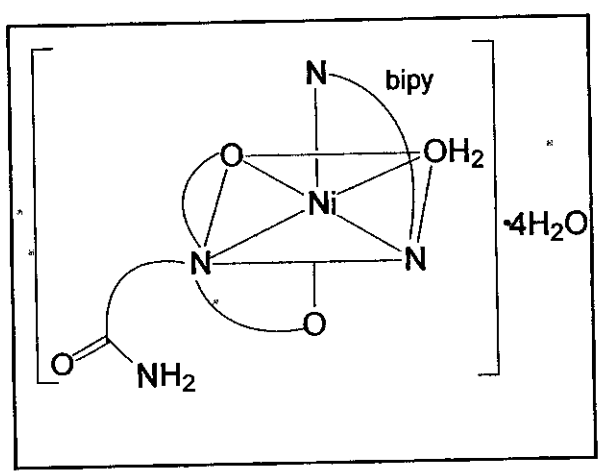

Figure 2.6: Structure of $[Ni(\eta^3\text{-ada})(bipy)(H_2O)]\cdot 4H_2O$.

Chromium(III)-nta complexes

Nitrilotriacetic acid (H_3nta) (**Figure 2.7**) is a tripodal polycaboxylate ligand and is a close analogue to ada^{2-}.

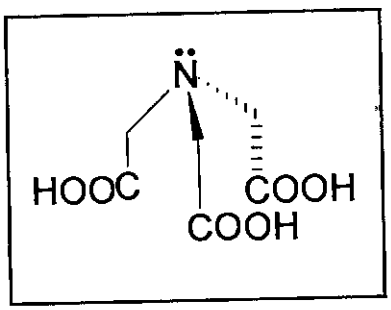

Figure 2.7: Nitrilotriacetic acid (H_3nta).

Uehara and co-workers (1968:2317) were the first to synthesize different chromium(III)-nta complexes. Two types of crystals with two distinctly different colours were isolated. Both complexes however had the same absorption spectra in solution and it was thus assumed that the two crystals were the same complex. It was suggested that the nta^{3-} ligand coordinated the chromium(III) centre through its three carboxylate groups and that the structure was $[Cr(\eta^3\text{-nta})(OH)(H_2O)]^-$. They based their assignment primarily on the maximum of the first electronic band, which is at considerably lower energy (585 nm) than that of typically observed for mononuclear $CrNO_5$-type complexes.

^2H NMR was used by Koine *et al.* (1986:2835) to investigate the solution behaviour of Cr(III) complexes with nta^{3-} by firstly blocking the *cis* positions with bidentate ligands to inhibit dimerisation. They observed three peaks with equivalent intensity for the ^2H NMR spectrum, which is consistent with a structure where nta^{3-} functions as a tetradentate ligand. An important part of this study was the investigation of the solution properties of the complexes prepared by Uehara *et al.* (1967:2317). The ^2H NMR spectrum of the complex in solution was consistent with fully coordinated nta^{3-} and not tridentate coordination as first postulated by Uehara *et al.* This was further confirmed by obtaining the ^2H_2O

solution IR spectrum as a function of pH. The carbonyl region was invariant with pH, consistent with full coordination of the nta^{3-} ligand to the metal centre.

Another important aspect of above-mentioned study is the first absorption maximum of the starting complex is 28 nm lower in energy than that of $[Cr(\eta^4\text{-nta})(H_2O)_2]$. Similar results were found for sym, *cis*-$[Cr(edda)(OH)]_2$ and sym, *cis*-$[Cr(edda)(H_2O)]_2^{+2}$ where a shift of 23 nm was observed (Srdanov *et al.*, 1980:37 and Radanovic, 1984:159) when moving from the dimer to the monomeric species. This motivated Koine *et al.* to propose that the complexes that Uehara and co-workers (1968:2317) prepared was actually a dimeric species, $[Cr(\eta^4\text{-nta})(OH)]_2^{2-}$. There are two possible isomers for this bis(μ-hydroxo)-nta complex, but only one species was observed in solution.

Koine and co-workers also observed a change in UV/VIS spectrum when moving from pH 7.1 to 3.5. At pH 4.6 a third species was observed spectophotometrically, but they were not able to characterise the intermediate. They postulated that it could be a mono-μ-hydroxo bridged intermediate that exists at pH 4.6 (**Scheme 2.4**).

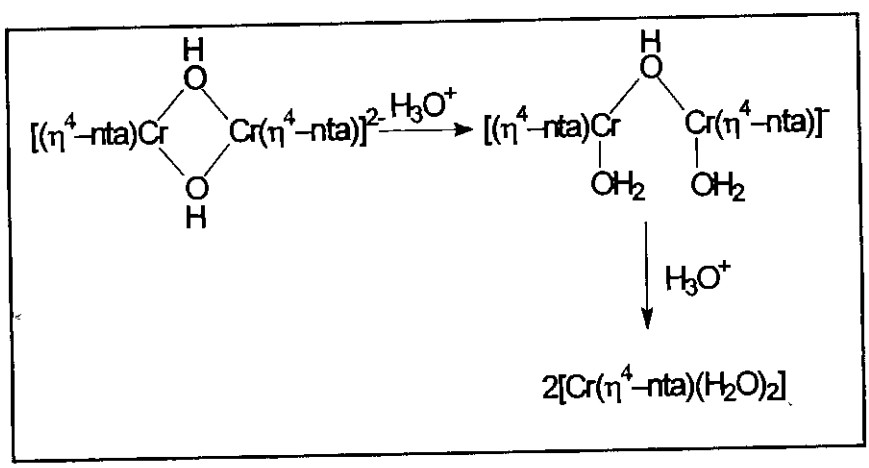

Scheme 2.4: Formation of intermediate Cr(III)-nta species in acidic solution.

Several chromium(III)-nta derivatives were prepared by Bocarsly *et al.* (1990:4898). The crystal structures for $[Cr((S)\text{-ida})(Im)_2]$ and $[Cr((S)\text{-pda})(Im)_2]$

were determined and was the first data in the literature where the *cis* positions of a Cr(III) complex with a nta^{3-} derivative are occupied by monodentate ligands.

$[Cr(\eta^4\text{-nta})(Im)_2]$ was also prepared and characterised by elemental analysis (Bocarseley *et al.* (1990:4898), but a slow hydrolysis reaction yielded the di-aqua complex. The UV/VIS spectra obtained for the hydrolysis of $[Cr(\eta^4\text{-nta})(Im)_2]$ showed that the reaction appears to involve two consecutive reactions. It was confirmed with ^2H NMR that the *trans*-imidazole aquates first to form an intermediate thought to be $[Cr(\eta^4\text{-nta})(Im)(H_2O)]$ (**Scheme 2.5**). It was explained that the *trans*-imidazole should be more labile due to the *cis*-labilisation of the carboxylate donors of nta^{3-}. The *trans*-imidazole is also affected by the three *cis*-carboxylate donors compared to the other imidazole which is only affected by two *cis*-carboxylates. The first order rate constants for this reaction were recorded as $5.9 \times 10^{-5}\ s^{-1}$ (pH 6) and $8.0 \times 10^{-5}\ s^{-1}$ (pH 7).

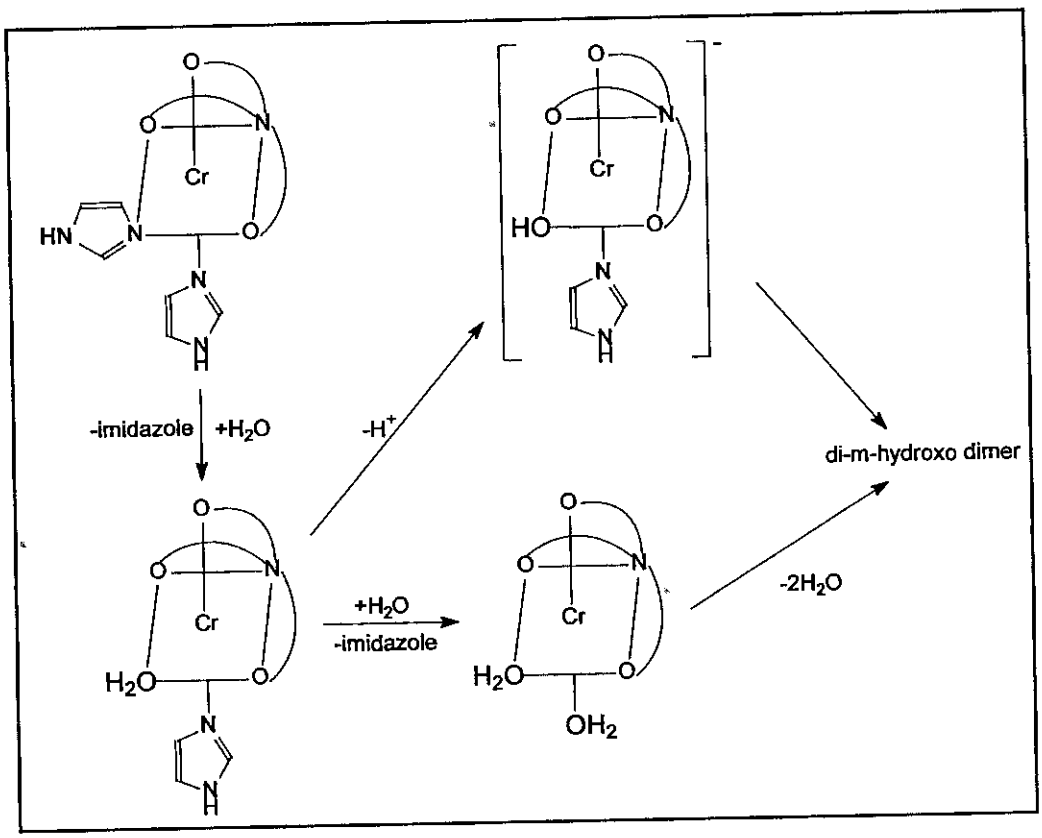

Scheme 2.5: Hydrolysis of $[Cr(\eta^4\text{-nta})(Im)_2]$.

Visser *et al.* (1999:2795) confirmed the existence of the dimeric, $[Cr(\eta^4\text{-nta})(OH)]_2^{2-}$ complex (see **Figure 2.8**), through their crystallographic characterisation of this complex. It was established that $Cs_2[Cr_2(\eta^4\text{-nta})_2(\mu\text{-OH})_2]\cdot 4H_2O$ crystallizes in two different space groups due to a slight variation in pH of the reaction mixtures. The spectra of the two complexes were found to be exactly the same in solution and the absorption maxima at 409.1 and 584 nm correlated well with the values of 409 and 585 nm obtained by Koine *et al.* (1986:2835) for $[Cr(\eta^4\text{-nta})(OH)]_2^{2-}$.

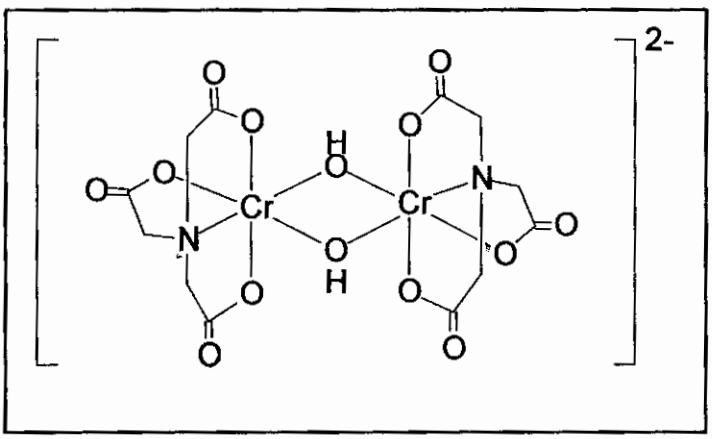

Figure 2.8: Structure of $[Cr(\eta^4\text{-nta})(\mu\text{-OH})]_2^{2-}$.

UV/VIS results obtained from this study by Visser *et al.* (1999:2795) also indicated a stable $[Cr(\eta^4\text{-nta})(\mu\text{-OH})]_2^{2-}$ complex in slightly alkaline solutions. A decrease in pH immediately led to a change in UV/VIS spectrum which was interpreted as the cleavage of the hydroxo bridges with the subsequent formation of the *cis*-diaqua complex. They also found that the addition of OH^- to this solution did not yield the original spectra and it was postulated that the increase in pH leads to the formation of an aqua-hydroxo complex. These reactions are indicated in **Scheme 2.6**.

$$[Cr_2(\eta^4\text{–nta})_2(\mu\text{-OH})_2]^{2-} \xrightarrow{2H^+} 2[Cr(\eta^4\text{–nta})(H_2O)_2] \underset{H^+}{\overset{OH^-}{\rightleftharpoons}} 2[Cr(\eta^3\text{–nta})(H_2O)(OH)]^-$$

Scheme 2.6: Formation of the *cis*-diaqua species, $[Cr(\eta^4\text{-nta})(H_2O)_2]$.

Visser *et al.* (1999:2795) using these results, also postulated that the different crystals (with distinctly different colours) prepared by Uehara *et al.* (1968:2317) were in fact not different, but possibly the $[Cr_2(\eta^4\text{-nta})_2(\mu\text{-OH})_2]^{2-}$ anion that crystallizes in two different space groups, namely tetragonal ($I4_1/a$) and monoclinical ($P2_1/c$) crystal systems, which was found in their study.

Ring strain in metal(II)-ada and similar complexes

The strain experienced by the acetate-metal rings of complexes containing polyamino polycarboxylate ligands such as $edta^{4-}$, $trdta^{4-}$, nta^{3-} and of course ada^{2-} brought about interesting, yet conflicting results. Weakliem and Hoard (1959:549) observed that the two co-planar carboxylate-containing, five-membered, equatorial rings (denoted G, or girdling rings) for $[Co(III)(\eta^6\text{-edta})]^-$ exhibit substantially more strain than the out-of plane rings (termed R, or relaxed rings), see **Figure 2.9**. It was postulated that the sum of the bond angles within the rings could be used tot determine the ring strain. The ideal value for the sum of the bond angles was calculated as 538.4°, which would allow the rings to be nearly planar.

Weakliem and Hoard explained that the strain in the G rings are primarily due to angular strain around the coordinated nitrogen atoms. It was argued that each ring attempts to impose its own stereochemical requirements on the nitrogen atom, which is also constrained to a tetrahedral geometry. The result is not only bond and angle abnormalities, but also significant distortions of the nitrogen tetrahedron. The R ring on the other hand, usually has an atom in the apical position of the complex and due to the Jahn-Teller effect (Jahn & Teller., 1937:220) the apical bonds are longer relative to the equatorial bonds around the metal centre. This elongated bond in the R ring could thus lessen the strain within the ring, causing it to be more planar and less strained than the corresponding G rings.

Nagao *et al.* (1972:1852) found in a similar study that the R rings are lesser strained than the G rings. The least squares calculations of the deviations of the non-bonded carboxylate atoms from the Co-N-O-C-C planes showed that the R ring was nearly planar. Furthermore, the Co-O_R bonding distance was slightly shorter than that of the Co-O_G bonding distance (1.861 Å compared to 1.904 Å). These results also suggested that the G ring is more strained than the R ring.

The results from the previous two studies were further supported by a study of Halloran and co-workers (1975:1762) on $[Co(\eta^4\text{-edda})(pn)]^+$ complexes, see **Figure 2.9**. Although it was observed that the total strain was more evenly distributed over the entire chelate.

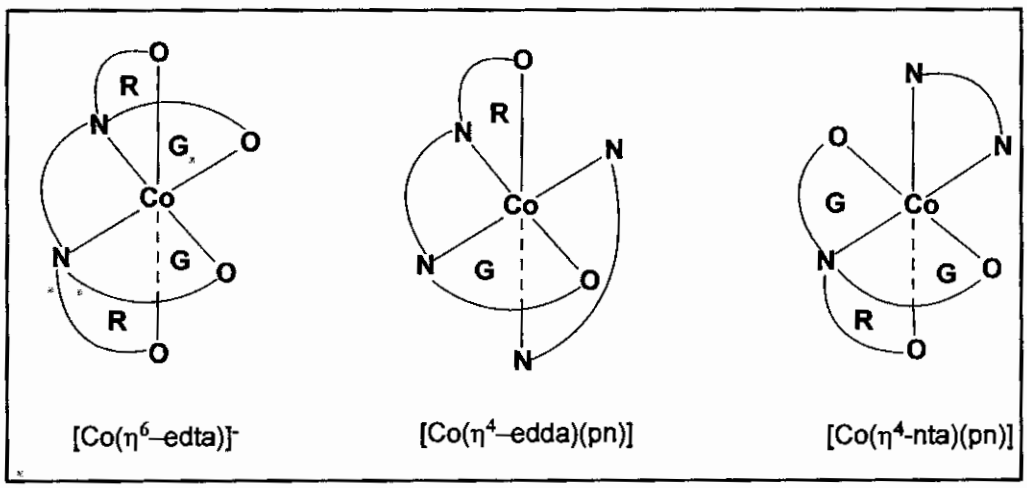

Figure 2.9: Illustration of R and G acetato rings for different Co(III) complexes.

In a study by Smith & Hoard (1959:556) it was demonstrated that the ring strain could influence the coordinating mode of ligands in these type of complexes. In the $[Ni(\eta^5\text{-edta})(H_2O)]^{2-}$ complex it was found that the $edta^{4-}$, which usually acts as a hexadentate ligand, acted as a pentadentate ligand. It was postulated that this was caused by the large metal ion. It was also established that the glycinato rings of this complex had less strain than the glycinato rings in the hexadentate $[Co(\eta^6\text{-edta})]^-$.

The influence of strain within the glycinato rings on the chemical behaviour of complexes was further illustrated by isotopic exchange studies preformed on $[Co(\eta^6\text{-edta})]^-$. Sudmeier and Occupati (1968:2524) as well as Terril and Reilly (1966:1988) showed that the α-carbon protons of the R rings of $[Co(\eta^6\text{-edta})]^-$ exhibit a much more rapid exchange rate in comparison with the G ring protons. It was concluded by these researchers that the strained environment of the G rings prevents the attainment of an enolate intermediate needed for proton exchange.

The strain in the glycinate rings were also measured in a structural study of two complexes containing different nta^{3-} derivatives, namely $[Cr(\eta^4\text{-pda})(Im)_2]$ and $[Cr(\eta^4\text{-ida})(Im)_2]$. A comparison of the ring torsion angles (O-C-CH_2-N) (the angles subtended by the atoms on the mutually perpendicular axes of the octahedron), were used in this comparison. It was found that the observed angles followed the anticipated order of ring strain, with the G rings being more strained than the R rings. Furthermore, the substituted G rings were found to be more strained than its unsubstituted counterparts in each case.

The strain in different Co(III)-nta complexes has been investigated by Visser and co-workers (2001:185). The study indicated that the sum of the endocyclic angles in $[Co(\eta^4\text{-nta})(CO_3)_2]^{2-}$ were 526.97(9) and 532.29(9)° for the G rings respectively while a value of 538.7(5)° was obtained for the R ring. These values indicated that the R ring once again experienced less strain than the G rings. They also stated that the nitrogen tetrahedron was slightly distorted from tetrahedral geometry with C-N-C angles ranging between 112.0(3)° and 114.3(2)°, which were different from the uncoordinated H_3nta where the C-N-C angles ranged between 112.3(1)° and 113.6(1)°.

Ring strain in metal-ada complexes

Results obtained in the study of the ring strain encountered in complexes containing ada^{2-} as a ligand, indicated that it does not follow the same tendency which was obtained for the metal-nta complexes.

The crystal structure of $[VO(O_2)(\eta^4\text{-ada})]^-$ (Sivak *et al.*, 1995:1057) revealed that the two glycinate rings are nearly co-planar (see **Figure 2.3**). The torsion angles, O-V-N-C, for the glycinate rings are 30.0(1) and -37.3(2)° compared to the torsion angle of 11.0(2)° which was obtained for the metal-glycinamide ring. This indicates that the latter ring is the least distorted of three pentagonal rings. In this structure the ada-amino nitrogen is also significantly distorted from the tetrahedral geometry with C-N-C angles varying between 109.7(2) and 112.8(2)°.

The structure determination of $[Ni(\eta^4\text{-ada})(H_2O)_2]$ (Bugella-Altamirano *et al.*, 2000:2463) indicated that the Ni-glycinamide ring is the most distorted of the three rings in the complex, while the $[M(\eta^4\text{-ada})(Im)(H_2O)]\cdot 1.5H_2O$ (M = Co, Ni) (Bugella-Altamirano *et al.*, 2000:2473) complexes it was found that the glycinamide rings is only the second most distorted ring. From the above studies it can be seen that the tendency of having specific rings carrying the most strain is not exhibited for metal-ada chelates as was observed for metal-nta complexes.

2.2.2 Reactions of chromium(III)-ada and similar complexes

Very few metal complexes containing ada^{2-} as a ligand is cited and to date no kinetic studies have been published on any of these complexes. It was therefore decided to focus the main part of this chapter on the substitution reactions of chromium(III)-nta and similar complexes.

Anation reactions of Cr(III)-nta complexes

Kinetic studies involving chromium(III) have been extensively investigated and the main characteristic of most of these results was the relative inertness of these complexes towards substitution reactions (Advanced Inorganic Chemistry, Edited by F.Cotton and G.Wilkinson 1966. p 558).

The kinetics of the formation and dissociation of $[Cr(\eta^4\text{-nta})(acac)]^-$ (see **Scheme 2.7**) have been investigated, but the complexity of the rate law prevented a full understanding of the mechanism (Bhatterchayya & Banerjee, 1997:4217).

$$[Cr(\eta^4\text{–nta})(H_2O)_2] + Hacac \underset{}{\overset{K_1}{\rightleftharpoons}} [Cr(\eta^4\text{–nta})(acac)]^- + H^+ + 2H_2O$$

Scheme 2.7: Formation of $[Cr(\eta^4\text{-nta})(acac)]^-$.

Two different kinetic studies investigated the reaction of $[Cr(\eta^4\text{-nta})(H_2O)_2]/[Cr(\eta^4\text{-nta})H_2O)(OH)]^-$ with different synthetic dyes, Solochrome Yellow 2G (Hualin & Xu, 1990:137) and Eriochrome Black T (Visser *et al.*,1994:1051). The second study also included the reaction with thiocyanate (NCS^-) and H^+ ions. Both these studies were complicated by the fact that the dyes have very large extinction coefficients and these reactions were thus rather performed with the [metal] in excess. The reaction scheme for the second study is represented in **Scheme 2.8**.

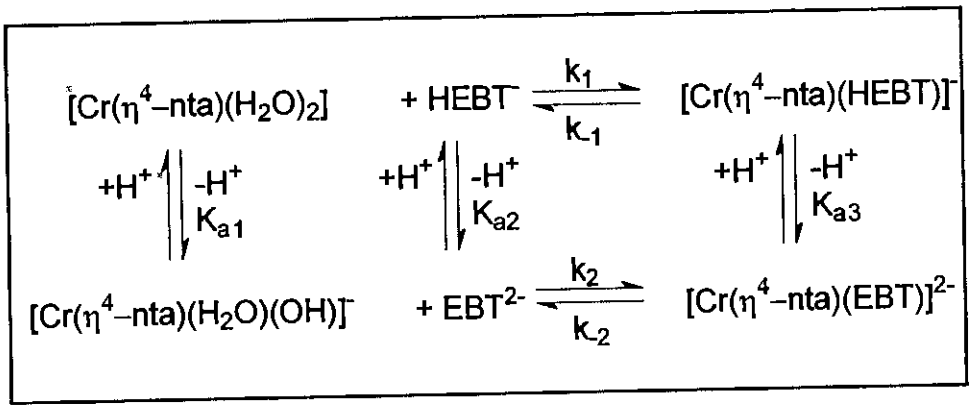

Scheme 2.8: Reaction scheme for the reaction of $[Cr(\eta^4\text{-nta})(H_2O)_2]$ with Eriochrome Black T, EBT^-.

This study was further complicated by the fact that EBT^- has an acid dissociation constant of 6.3 (Vogel, 1989), which is very close to that of $[Cr(\eta^4\text{-nta})H_2O)(OH)]^-$ (pK_a = 5.47). The elucidation of the mechanism was then even further complicated by the fact that a precipitate formed at pH 6.

In spite of these difficulties, very useful information was obtained from their study. It was found that the reaction between $[Cr(\eta^4\text{-nta})(H_2O)_2]$ and EBT^- is 16 times faster (9.5×10^{-2} $M^{-1}s^{-1}$ at 30°C) than the corresponding reaction with NCS^- (5.8×10^{-3} $M^{-1}s^{-1}$ at 25°C). This was attributed to the chelating effect of the EBT^- ligand during the reaction.

Haulin and Xu proposed a different mechanism for the reaction of $[Cr(\eta^4\text{-nta})(H_2O)_2]$ with Solochrome Yellow 2G. They suggested a two-step mechanism (ion pair formation) that involved rapid formation of the monodentate coordinated dye intermediate, followed by the rate determining ring-closure (**Scheme 2.9**). The rate constants, k_1 and k_2, for the ring closure steps were determined as 2.3×10^{-2} s^{-1} and 1.7×10^{-2} s^{-1} respectively.

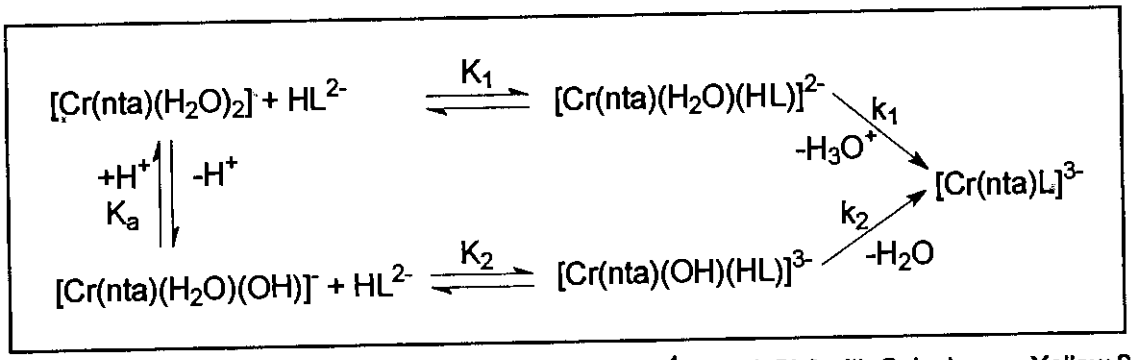

Scheme 2.9: Reaction scheme for the reaction of $[Cr(\eta^4\text{-nta})(H_2O)_2]$ with Solochrome Yellow 2G (HL).

Both these studies found that the electron donating ability of nta^{3-} improved the reactivity of the chromium(III) complex by several orders of magnitude. The second order rate constant (5.8×10^{-3} $M^{-1}s^{-1}$) for the reaction of $[Cr(\eta^4\text{-nta})(H_2O)_2]$ with NCS^- compares well with the k_1 value of 4.7×10^{-3} $M^{-1}s^{-1}$ which was obtained for the reaction between $[Cr(\eta^4\text{-TPPS})(H_2O)_2]^{3-}$ and NCS^- (Ashley *et al.*, 1980:1608). Porphyrins like $TPPS^{6-}$ are known to enhance the rate of substitution of inert metal(III) complexes by several orders of magnitude. The main reason for this is believed to be the electron donating ability of the porphyrin, which in turn increases the electron density on the central metal ion, making it react more like the labile metal(II) species.

Chelate ring opening reactions of metal(III) complexes

Research data on the acid-catalyzed aquation of tripodal aminopolycarboxylate systems is very scarce in literature. Even less data is available on the chelate ring opening of these systems where the metal-carboxylate bond is broken.

The reaction between $[Cr(\eta^4\text{-nta})(H_2O)_2]$ and H^+ was investigated by Visser *et al.* (1994:1051). It was proposed that the mechanism for the reaction involved the formation of an ion pair. Subsequent protonation of one of the carboxylate groups of nta^{3-} then occurs, which results in the dissociation of this bond to give

the aquated tridentate complex, $[Cr(\eta^3\text{-nta})(H_2O)_3]^+$. A possible reaction scheme is presented in **Scheme 2.10**.

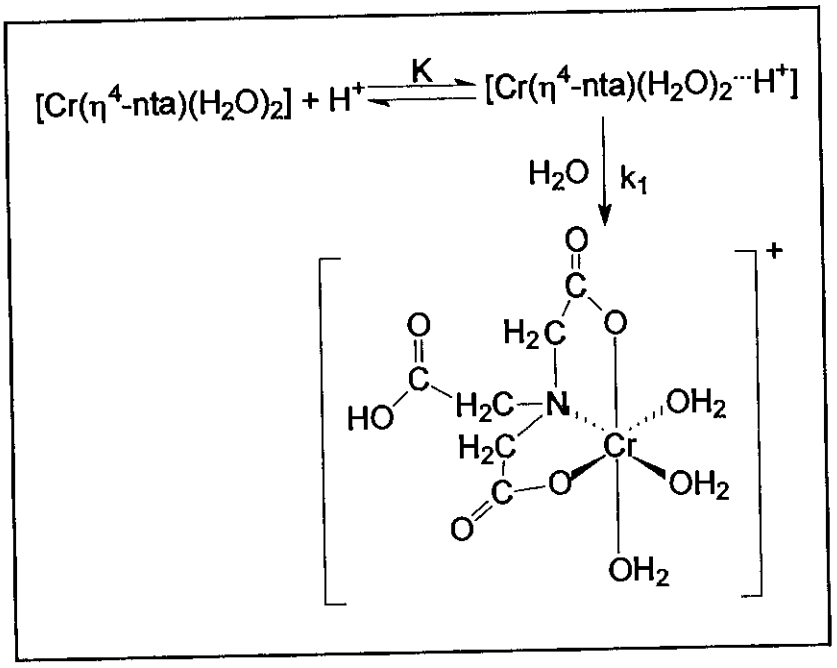

Scheme 2.10: Formation of $[Cr(\eta^3\text{-nta})(H_2O)_3]^+$.

During a later study by Visser *et al.* (2002:461) the kinetic study of a similar reaction between $[Co(\eta^4\text{-nta})(H_2O)_2]$ with H^+ ions was reported. Once again it was found that the addition of it lead to the formation of an ion associated species, $[Co(\eta^4\text{-nta})(H_2O)_2{\cdots}H^+]$. This species dissociates in a rate-determining step to form the tridentate cation, $[Co(\eta^3\text{-nta})(H_2O)_3]^+$. The mechanism that was proposed is analogous to that found for the reaction between $[Cr(\eta^3\text{-nta})(H_2O)_3]^+$ and H^+ ions, see **Scheme 2.10**.

The $Na[Cr(\eta^4\text{-cida})(pic)]{\cdot}2H_2O$ complex was characterised by Chatterjee and Stephen (2002:2917). The $cida^{3-}$ also acts as a tripodal tetradentate ligand in complex formation reactions and is similar to ada^{2-} and nta^{3-}. The complex was showed to form the $[Cr(\eta^4\text{-cida})(H_2O)_2]$ and picolinic acid (picH) as the final products upon acidification of a $Na[Cr(\eta^4\text{-cida})(pic)]{\cdot}2H_2O$ solution (see **Scheme 2.11**). The variation of the pseudo-first order rate constants with

variation of perchloric acid concentration suggests the operation of two concurrent pathways namely an uncatalyzed as well as an acid-catalyzed pathway. The solvent deuterium isotope effect that was obtained was consistent with a rapid pre-equilibrium protonation followed by a rate determining ring opening step. This study clearly eliminated a concerted [H^+] attack on the metal complex as a possibility. The uncatalyzed path is believed to involve the attack of a solvent molecule in the rate determining step while the acid catalyzed pathway seems to involve dissociation of the conjugate acid formed by the protonation of the complex in a rapid pre-equilibrium step.

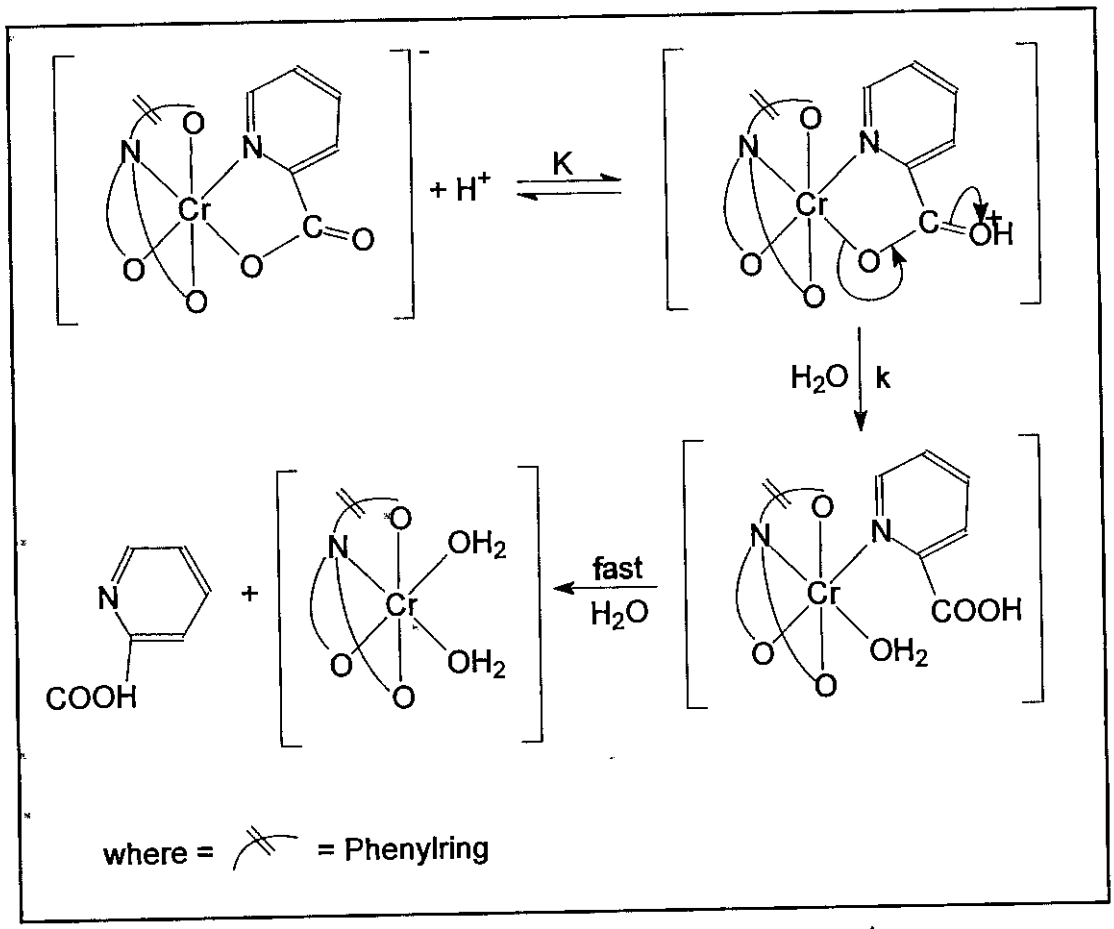

Scheme 2.11: Acid catalysed mechanism of hydrolysis of [Cr(η^4-cida)(pic)]$^-$.

The same study investigated the effect of different metal(II) ions (M^{2+} = Cu(II), Ni(II) and Zn(II)) on the aquation of Na[Cr(η^4-cida)(pic)]·$2H_2O$ (see

Scheme 2.12). Results obtained indicated an increase in rate constant values with an increase in $[M^{2+}]$ at a constant $[H^+]$.

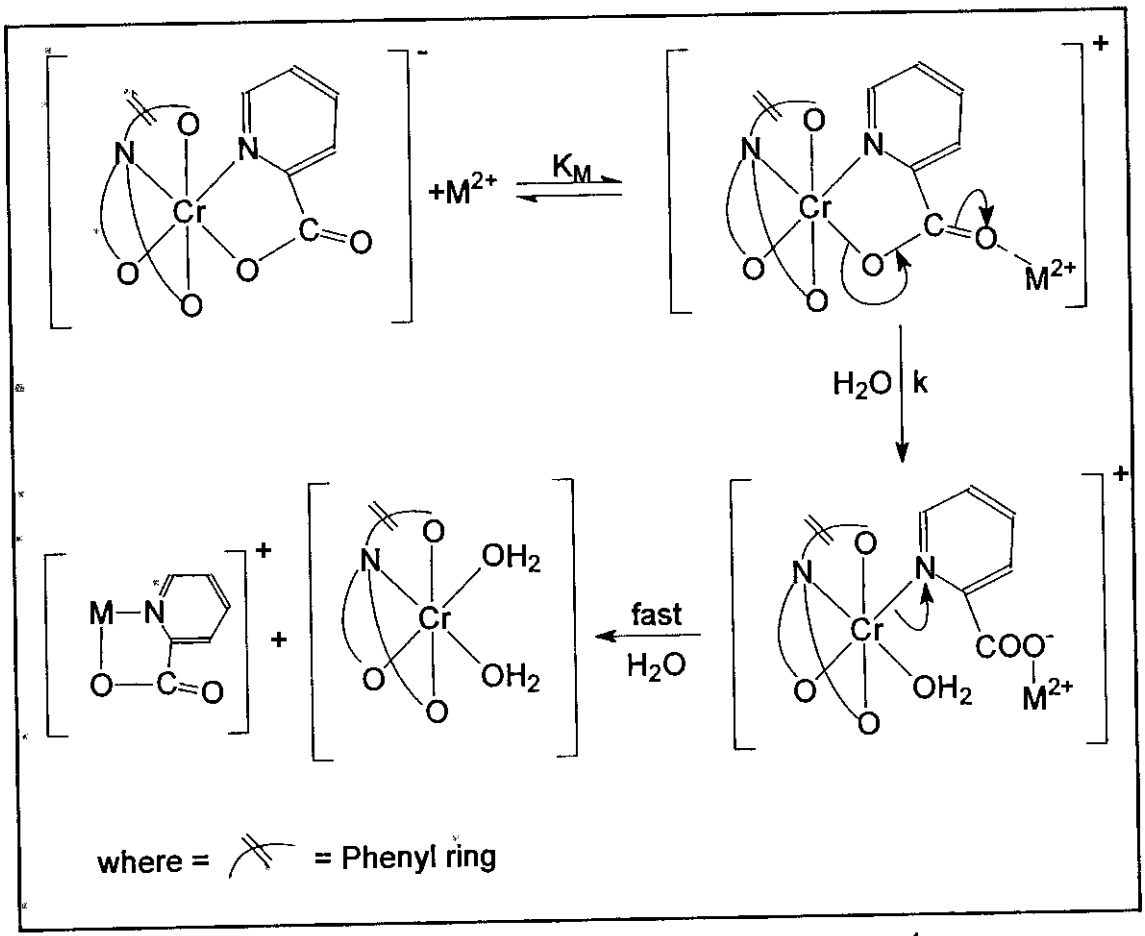

Scheme 2.12: Metal ion promoted mechanism of hydrolysis of $[Cr(\eta^4\text{-cida})(pic)]^-$.

Anation reactions of Co(III)-nta complexes

The first study on the anation reactions of *cis*-$[Co(\eta^4\text{-nta})(H_2O)_2]$ was performed by Thacker and Higginson (1975:704). They studied the redox substitution reactions of *cis*-$[Co(\eta^4\text{-nta})(H_2O)_2]$ with various ligands. They found that only NCS^- ions did not show redox properties in the pH region they used during their investigation (pH = 3 – 5). Their results were however not good due to, among other things, the interference of the buffer solutions used during these kinetic studies.

The influence of H^+ ions on the Co(II)-nta system was studied by Visser *et al.* (2002:461). It was observed that the aqua-hydroxo complex, $[Co(\eta^4\text{-nta})H_2O)(OH)]^-$, reverts back to the dimer at pH 6 – 7 upon standing for several days (**Scheme 2.13**). They therefore studied the pH dependence of the $[Co(\eta^4\text{-nta})(H_2O)_2]$ complex between pH 2 and 7 to avoid complication of competing reactions. The acid dissociation constant of $[Co(\eta^4\text{-nta})(H_2O)_2]$, pK_{a2}, was determined as 6.52(2), which compares well with the value of 6.71(1) determined by Thacker and Higginson (1975:704) for the β-form of the Co(III)-nta study, but is higher than the value obtained (pK_a = 5.43) for the same reaction by Haulin & Xu (1990:137).

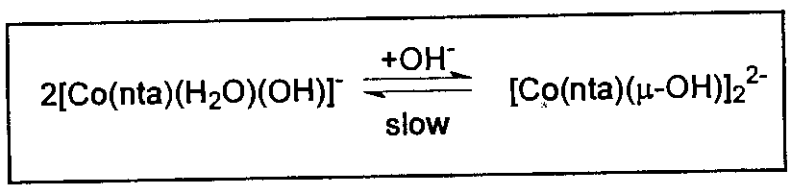

Scheme 2.13: $Co(\eta^4\text{-nta})(H_2O)(OH)]^-$ reverting back to the dimer at pH 6 – 7.

Visser *et al.* (2002:461) extended their study by investigating the reaction of $[Co(\eta^4\text{-nta})(H_2O)_2]/[Co(\eta^4\text{-nta})(H_2O)(OH)]^-$ with NCS^- ions (see **Scheme 2.14**). The reaction was studied at pH values between 2 and 7, which allow both Co(III)-nta species to react with NCS^-. The following scheme was proposed:

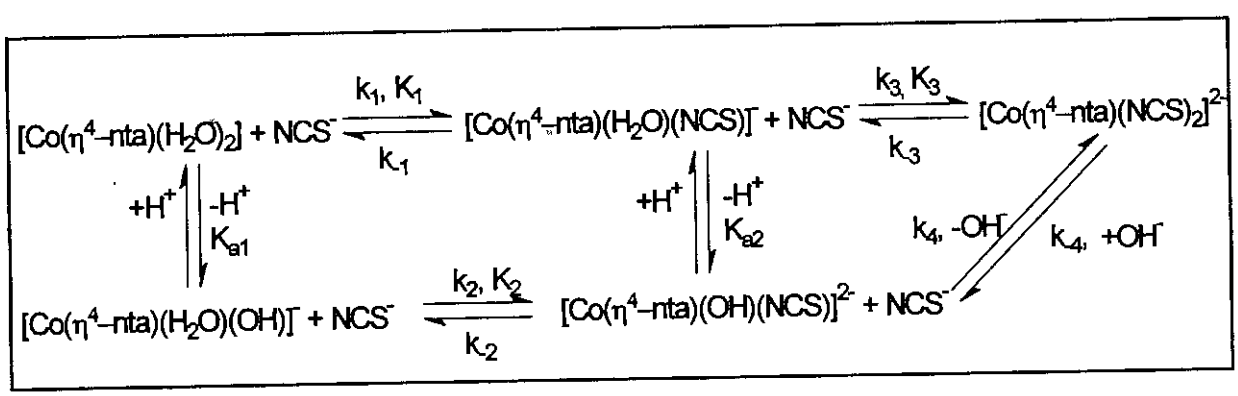

Scheme 2.14: Reactions of $[Co(\eta^4\text{-nta})(H_2O)_2]/Co(\eta^4\text{-nta})(H_2O)(OH)]^-$ with NCS^- ions.

The final product in **Scheme 2.14** were substantiated by the synthesis and successful characterisation of $[Co(\eta^4\text{-nta})(NCS)_2]^{2-}$.

The $[Co(\eta^4\text{-nta})(H_2O)(OH)]^-$ complex was found to react 70 times faster at 24.7°C with NCS^- than $[Co(\eta^4\text{-nta})(H_2O)_2]$ with NCS^- (k_2 = 1.68(5) $M^{-1}s^{-1}$ *vs.* 2.4(1) × 10^{-2} $M^{-1}s^{-1}$ for k_1 at 24.7°C). The increase in substitution rate is attributed to the labilizing effect of the hydroxo ligand. The *cis*-labilizing effect for the hydroxo ligand was also observed for the corresponding reaction between $[Cr(\eta^4\text{-nta})H_2O)(OH)]^-$/$[Cr(\eta^4\text{-nta})H_2O)_2]$ and NCS^- an increase of about 8 times was observed for the hydroxo complex (Visser *et al.*, 1994:1051).

Other similar Co(III) and Cr(III) complexes.

Only a few articles are available in the literature that covers the anation and aquation reactions of *cis*-$[Co(\eta^4\text{-edda})(X_2)]$ complexes (X = Cl^-, H_2O) (Weyh *et al.*, 1973:2374 and Garnett & Watts, 1947:307). There are also only a few reports on the substitution reactions of mono-aqua complexes of chromium(III) where the other five coordination positions are occupied by five-coordinate, edta-type ligands (Ogino *et al.*, 1975:2093 and Sulfab *et al.*, 1976:2388). All of these studies illustrated that these type of ligands (multidentate N, O donors) labilise the metal center and enhance the rate of substitution by several orders of magnitude.

Bridge cleavage reactions by hydrogen ions

Sykes and Weil (1970) wrote a comprehensive review on the acidic bridge cleavage reactions of binuclear cobalt(II) complexes. Bridging ligands can vary from peroxo, amido, superoxo, phosphato, nitrito, halido, acetato and hydroxo ligands.

It has been suggested that cobalt complexes containing aminocarboxylic acids such as nta^{3-} and $edta^{4-}$ do not appear to combine with O_2 to form peroxo- or superoxo-bridged species (Fallab, 1967:496). The reason that was given for this phenomenon is that these ligands contain too many oxygenic groups which are bonded to the cobalt(II). These groups reduce the ability with which these complexes can form stable molecular oxygen adducts. On the other hand, there are countless examples of hydroxo-bridged species of cobalt complexes such as $[Co(\eta^4\text{-nta})(\mu\text{-OH})]_2^{2-}$ one of which was prepared by Visser *et al.* (2003:235).

The stability of Co(II) di- and tri-μ-hydroxo complexes in aqueous solutions is very much dependent on the hydrogen ion concentration. Hoffman and Taube (1968:903) studied the kinetics of the reaction of hydrogen ions with $[Co(NH_3)_4(\mu\text{-OH})]_2^{4+}$, see **Scheme 2.15.** The hydroxo bridge cleavage of $[Co(C_2O_4)_2(OH)]_2^{4-}$ at pH 3.5 – 4.5 was investigated by Lee Hin-Fat and Higginson (1971:2589). They also found a first order $[H^+]$ dependence for this reaction.

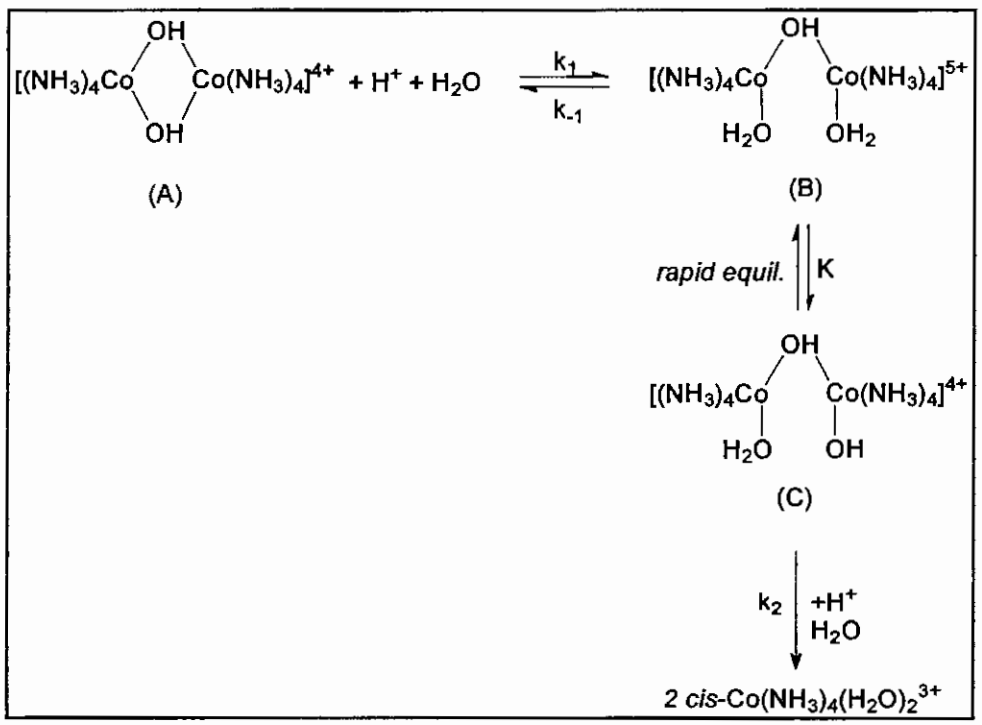

Scheme 2.15: Acidic cleavage of $[Co(NH_3)_4(\mu\text{-OH})]_2^{4+}$.

The acid-assisted cleavage of the di-μ-hydroxo bonds in $[Co(en)_2(OH)]_2^{4+}$ was also studied by different research groups (El-Awady & Hugus, 1971:1415 and Demaine & Hunt, 1971:2106). The study of Demaine and Hunt (1971:2106) suggested the same mechanism as the one proposed for $[Co(NH_3)_4(\mu\text{-}OH)]_2^{4+}$ (as indicated in **Scheme 2.15**) while the study of El-Alwady and Hugus (1971:1415) proposed two possible mechanisms for the acid assisted cleavage for this reaction. According to El-Alwady both mechanisms involve the formation of a single hydroxo-bridged dimeric species as an intermediate. It is proposed that the one mechanism involves the protonation of the dimer and the intermediate in a fast reversible step (**Scheme 2.16**). The second mechanism which involves the second protonation of the mono-μ-hydroxo complex is very similar to that proposed by Hoffman and Taube (1968:903) (**Scheme 2.15**).

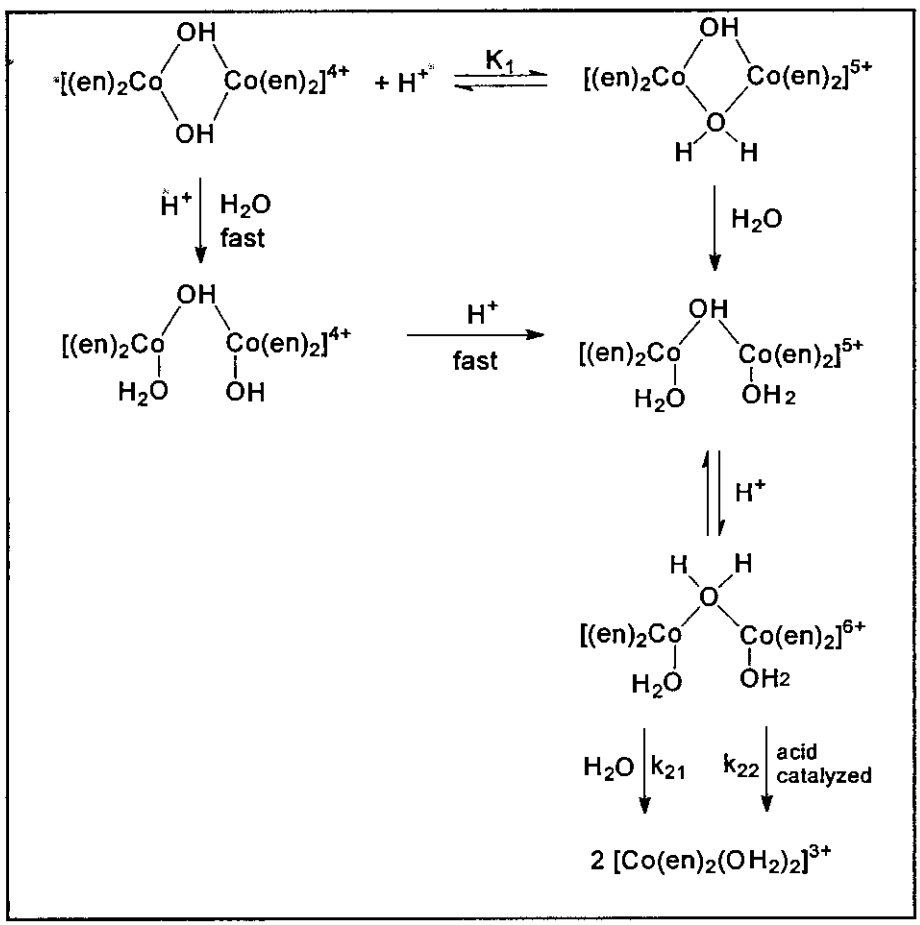

Scheme 2.16: Acid assisted cleavage of the di-μ-hydroxo bridges in $[Co(en)_2(OH)]_2^{4+}$.

Ellis and co-workers (1972:2565), later provided a possible solution for the differences in the observed [H^+] dependence in the above-mentioned studies. According to their results the rate laws for the acid cleavage of μ-hydroxo-cobalt(III) complexes sometimes involve an acid dependent term and invariably show an acid dependence for the reaction, which varies from simple first-order to a combination of first- and second-order terms. Complexes with a single hydroxo bridge on the other hand yield a linear dependence between the observed rate constant and the [H^+]. Any deviation from such a dependence in di-μ- hydroxo bridged complexes must be a function of the second hydroxo bridge. The mechanism they predicted for the acidic cleavage of a μ-hydroxo cobalt(III) complex is shown in **Scheme 2.17**.

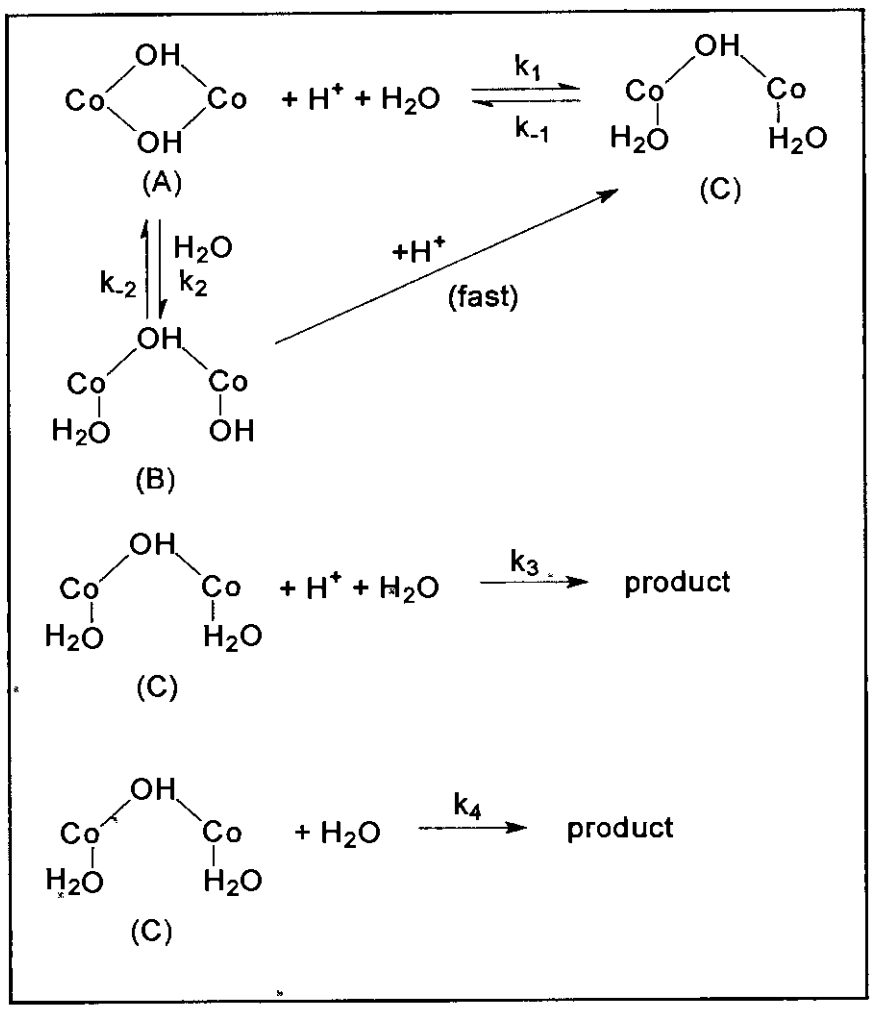

Scheme 2.17: Acidic cleavage of a μ-hydroxo cobalt(III) complex.

The pseudo first-order rate constant, k_{obs} is given in Equation 2.1.

$$k_{obs} = (k_2k_4 + k_1k_3 + k_1k_4[H^+] + k_1k_3[H^+]^2)/(k_{-1} + k_4 + k_3[H^+]) \quad (2.1)$$

It can be seen from Equation 2.1 that the rate constant k_{-2} was ignored. The reason given for this is that the intermediate, (B) (**Scheme 2.17**), can partially rotate to form hydrogen bonds with another intermediate complex or the dimer, especially through the OH^- ligand. It was therefore concluded that k_{-2} will only make a contribution at very small hydrogen ion concentrations.

The acidic cleavage of the hydroxo bridges of $[Co(\eta^4\text{-nta})(\mu\text{-OH})]_2^{2-}$ has been investigated by other workers (Thacker & Higginson. 1975:704 and Meloon & Harris, 1977:434). Both these studies observed a fast initial reaction followed by a slower second reaction upon allowing $[Co(\eta^4\text{-nta})(\mu\text{-OH})]_2^{2-}$ to remain in moderately acidic solutions (*ca.* pH 4) for 20 to 30 minutes. It was observed that the aqueous solutions of $[Co(\eta^4\text{-nta})(\mu\text{-OH})]_2^{2-}$ did not show any evidence of normal acidic or basic properties when titrated rapidly with dilute acid and back-titrated with a base. It was postulated that these two reactions involved the formation of a mono-hydroxo-bridged species that dissociates to form *cis*-$[Co(\eta^4\text{-nta})(H_2O)_2]$ in the second slower step (**Scheme 2.18**).

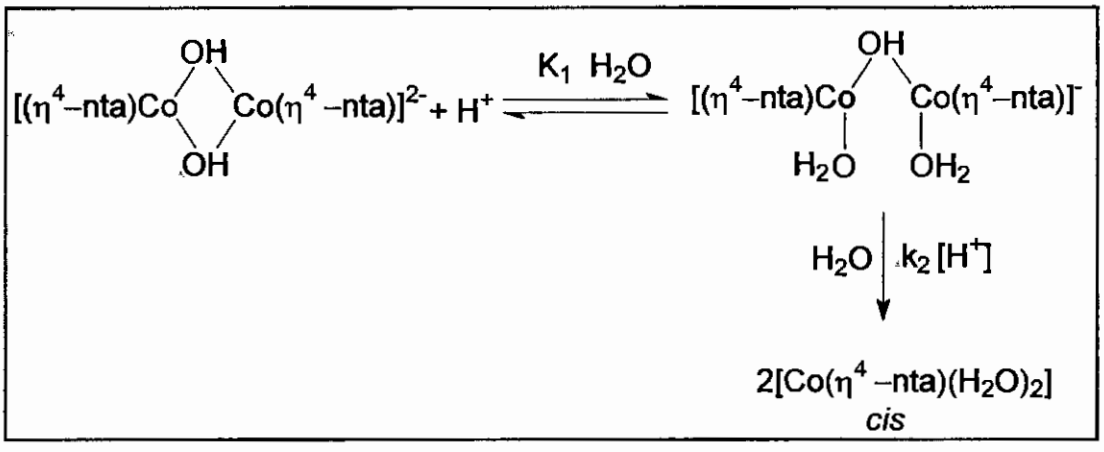

Scheme 2.18: Acidic cleavage of $[Co(\eta^4\text{-nta})(\mu\text{-OH})]_2^{2-}$.

Thacker & Higginson also calculated the acid dissociation constant (pK_a = 6.71(1)) for the formation of *cis*-$[Co(\eta^4\text{-nta})(H_2O)(OH)]^-$ from *cis*-$[Co(\eta^4\text{-nta})(H_2O)_2]$. It was mentioned that *cis*-$[Co(\eta^4\text{-nta})(H_2O)(OH)]^-$ is not very stable in solution. Research by Koine *et al.* (1986:2835) showed with ^2H NMR that an intermediate species is formed upon acidification of $[Cr(\eta^4\text{-nta})(OH)]_2^{2-}$. They concluded that the intermediate might also be a mono-hydroxo-bridged species. Other observers also support this assumption (Toftlund & Springborg, 1976:1017 and Grant & Hamm, 1958:4166).

The acidic cleavage reaction of $[Co(\eta^4\text{-nta})(\mu\text{-OH})]_2^{2-}$ (**Scheme 2.19**) during the slow addition of acid (pH 2 - 6) was investigated by Visser *et al.* (2002:461). Their results did not exhibit the expected diprotic behaviour for the protonation of $[Co(\eta^4\text{-nta})(\mu\text{-OH})]_2^{2-}$. Instead only one protonation step was observed under the experimental conditions. Previous studies proved that the cobalt(III)-nta species present in solution with pH 6 – 7 is in fact the di-μ-hydroxo complex and that the main complex present at pH 2 is $[Co(\eta^4\text{-nta})(H_2O)_2]$ (Visser *et al.*, 1997:2851). Furthermore, the results presented in previous studies (Hoffman & Taube, 1968:903), Demaine & Hunt, 1971:2106 and Linhart & Siebert, 1969:24) for the stepwise bridge cleavage of di-μ-hydroxo complex ions support this type of protonation. Reactions 2 and 3 (**Scheme 2.19**) were proposed for the protonation of $[Co(\eta^4\text{-nta})(\mu\text{-OH})]_2^{2-}$.

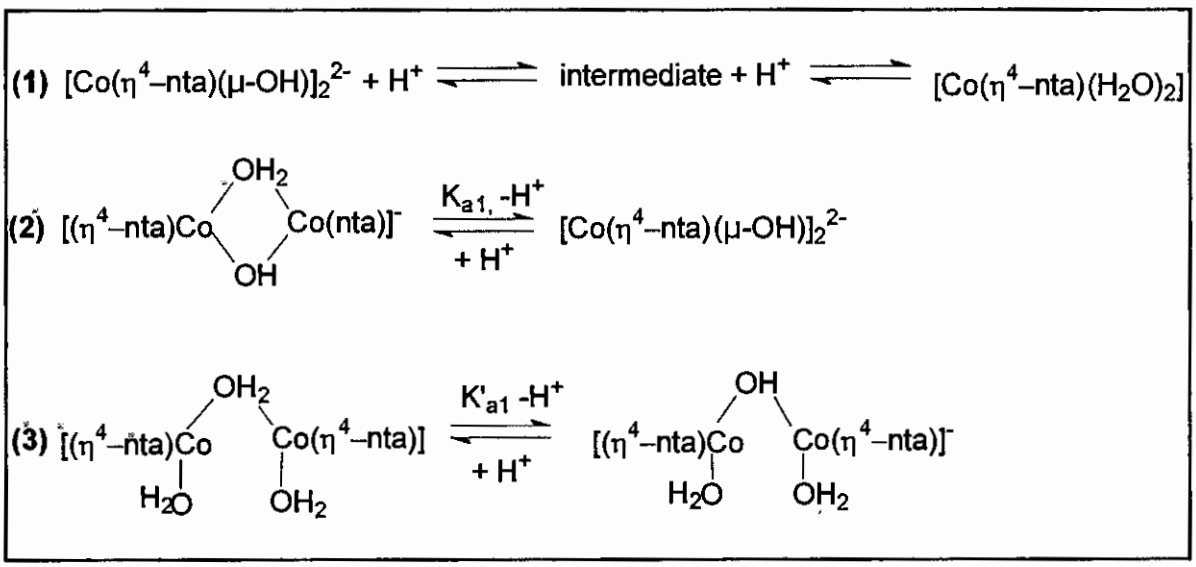

Scheme 2.19: Proposed protonation reactions of $[Co(\eta^4\text{-nta})(\mu\text{-OH})]_2^{2-}$.

In Reactions 1 and 2 (**Scheme 2.19**), K_{a1} and K'_{a1} represent the acid dissociation constants of the di-μ-hydroxo complex ion and singly bridged μ-hydroxo species, respectively. The fact that only one protonation step was experimentally observed, Equation 2.2 was found to be applicable.

$$A = (A_h + A_0(K_{a1}/[H^+]))/(1 + (K_{a1}/[H^+])) \qquad (2.2)$$

The pK_{a1} of $[Co(\eta^4\text{-nta})(\mu\text{-OH})]_2^{2-}$ was determined spectr ophotometrically as 3.09(3). According to their study, a possible reason for only one protonation step and not two, as expected, was due to the fact that the UV/VIS spectra of the intermediate species (Reaction 1 – 3 in **Scheme 2.19**) were very similar under their experimental conditions. Therefore, it was impossible to decide on the basis of available information which of K_{a1} or K'_{a1} (**Scheme 2.19**) was actually detected in this study.

The kinetic study of the acid cleavage of $[(phen)_2Cr(\mu\text{-OH})]_2^{4+}$ (Wolcott & Hunt, 1968:755) showed completely different mechanistic results. It was proposed that proton transfer reactions in aqueous solutions are far too rapid for the acid

dependence of the cleavage rate to be explained in terms of rate-determining addition of a proton to the dimer (**Scheme 2.20**).

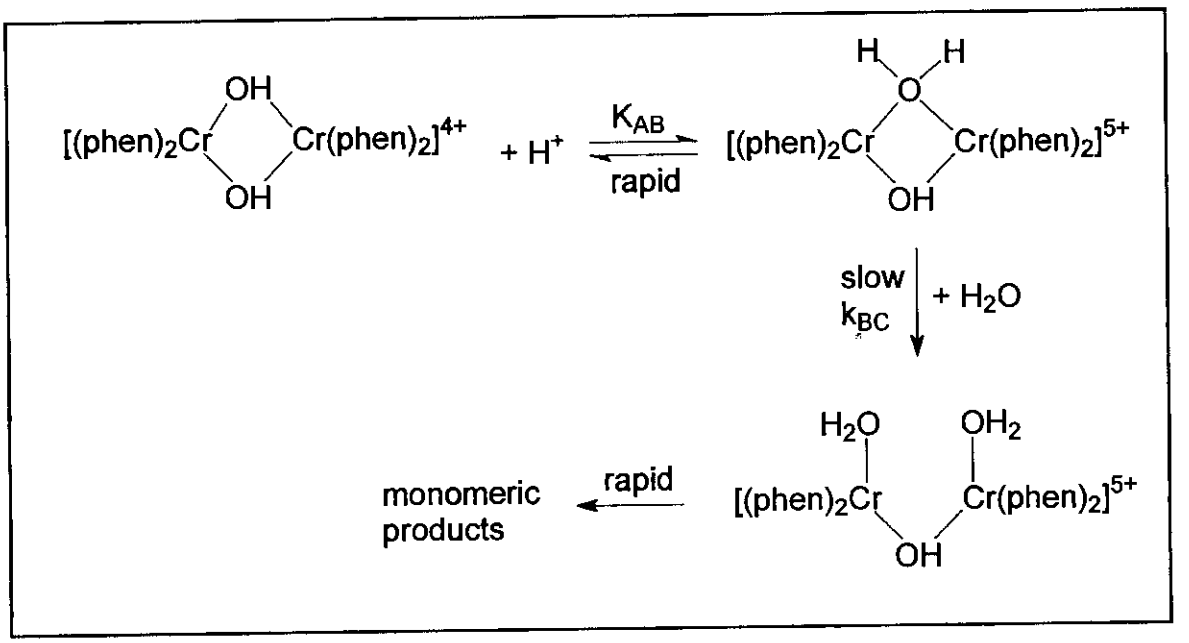

Scheme 2.20: Acidic cleavage of $[(phen)_2Cr(\mu\text{-}OH)]_2^{4+}$.

They suggested that the first-order $[H^+]$ dependence of the rate law is due to a rapid acid-base reaction preceding the rate-determining step which involves the addition of a proton to the dimer.

It can be seen from the previous paragraphs that by making the appropriate assumptions concerning the magnitude of the various constants, one can readily derive an expression corresponding to any of the observed mechanisms for related cobalt(III) complexes. The complexity of these type of reactions is underlined by the fact that different workers suggested different types of mechanisms for bridge cleavage reactions for the same reaction. The above discussion represents a fairly complete set of results on these types of reactions to date, making the investigation of these reactions very interesting due to the limited data available on these type of complex reactions.

2.3 Conclusion

It can be seen from this chapter that there are many possibilities in the investigation of metal-ada complexes. A number of metal(II)-ada complexes have been characterised but to date no metal(III)-ada complex has been synthesized and characterised by means of IR, UV/VIS and X-ray crystallography. The isolation and characterisation of such a complex will shed more light on the mode of coordination of ada^{2-} toward a metal(III) cation and the strain in these complexes. No kinetic studies have been undertaken on any metal-ada complexes. The kinetic study of a Cr(III)-ada complex would provide a lot of information on the mechanism of the substitution reactions of these type of complexes.

Further studies on these complexes could provide much needed information on the behaviour of biological systems in the presence of transition metals.

3 Synthesis and identification of Cr(III)-ada complexes

In this chapter...

The synthesis and characterisation of the different water soluble chromium(III)-ada complexes are presented in this chapter. The results are summarised in the final paragraphs.

3.1 Introduction

It was shown in the previous chapters that there are only a few reports on the synthesis and identification of metal-ada complexes, and none to date on metal(III)-ada complexes. The identification of the starting complex and the final products in this study was also vitally important for the determination of the mechanism for the acid-catalyzed reaction and substitution reactions of the Cr(III)-ada complexes, which will be discussed in Chapter 5.

Most of the studies on ada^{2-} and nta^{3-} complexes (Chapter 2) relied heavily on X-ray crystallography, IR and UV/VIS spectroscopy. The identification of these types of complexes by IR is complicated and not always conclusive, but can be very useful in obtaining some information on its structures. The difficulty in the correct identification of these complexes is illustrated by the fact that the oxygen atoms of the carboxyl groups which are not bonded to the metal can either be hydrogen-bonded, weakly bonded to the amino group of the neighbouring molecule, or to the water of crystallisation, or weakly bonded to the metal of a neighbouring complex (Nakamoto, 1963:206). The COO–M stretching

frequencies of complexes containing ada^{2-}, nta^{3-} and related compounds are therefore affected by coordination as well as by intermolecular interaction, making the assignment of IR stretching frequencies complicated. IR can, in spite of all the above mentioned complications, be useful in the characterisation of these type of metal complexes. COO^- groups have according to Nakamoto (1963:206) stretching frequencies of 1650 – 1620 cm^{-1} when coordinated to metals such as chromium(III) and stretching frequencies of 1750 – 1700 cm^{-1} when un-ionised or uncoordinated.

This chapter deals mainly with the isolation of different Cr(III)-ada complexes. The characterisation of these complexes with IR- and UV/VIS- spectroscopy are discussed. The paramagnetic nature of Cr(III) prevented the use of ^1H NMR as an identification method. A schematic representation of the formation of different Cr(III)-ada complexes investigated in this study is shown in **Scheme 3.1**.

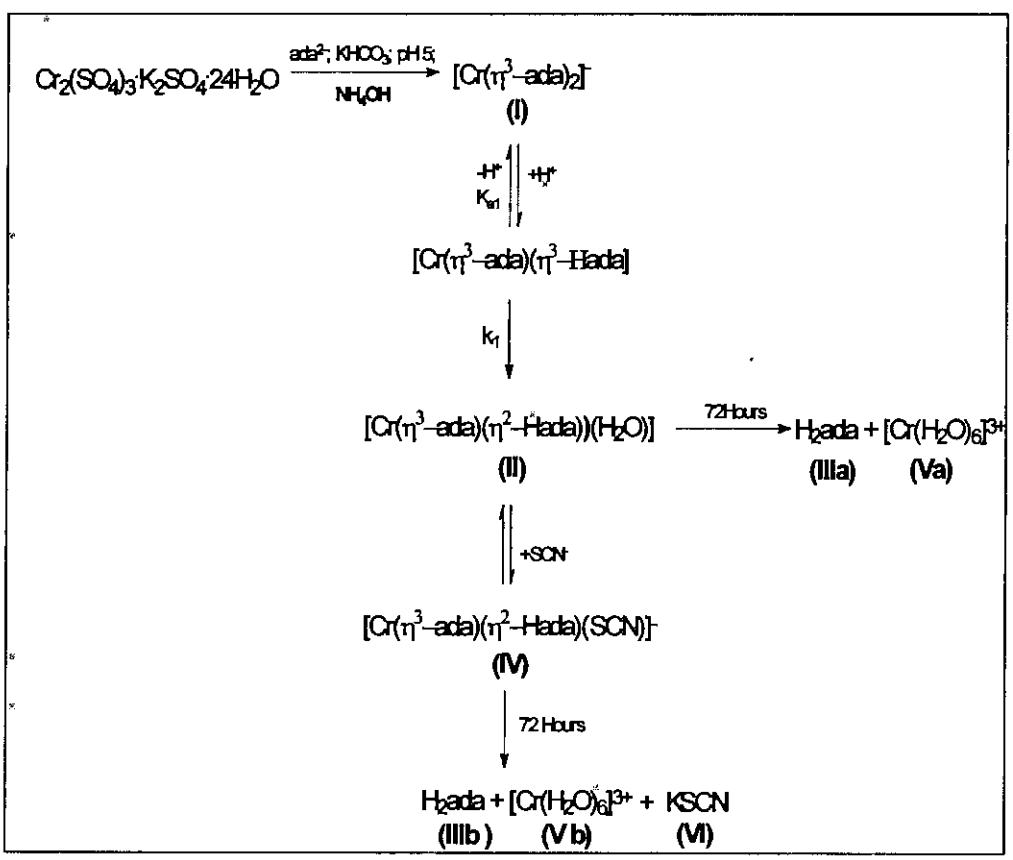

Scheme 3.1: Synthesis and reactions of chromium(III)-ada complexes.

3.2 Apparatus and chemicals

All reagents were of reagent grade. All pH measurements were performed with a pH 211 microprocessor pH meter, which was calibrated with two buffer solutions, at a pH 7.01 (HI7007) and pH 4.01 (HI7004) that were all obtained from Hanna instruments. UV/VIS measurements were performed on a Cary 50 (Conc.) spectrophotometer equipped with a constant temperature cell holder (accuracy within 0.1 °C). The infrared spectra were recorded on a Digilab FTS2000 f.t.I.R. spectrometer (s = strong, sh = shoulder, w = weak peak heights), (υ = stretching frequency, δ = bending mode frequency).

3.3 Synthesis and isolation of different complexes/compounds

3.3.1 Synthesis of $Cs[Cr(\eta^3\text{-ada})_2]\cdot 2H_2O$ (I)

$Cr_2(SO_4)_3\cdot K_2SO_4\cdot 24H2O$ (5.252 g) was dissolved in H_2O (40 cm^3). Concentrated NH_4OH was added dropwise to this solution to precipitate chromium(III) hydroxide. The precipitate was added to a solution containing H_2ada (2 g) and H_2O (40 cm^3) and heated on a water bath until almost dry. Hot H_2O (30 cm^3) was added to this reaction solution and immediately filtered. Orange-pink crystals precipitated after a few hours. The title compound was obtained by dissolving the compound in minimum H_2O and adding an excess of CsCl (2.91 g).

Yield: 3.53 g (77 %)
IR (υ-COO-(cm^{-1})): 1615 (s)
IR ($\delta(NH_2$ (cm^{-1})): 1681 (sh)
UV/VIS (λ_{max} (nm)(ε, M^{-1} cm^{-1})): 355 (38), 501 (46)

3.3.2 Isolation and characterisation of $[Cr(\eta^3\text{-ada})(\eta^2\text{-Hada})(H_2O)]$ (II)

$Cs[Cr(\eta^3\text{-ada})_2]\cdot 2H_2O$ (0.5 g) was dissolved in water (30 cm^3) and the pH was adjusted to 0.8 (HCl, 1.0 M). The reaction mixture was allowed to react at 25 °C for 2 minutes (to allow for completion of the first reaction (see k_1 step in **Scheme 3.1, Figure 3.1**). Ethanol (75 cm^3) was added slowly to the mixture until precipitation of the product was completed. The precipitate was dried under vacuum in a dessicator in the presence of P_2O_5.

IR (υ_{-COO-}(cm^{-1})): 1607.2 (s)
IR (υ_{-COOH}(cm^{-1})): 1734.8 (s)
IR ($\delta(NH_2)$ (cm^{-1})): 1671.2(s)
IR ($\upsilon_{Cr\text{-}OH_2}$($cm^{-1}$)): 546.9 (w)
UV/VIS (λ_{max} (nm)(ε, M^{-1} cm^{-1})): 564 (98), 405 (110)

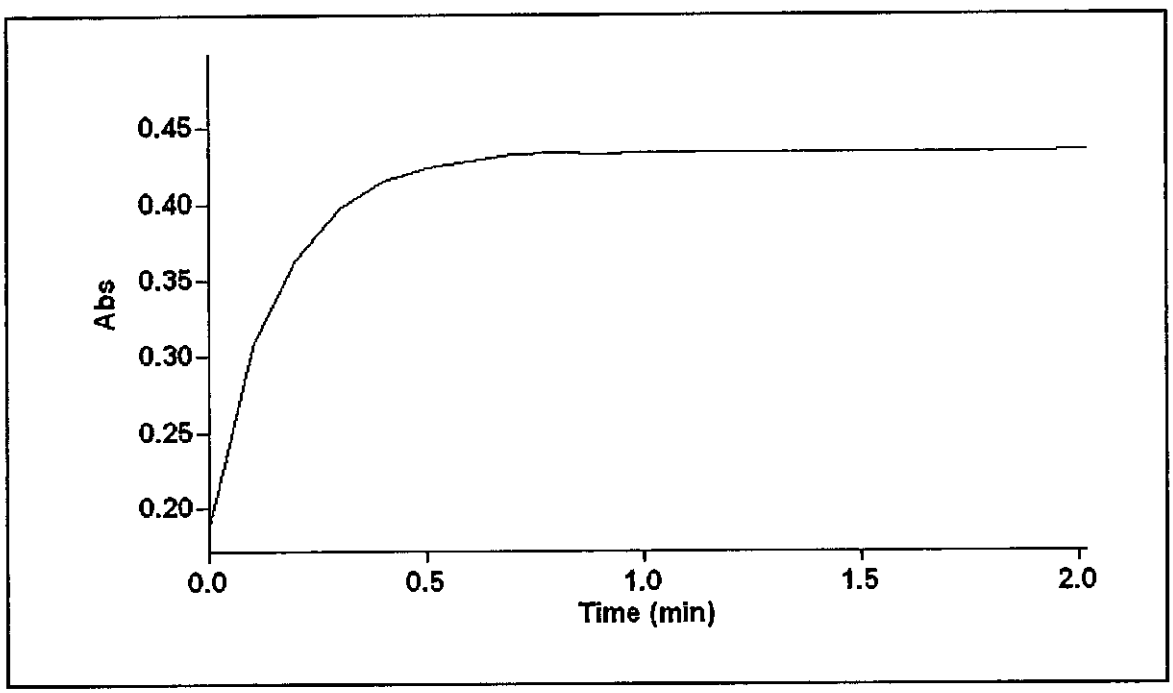

Figure 3.1: Absorbance *vs.* time spectrum for the reaction between $Cs[Cr(\eta^3\text{-ada})_2]\cdot 2H_2O$ (5.0×10^{-3} M) and H^+ (1 M), μ = 0.05M ($NaClO_4$), λ = 405 nm at 25°C.

3.3.3 Isolation of H_2ada (IIIa)

$Cs[Cr(\eta^3\text{-ada})_2]\cdot 2H_2O$ (0.5 g) was dissolved in water (30 cm^3) and the pH was adjusted to 0.8 with concentrated HCl. The reaction mixture was stirred for 5 minutes at 25 °C. The solution was allowed to stand for several days. After 3 days white crystals suitable for X-ray crystallography (discussed in Chapter 4) were obtained.

Yield: 0.1760 g (84 %).
IR (υ-$_{COOH}$(cm^{-1})): 1696.8 (s)
IR ($\delta(NH_2)$ of (cm^{-1})): 1676.0 (sh)

3.3.4 Isolation of $[Cr(H_2O)_6]Cl_3$ (Va)

$Cs[Cr(\eta^3\text{-ada})_2]\cdot 2H_2O$ (2 g) was dissolved in H_2O (100 cm^3) and the pH of the solution was adjusted to 0.8 by the addition of HCl (1M). The solution was allowed to stand for three days after which white crystals were separated from the solution by filtration. The resulting violet solution was divided in two parts and treated as follows, Part 1: The water was removed under reduced pressure. The precipitate was dried in a vacuum desiccator in the presence of P_2O_5. IR spectra was obtained from this violet precipitate. Part 2: The UV/VIS spectra was obtained for this solution.

IR (υ-$_{Cr\text{-}OH_2}$ (cm^{-1})): 550.8 (w)
IR (υ-$_{O\text{-}H}$ (cm^{-1})): 3440.1 (w)
IR ($\delta(H_2O)$ (cm^{-1})): 1620.2 (w)
UV/VIS (λ_{max} (nm)(ε, M^{-1} cm^{-1})): 407.0 (30), 574.0 (26)

3.3.5 Isolation of $[Cr(\eta^3\text{-ada})(\eta^2\text{-Hada})(SCN)]^-$ (IV)

$Cs[Cr(\eta^3\text{-ada})_2]\cdot 2H_2O$ (0.5 g) was dissolved in water (30 cm^3) and the pH was adjusted to 0.8 (HCl , 1.0 M). The reaction mixture was allowed to react at 25 °C for 2 minutes (see **Figure 3.1**). Ethanol (75 cm^3) was added to the mixture until precipitation occurred. The precipitate was dissolved in water (30 cm^3) and an aqueous (20 cm^3) solution containing KSCN (0.1127 g) was added dropwise. The reaction mixture was allowed to react at 25°C for 10 minutes (until the completion of the reaction (see k_2 step in **Scheme 3.1** and **Figure 3.2**). The solvent was removed under reduced pressure at 40°C. The solid was dried under vacuum in a desiccator in the presence of P_2O_5.

IR (υ-COO^-(cm^{-1})): 1597.2 (s)
IR (υ-COO^-(cm^{-1})): 1734.8 (s)
IR (υ-CN(cm^{-1})): 2082.9 (s)
IR (δ(NH_2 (cm^{-1})): 1671.3 (s)
UV/VIS (λ_{max} (nm)(ε, M^{-1} cm^{-1})): 295 (268)

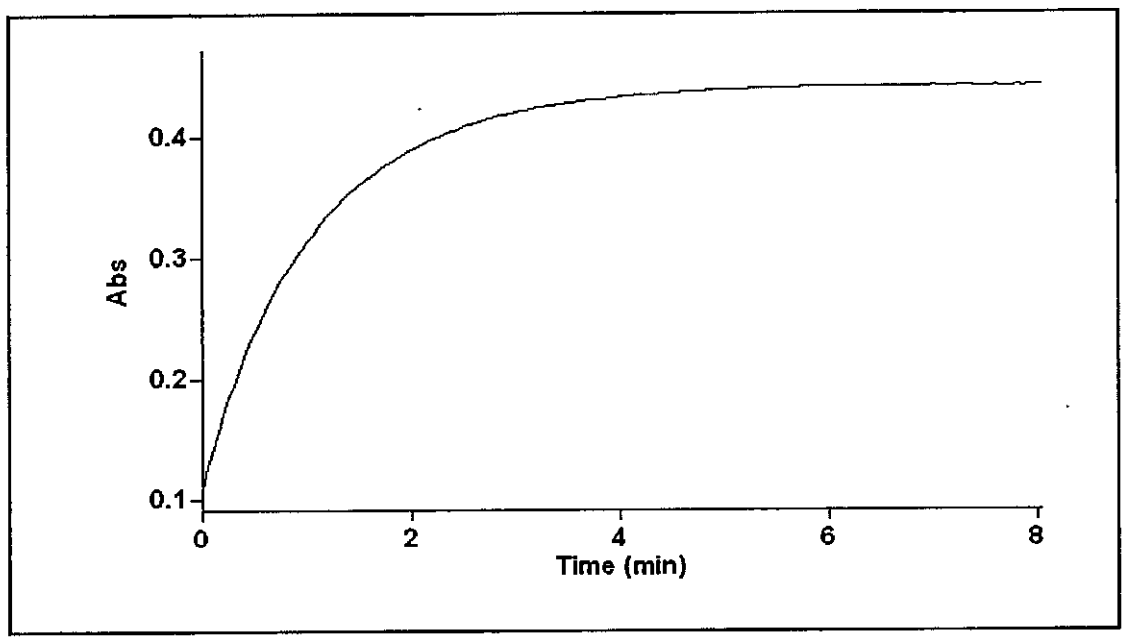

Figure 3.2: Reaction between $[Cr(\eta^3\text{-ada})(\eta^2\text{-Hada})(H_2O)]$ and NCS^- (5.0×10^{-2} M) at pH = 0.8. $Cs[Cr(\eta^3\text{-ada})_2]\cdot 2H_2O$ = (5.0×10^{-4} M) , μ = 0.05M ($NaClO_4$), λ = 295 nm at 25°C.

3.3.6 Isolation of H_2ada (IIIb)

$Cs[Cr(\eta^3\text{-ada})_2]\cdot 2H_2O$ (0.5 g) was dissolved in water (30 cm^3) and the pH was adjusted to 0.8 (HCl , 1.0 M). The reaction mixture was allowed to react at 25 °C for 2 minutes (to allow completion of reaction, see **Figure 3.1**). Ethanol (75 cm^3) was added to the mixture until precipitation occurred. The precipitate was dissolved in water (30 cm^3) and an aqueous solution (20 cm^3) containing KSCN (0.1127 g) was added dropwise. The solution was allowed to stand and after 3 days white crystals were isolated.

Yield: 0.1420 g (67.78 %).
IR (υ-$_{COOH}$(cm^{-1})): 1696.8 (s)
IR ($\delta(NH_2)$ (cm^{-1})): 1676.0 (sh)

3.3.7 Isolation of KSCN

$Cs[Cr(\eta^3\text{-ada})_2]\cdot 2H_2O$ (0.5 g) was dissolved in water (30 cm^3) and the pH was adjusted to 0.8 (HCl , 1.0 M). The reaction mixture was allowed to react at 25 °C for 2 minutes (to allow completion of reaction, see **Figure 3.1**). Ethanol (75 cm^3) was added to the mixture until precipitation occurred. The precipitate was dissolved in water (30 cm^3) and an aqueous solution (20 cm^3) containing KSCN (0.1127 g) was added dropwise. The solution was allowed to stand for three days after which H_2ada crystals were separated from the solution by filtration. The solution was allowed to stand for another 24 hours, after which a white precipitate was isolated.

Yield: 0.0794 g (70.5 %)
IR (υ-$_{CN}$(cm^{-1})): 2068.1 (s)

3.3.8 Isolation of $[Cr(H_2O)_6]Cl_3$ (Vb)

$Cs[Cr(\eta^3\text{-ada})_2]\cdot 2H_2O$ (0.5 g) was dissolved in water (30 cm^3) and the pH was adjusted to 0.8 (HCl , 1.0 M). The reaction mixture was allowed to react at 25 °C for 2 minutes (see **Figure 3.1**). Ethanol (75 cm^3) was added to the mixture until precipitation occurred. The precipitate was dissolved in water (30 cm^3) and an aqueous solution (20 cm^3) containing KSCN (0.1127 g) was added dropwise. The solution was allowed to stand for three days after which H_2ada crystals were separated from the solution by filtration. The solution was allowed to stand for another 24 hours, after which a white precipitate (KSCN) was removed by filtration. The remaining violet solution was divided in two parts and treated as follows, Part 1: The water was removed under reduced pressure. The precipitate was dried in a vacuum desiccator in the presence of P_2O_5. IR spectra was obtained from this violet precipitate. Part 2: The UV/VIS spectra was obtained for this solution.

IR ($\upsilon_{Cr\text{-}OH_2}$ (cm^{-1})): 547.2 (w)
IR ($\upsilon_{O\text{-}H}$ (cm^{-1})): 3402.7 (w)
IR ($\delta(H_2O)$ (cm^{-1})): 1619.2 (w)
UV/VIS (λ_{max} (nm)(ε, M^{-1} cm^{-1})): 406.0 (31), 573.0 (26)

3.4 Discussion of results

3.4.1 Characterisation of $Cs[Cr(\eta^3\text{-ada})_2]\cdot 2H_2O$ (I)

IR spectrum

The IR spectrum of $Cs[Cr(\eta^3\text{-ada})_2]\cdot 2H_2O$ (I) presents two strong vibrational frequencies at 1615.2 and 1685 cm^{-1} (see **Figure 3.3**). This IR spectrum differs substantially from the spectrum of the free acid, H_2ada, which had vibrational

frequencies of 1681 and 1700 cm^{-1} (Bugella-Altamirano *et al.*, 2000:2463). The value of 1615.2 cm^{-1} corresponds accurately to bonded COO^- groups (values between 1620 and 1650 cm^{-1}, Nakamoto (1963:206)) while the vibrational frequency at 1685.7 cm^{-1} can be assigned to $\delta(NH_2)$, a bending mode for the amido group. Nakamoto (1963:206) postulated values between 1700 and 1750 cm^{-1} for uncoordinated COO^- groups. It is clear from the results obtained for this complex that coordination of the COO^- to the metal ion substantially lower the υ(COOH). The value of 1685.7 cm^{-1} for $\delta(NH_2)$ of the metal complex corresponds closely to the 1681 cm^{-1} that was obtained for the free H_2ada, suggesting uncoordinated $CONH_2$ groups in the complex. The slight variation in vibrational frequency can be attributed to a slight change in chemical environment.

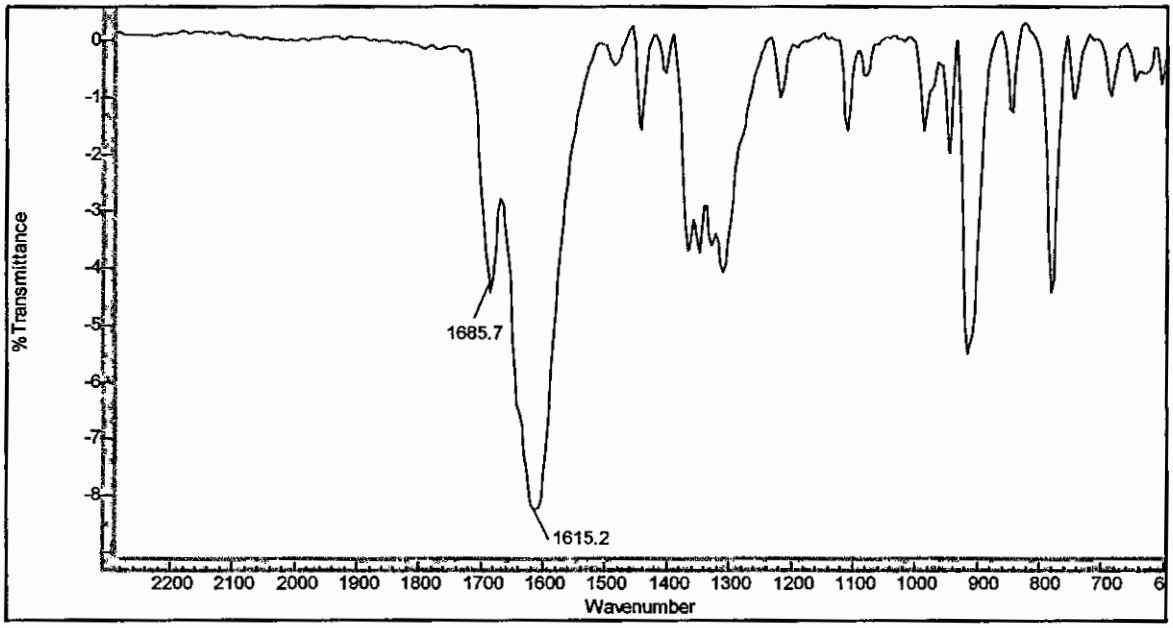

Figure 3.3: IR spectrum of $Cs[Cr(\eta^3\text{-ada})_2]\cdot 2H_2O$ (I).

The relatively close proximity of the vibrational frequencies for $\upsilon(COO^-)$ and the $\delta(NH_2)$ does cause some problems in the correct assignment of these values to the different groups. Previous workers observed the overlapping of $\upsilon(COO^-)$ and the $\delta(NH_2)$ in the 1600-1700 cm^{-1} region and) for the $[Ni(\eta^4\text{-ada})(H_2O)_2]$ (1603 and 1587cm^{-1}) (Bugella-Altamirano *et al.*, 2000:2463) and

$[M(\eta^4\text{-ada})(ImH)(H_2O)]\cdot 1.5H_2O$ (M = Co/Ni) (Bugella-Altamirano *et al.*, 2000:2473) complexes (1610 cm^{-1} for both vibrational frequencies) in which ada^{2-} acted as a tetradentate ligand (see **Table 3.1**).

3.4.2 Characterisation of $[Cr(\eta^3\text{-ada})(\eta^2\text{-Hada})(H_2O)]$ (II)

IR spectrum

The IR spectrum of $[Cr(\eta^3\text{-ada})(\eta^2\text{-Hada})(H_2O)]$ (**Figure 3.4**) showed three vibrational frequencies at 1602.9, 1677.9 and 1733.4 cm^{-1}. The stretching frequency at 1607.2 cm^{-1} correlates well with the stretching frequency of 1615.0 cm^{-1} that was obtained for $Cs[Cr(\eta^3\text{-ada})_2]\cdot 2H_2O$ (I) (**Figure 3.3**) which indicated the presence of coordinated COO^- groups in the metal complex. The vibrational frequency at 1671.2 cm^{-1} is also similar to the vibrational frequency observed for $\delta(NH_2)$ in $Cs[Cr(\eta^3\text{-ada})_2]\cdot 2H_2O$ (**Figure 3.3**) and H_2ada at 1681 cm^{-1} and 1676 cm^{-1} respectively indicating that the glycinamido group is still uncoordinated in this complex. The stretching frequency of importance is the one at 1733.4 cm^{-1} which points to uncoordinated COO^- group/s according to Nakamoto (1963:206).

According to Best *et al.* (1980:1958) a stretching frequency at *ca* 555 cm^{-1} indicates an aqua ligand coordinated to a chromium(III) centre in $[Cr(H_2O)_6]Cl_3$. The IR spectrum for $[Cr(\eta^3\text{-ada})(\eta^2\text{-Hada})(H_2O)]$ (**Figure 3.4**) presents a stretching frequency at 546.9 cm^{-1}, suggesting the presence of at least one aqua ligand in the coordination sphere. The vibrational frequency at 1602.9 cm^{-1} is a broad peak, which means that the presence of 1620 cm^{-1}, which corresponds to the H-O-H wagging mode (Nakamoto, 1963:166), can not be seen.

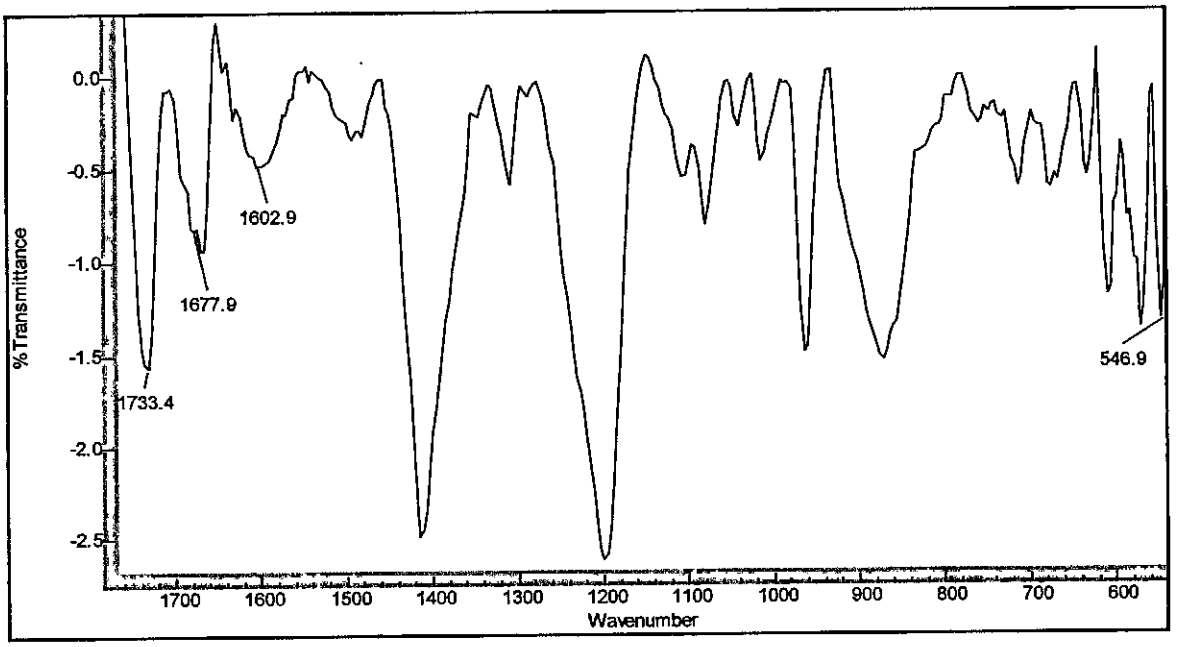

Figure 3.4: IR spectrum of $[Cr(\eta^3\text{-ada})(\eta^2\text{-Hada})(H_2O)]$

UV/VIS spectra

The UV/VIS spectrum for $[Cr(\eta^3\text{-ada})(\eta^2\text{-Hada})(H_2O)]$ in H_2O (see (B) in **Figure 3.5**) has absorption maxima at 405 and 564 nm. These values are significantly different from the values for $[Cr(\eta^3\text{-ada})_2]^-$ see (A) in **Figure 3.5**) (355 and 501 nm). This shift in spectrum is accompanied with a drastic increase in absorbance.

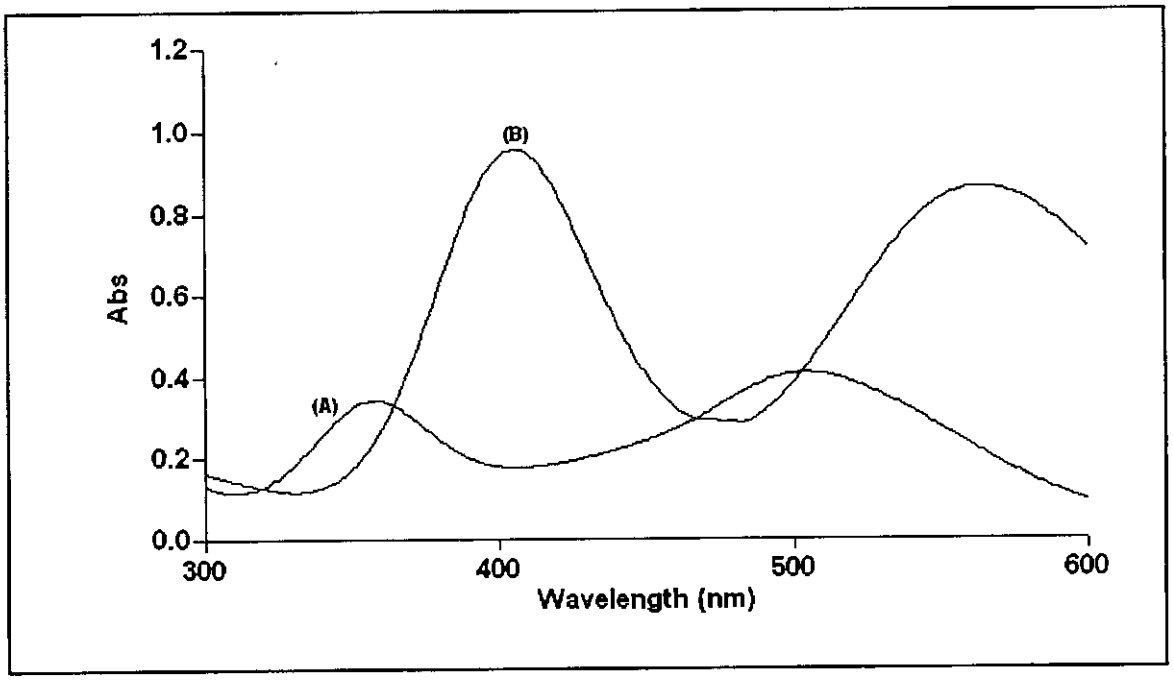

Figure 3.5: UV/VIS spectrum of a solution of $[Cr(\eta^3\text{-ada})_2]^-$ (A) (5.0 x 10^{-3} M), pH = 6 and a solution of $[Cr(\eta^3\text{-ada})(\eta^2\text{-Hada})(H_2O)]$ (B) (5.0 x 10^{-3} M), pH = 0.8. T = 25°C.

3.4.3 Characterisation of H_2ada (IIIa) and (IIIb)

IR spectra

The IR spectra of the products (IIIa and IIIb) (**Figure 3.6** and **Figure 3.7**) were almost identical to the IR spectrum of the free acid, H_2ada, that is of reagent grade and was bought from Sigma. The values obtained from the IR spectrum for (IIIa) (1696.8 and 1676.0 cm^{-1}) as well as (IIIb) (1696.4 and 1675.5 cm^{-1}) also compares very well to the vibrational frequencies obtained by Bugella-Altamirano *et al.* (2000:2463) for the free acid, H_2ada. As mentioned earlier these values were assigned to $\delta(NH_2)$ and υ(COOH) respectively.

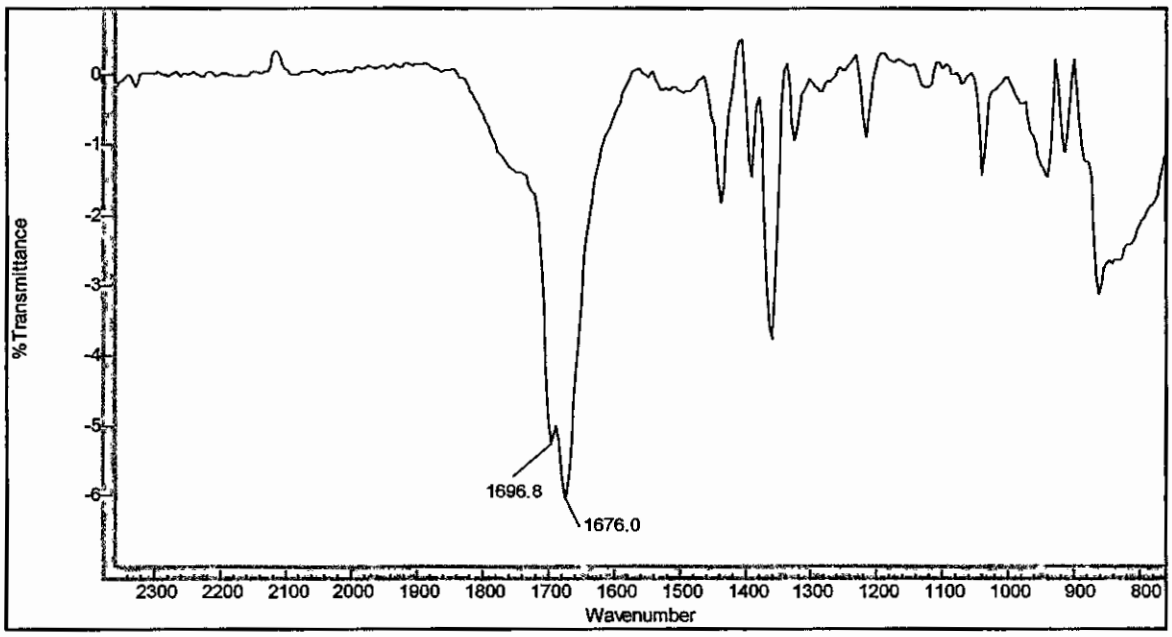

Figure 3.6: IR spectrum of H_2ada (IIIa).

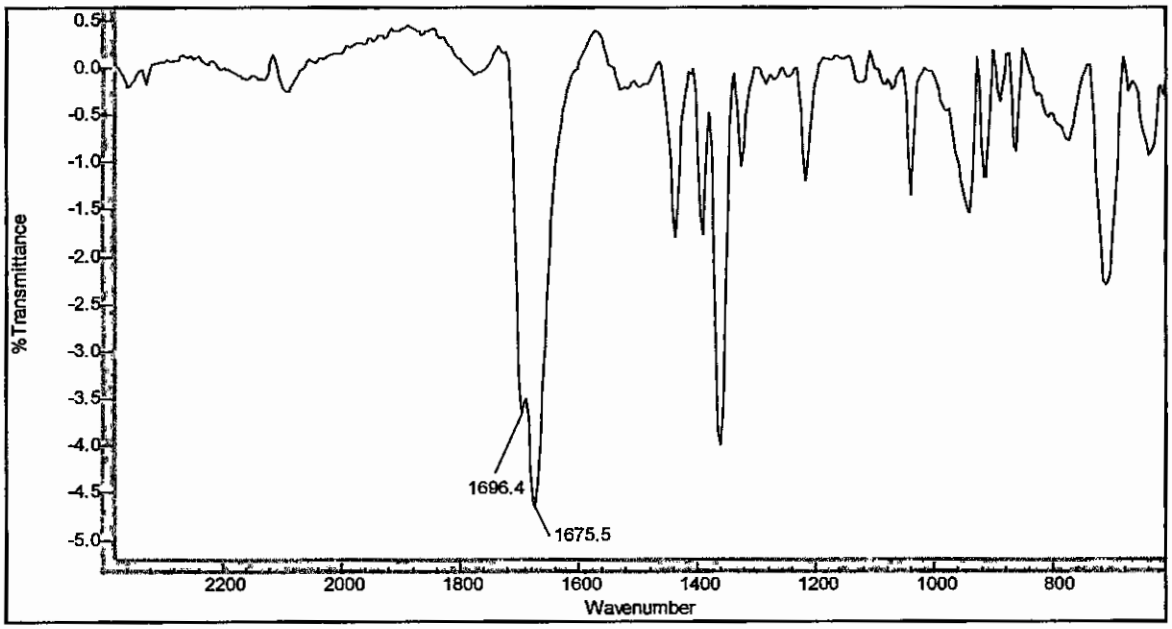

Figure 3.7: IR spectrum of H_2ada (IIIb).

3.4.4 Characterisation of $[Cr(H_2O)_6]Cl_3$ (Va) and (Vb)

IR spectrum

The IR spectrum for $[Cr(H_2O)_6]Cl_3$ (Va and Vb) revealed three weak vibrational frequencies 550.8, 1620.2 and 3440.1 cm^{-1} for (Va) (see **Figure 3.8**) and 547.2, 1619.2 and 3402.7 cm-1 for (Vb) (see **Figure 3.9**). These peak values are not particularly strong and this is due to the fact that the chromium(III) centre is surrounded by aqua ligands, which do not give rise to strong vibrational frequency peaks.

As mentioned previously the characteristic stretching frequency for a Cr(III)-aqua bond for $[Cr(H_2O)_6]Cl_3$ is *ca* 555 cm^{-1} (Best *et al.*, 1980:1958). According to Nakamoto (1963:166) the vibrational frequency for coordinated water is between 1600 and 1630 for the wagging mode of H_2O and a stretching frequency between 3200 and 3200 for the O-H bond. The vibrational frequencies of 550.8, 1620.2 and 3440.1 cm^{-1} for (Va) (see **Figure 3.8**) and 547.2, 1619.2 and 3402.7 cm^{-1} for (Vb) (see **Figure 3.9**) corresponds well with the above mentioned values. The fact that the vibrational frequencies which correspond to coordinated ada^{2-} (as described in Paragraph 3.3.1 are absent from the IR spectrum indicates that both ada^{2-} ligands (from the Cr(III)-ada complexes) dissociated from the metal ion over a long period (3 days) in acidic conditions (pH = 0.8).

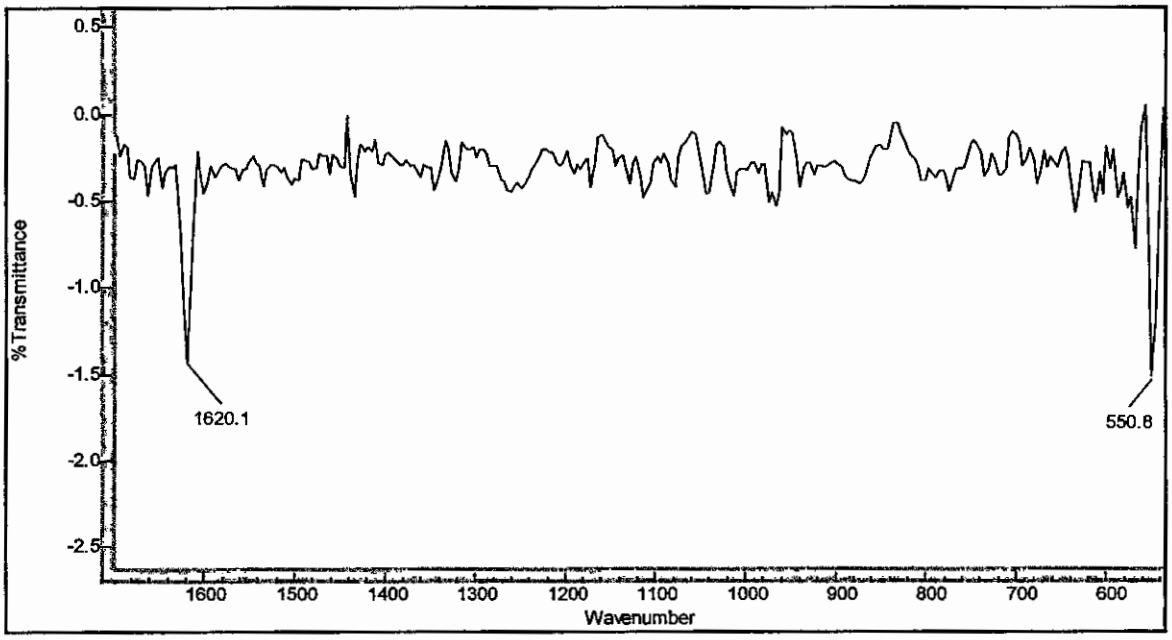

Figure 3.8: IR spectrum of $[Cr(H_2O)_6]^{3+}$(Va).

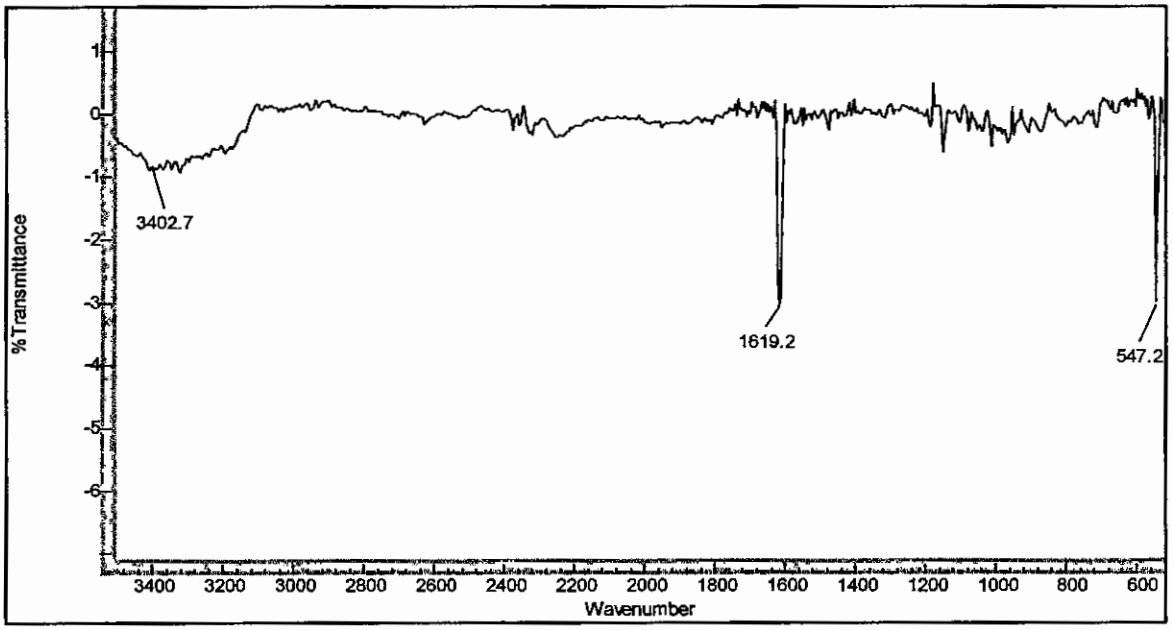

Figure 3.9: IR spectrum of $[Cr(H_2O)_6]^{3+}$(Vb).

UV/VIS spectra

The UV/VIS spectra for $[Cr(H_2O)_6]^{3+}$ (Va and Vb) (**Figure 3.10**) (Paragraph 3.3.4 and 3.3.8) shows absorption maxima at 407.0 and 574 nm for (Va) (see (1) in **Figure 3.10**) and 406 and 573 nm for (Vb) (see (2) in **Figure 3.10**). This

compares well with the spectrum of $[Cr(H_2O)_6]^{3+}$ (Barbier *et al.*, 1972:204) namely 407.0 and 573.0 nm. The UV/VIS spectrum for $[Cr(H_2O)_6]Cl_3$ in aqueous solution as prepared by the procedure described by Barbier *et al.* (1972:204) is represented in **Figure 3.10**, see (3). These values suggest the presence of aqua ligands in the primary coordination sphere of the metal ion.

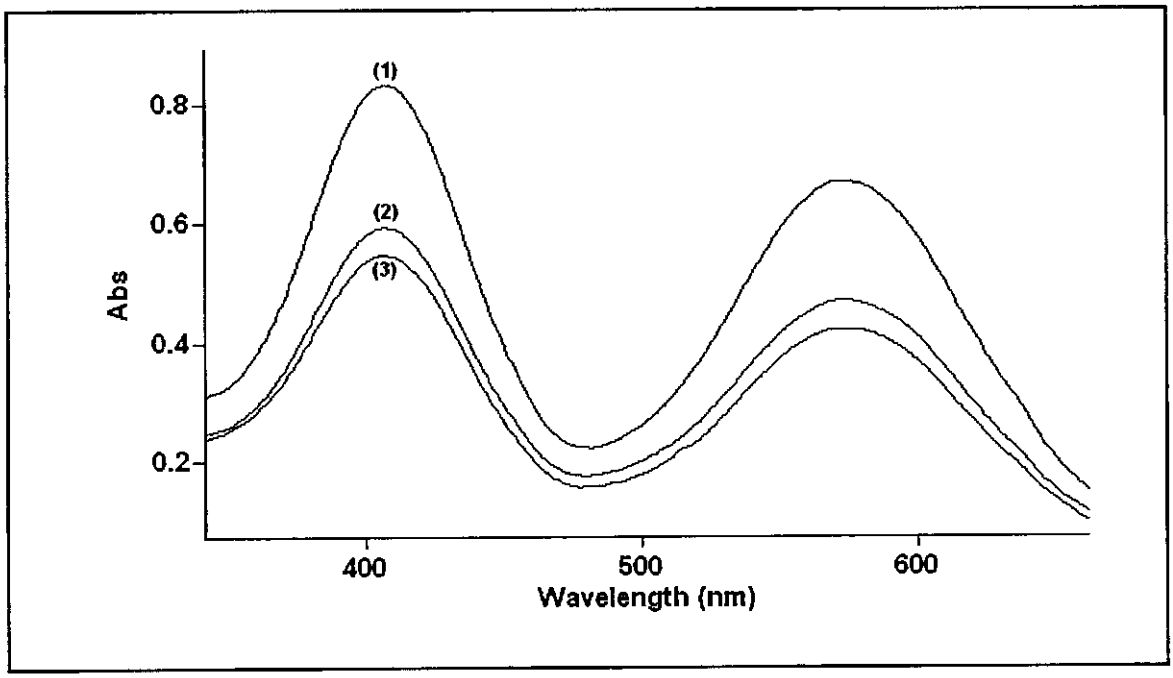

Figure 3.10: UV/VIS spectrum of $[Cr(H_2O)_6]^{3+}$ (Va (0.03 M) (1) and Vb (0.02 M) (2)) and $[Cr(H_2O)_6]^{3+}$ (0.019M) (prepared in the laboratory (3), T = 25°C.
(1) = $[Cr(H_2O)_6]^{3+}$ Va (pH = 0.8).
(2) = $[Cr(H_2O)_6]^{3+}$ Vb (pH = 0.8).
(3) = $[Cr(H_2O)_6]^{3+}$ prepared in the laboratory (pH = 0.8).

3.4.5 Characterisation of $[Cr(\eta^3\text{-ada})(\eta^2\text{-Hada})(SCN)]^-$ (IV)

IR spectrum

The IR spectra obtained for this complex also gives a good indication of the coordination environment of the Cr(III) centre. The vibrational frequencies at 1609.4, 1671.1 and 1732.9 cm^{-1} correspond to the presence of coordinated COO^- groups, to an uncoordinated amido groups and the presence of an

uncoordinated COO^- group respectively. The stretching frequency at 2082.1 cm^{-1} (**Figure 3.11**) correlates well with the stretching frequency of 2082.0 cm^{-1} that was assigned to υ(CN) for the $[Cr(NCS)_3py_3]$ complex, reported by DasSarma *et al.* (1979:3618). The absence of a peak at *ca* 555 cm^{-1}, which was assigned to a metal coordinated aqua ligand, indicates that the aqua ligand was substituted by the NCS^- ligand (see **Figure 3.12**).

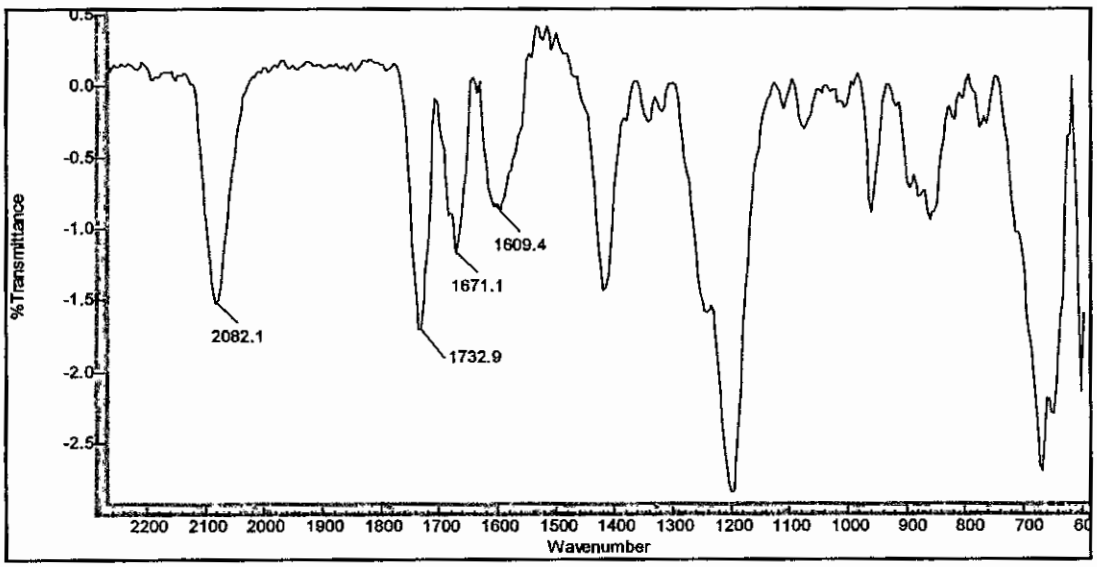

Figure 3.11: IR spectrum of $[Cr(\eta^3\text{-ada})(\eta^2\text{-Hada})(SCN)]^-$ (2260 – 600 cm^{-1}).

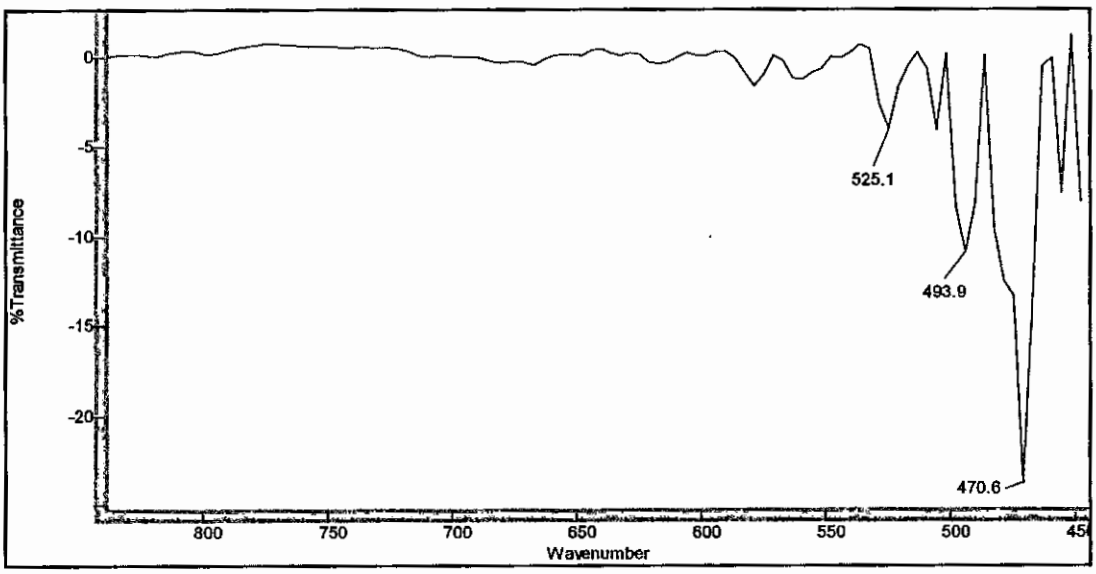

Figure 3.12: IR spectrum of $[Cr(\eta^3\text{-ada})(\eta^2\text{-Hada})(SCN)]^-$ (880 - 450 cm^{-1}).

UV/VIS spectra

The UV/VIS spectral change of a solution of $[Cr(\eta^3\text{-ada})(\eta^2\text{-Hada})(H_2O)]$ (pH = 0.8) upon the addition of SCN^- (0.1 M, pH 0.85) was recorded (**Figure 3.13**). The spectrum shows an increase in absorption with a peak formation at 295 nm. The kinetics of this reaction is discussed in Chapter 5.

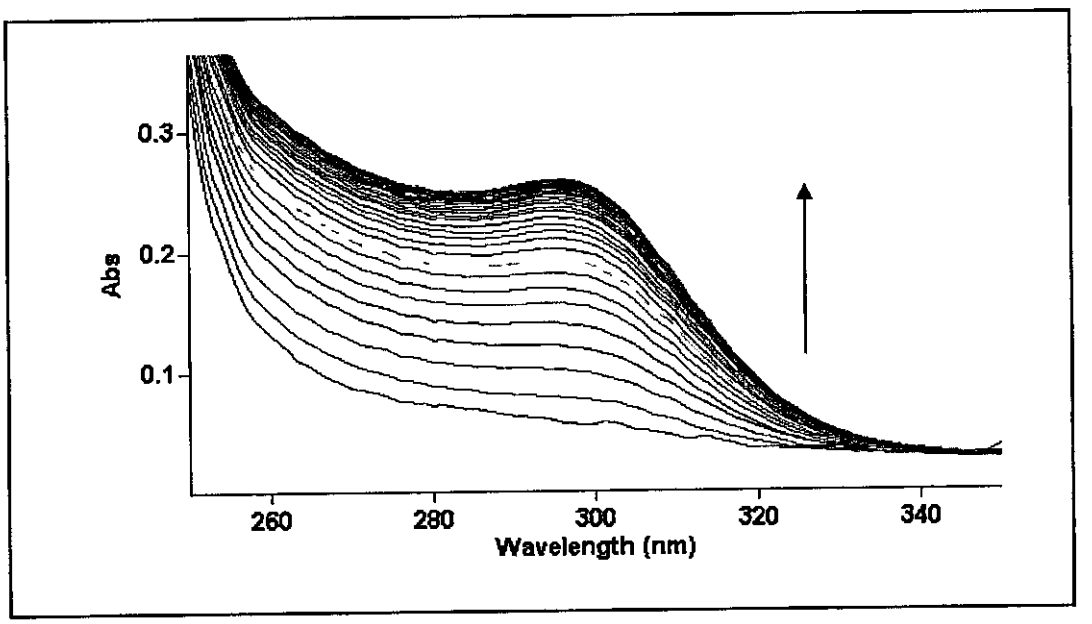

Figure 3.13: UV/VIS spectral change upon addition of a solution of NCS^- (pH = 0.8) to a solution of $Cs[Cr(\eta^3\text{-ada})_2]\cdot 2H_2O$ (5.0×10^{-4} M) (pH = 0.85). T = 25°C, $[NCS^-] = 5.0 \times 10^{-2}$M.

3.4.6 Characterisation of KSCN (VI)

IR spectra

The IR spectrum of the white product/crystals that was isolated from the purple solution after several days, showed a very strong stretching frequency at 2068.3 cm^{-1}. It corresponds very well with the value that was obtained in the laboratory using reagent grade KSCN (2067.6 cm^{-1}) as well as to the value of 2053 cm^{-1} according Nakamoto, (1963:188). The difference between the stretching frequency of the free NCS^- ion and that of the value obtained for the

$[Cr(\eta^3\text{-ada})(\eta^2\text{-Hada})(SCN)]^-$ complex clearly suggest the bonding of the ligand to the metal centre.

3.5 pH dependence of $Cs[Cr(\eta^3\text{-ada})_2]\cdot 2H_2O$ – UV/VIS spectral studies

A detailed pH study was undertaken in order to investigate all the possible complexes that formed in solution. $Cs[Cr(\eta^3\text{-ada})_2]\cdot 2H_2O$ crystals were dissolved in water (pH *ca.* 6) and the UV/VIS spectrum was recorded which showed peaks at 355.0 and 501 nm. No spectral change was observed over a time of 48 hours, confirming that this complex is stable at pH *ca* 6.

In a second experiment the $Cs[Cr(\eta^3\text{-ada})_2]\cdot 2H_2O$ crystals (see Paragraph 3.3.1 for synthesis) were dissolved (pH *ca.* 6) in H_2O after which HCl (1 M) was added to the solution (pH 0.3). The spectral change for this reaction was recorded (**Figure 3.14** and **Figure 3.1**). The addition of HCl resulted in a shift of the absorption maxima of 355.0 and 501 nm to 405.0 and 564 nm respectively with a large increase in absorption in both cases. Three isosbestic points were also observed at 366.2, 464.5 and 510 nm respectively.

A second, slower reaction was also observed upon the addition of H^+ to a solution containing $Cs[Cr(\eta^3\text{-ada})_2]\cdot 2H_2O$ where the absorption bands at 405.0 and 566.0 nm slowly decreased (*ca* 24 hours). The solution was allowed to stand for three days (pH = 0.8) after which a white precipitate was filtered off. The pH of the violet filtrate was adjusted to approximately pH = 6, resulting in the immediate formation of an insoluble green precipitate which did not allow for a UV/VIS spectrum determination. The IR spectrum obtained from this precipitate gave vibrational frequencies at 551.2 and 3502.3 cm^{-1}, indicating the presence of possible Cr(III)-OH and O-H bonds respectively. The disappearance of the

1620 cm^{-1} vibrational frequency points to the presence of coordinated hydroxide groups and not aqua ligands according to Nakamoto (1963:168).

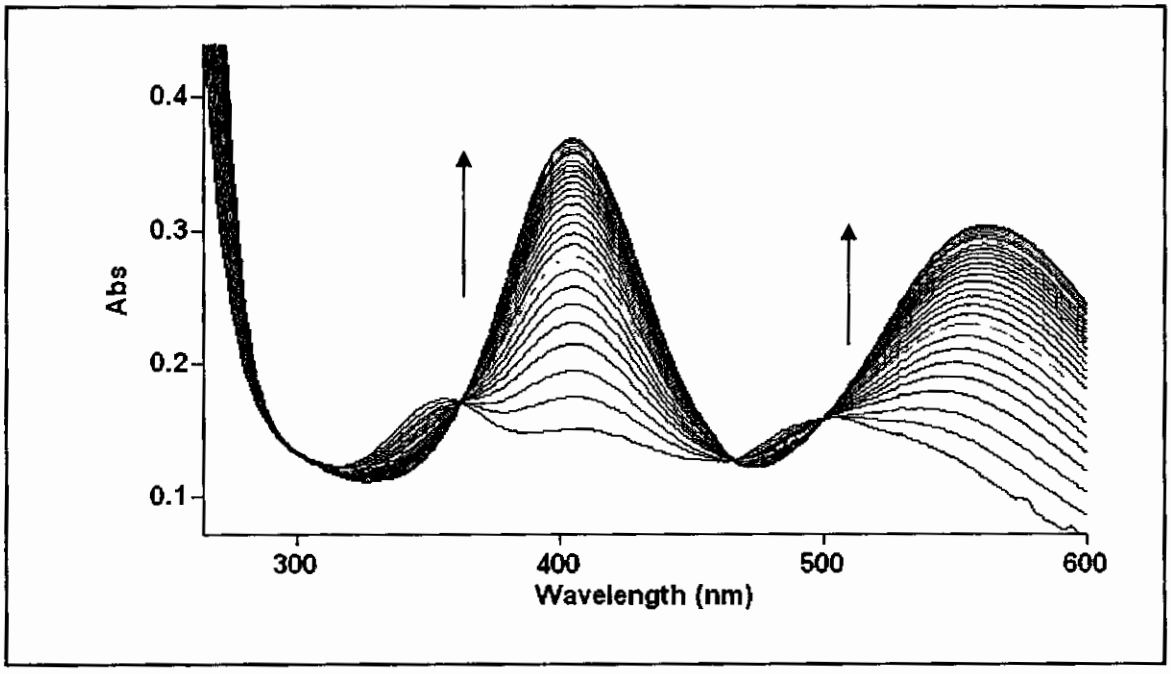

Figure 3.14: Spectral change of $Cs[Cr(\eta^3\text{-ada})_2]\cdot 2H_2O$ (5.0×10^{-3} M) upon the addition of HCl (1 M) with scans recorded every 30 seconds at 10°C (final pH = 0.3).

Crystals of $Cs[Cr(\eta^3\text{-ada})_2]\cdot 2H_2O$ were again dissolved in water (pH = 6, T = 5°C) and the spectrum was recorded (see (1) in **Figure 3.15**). The pH of this solution was adjusted to 0.8 (HCl, 1.0 M) and the spectrum was immediately recorded (see (2) in **Figure 3.15**). The pH of the solution for (2) was re-adjusted to pH ~ 6 (see (3) in **Figure 3.15**) (KOH, 1M) as soon as possible after the spectrum of (2) was recorded in order to prevent the reaction of $[Cr(\eta^3\text{-ada})_2]^-$ with H^+ (see **Figure 3.13**) from proceeding too far. The temperature of the solution was maintained at 5°C in order to try to suppress the reaction just mentioned.

It can be seen from **Figure 3.15** that there seems to be an acid association equilibrium present as depicted in **Scheme 3.1** and **Scheme 3.2**. The fact that the spectrum (1) was not totally re-obtained after re-adjusting the pH of (2) could be ascribed to dilution effects and the fact that the reaction with H^+ could not be

suppressed as a whole. The small difference in absorption between (1) and (2) makes an accurate determination of the equilibrium constant impossible, see Chapter 5.

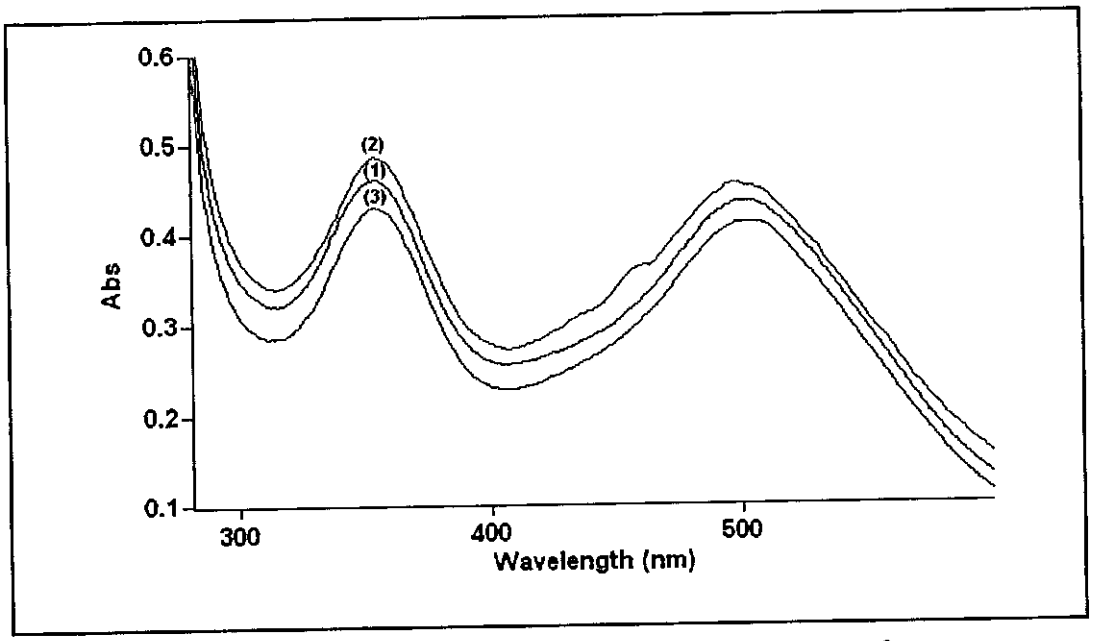

Figure 3.15: pH adjustment of $[Cr(\eta^3\text{-ada})_2]^-$, $Cs[Cr(\eta^3\text{-ada})_2]\cdot 2H_2O$ (7.0×10^{-3}M). T = 5°C, total time = 60 seconds.

(1) = $[Cr(\eta^3\text{-ada})_2]^-$ solution (pH = 6)

(2) = $[Cr(\eta^3\text{-ada})(\eta^3\text{-Hada})]$ solution (pH = 0.78)

(3) = $[Cr(\eta^3\text{-ada})_2]^-$ solution (pH = 6), after pH re-adjustment of (2)

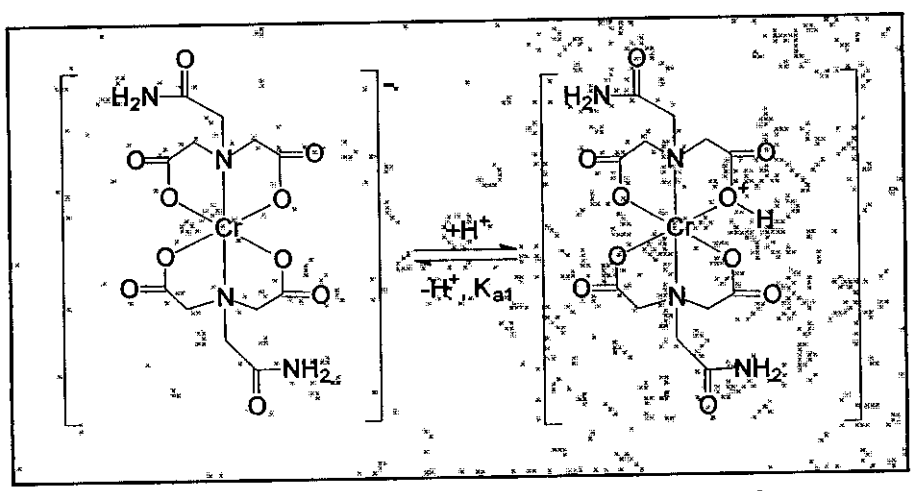

Scheme 3.2: Proposed acid dissociation reaction for $[Cr(\eta^3\text{-ada})_2]^-$.

During the next experiment, $Cs[Cr(\eta^3\text{-ada})_2]\cdot 2H_2O$ crystals were dissolved (pH *ca.* 6) (see (1) in **Figure 3.16**) and the pH was adjusted to approximately 0.8 (see (2) in **Figure 3.16**). The solution was allowed to stand for 2-3 minutes (see (2) in **Figure 3.16**) after which the pH was adjusted to 5.9 (KOH, 1 M) and the spectrum was recorded after 48 hours (see (3) in **Figure 3.16**). This evidence indicates that the starting product is re-obtained after 48 hours, thereby providing further evidence of the existence of $[Cr(\eta^3\text{-ada})(\eta^2\text{-Hada})(H_2O)]$ which forms the starting complex (see (I) in **Scheme 3.1**) after adjusting the pH to 6.

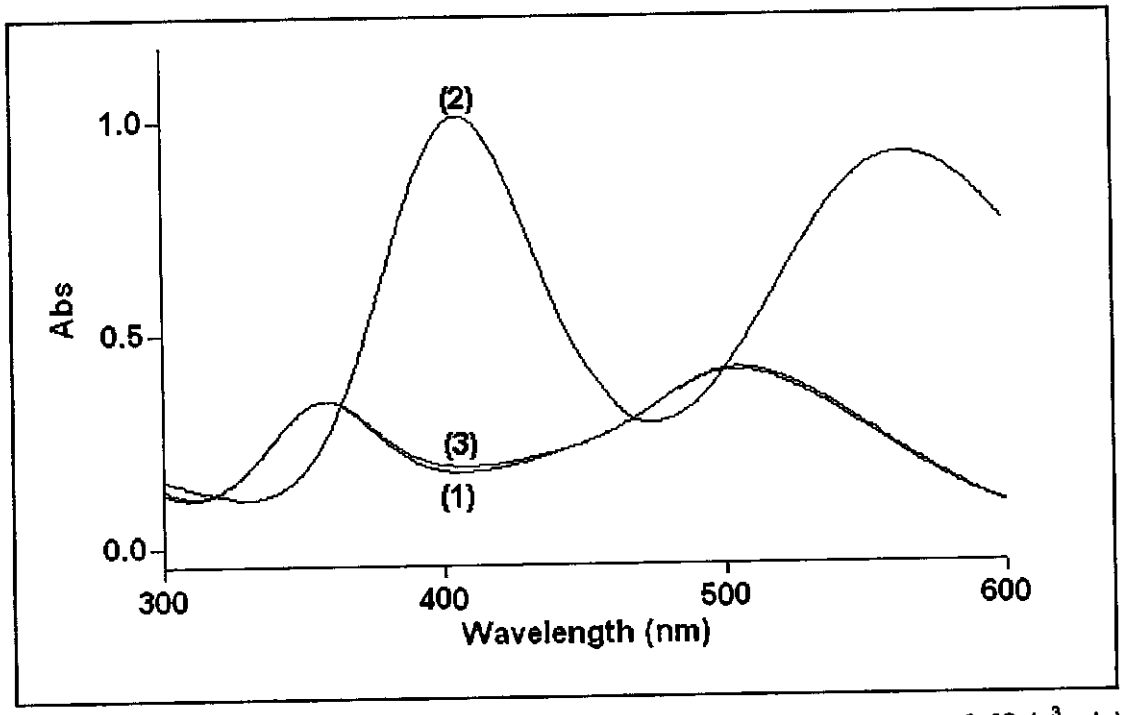

Figure 3.16: UV/VIS spectrum of the reversible reaction of a solution of $[Cr(\eta^3\text{-ada})_2]^-$ (5.0×10^{-3} M) upon pH variation. T = 25°C.
(1) = $[Cr(\eta^3\text{-ada})_2]^-$ (5.0×10^{-3} M) (pH = 6.0).
(2) = $[Cr(\eta^3\text{-ada})_2]^-$ (5.0×10^{-3} M) (pH = 0.8) after 2-3 minutes.
(3) = $[Cr(\eta^3\text{-ada})_2]^-$ (5.0×10^{-3} M) (pH = 5.9) after 48 hours.

During the next experiment the UV/VIS spectrum was obtained for a solution containing $[Cr(\eta^3\text{-ada})_2]^-$ (pH = 6) (see (1) in **Figure 3.17**). The pH of the solution was adjusted to 0.8 (HCl, 1M) and left to stand for 2-3 minutes and the spectrum was recorded (see (2) in **Figure 3.17**). This allowed for the completion of the

reaction between $[Cr(\eta^3\text{-ada})_2]^-$ and H^+ ions (k_1 step in **Scheme 3.1**). Another spectrum of the solution in (2) was recorded after 24 hours (see (3) in **Figure 3.17**) and again after 3 days (see (4) in **Figure 3.17**).

The absorption maxima of (2) in **Figure 3.17** were recorded as 405 and 564 nm. This corresponds to the spectra of the partial dechelation for one of the ada^{2-} ligands, Paragraph 3.4.2. The spectrum of (4) in **Figure 3.17** corresponds to the presence of $[Cr(H_2O)_6]^{3+}$, see Paragraph 3.4.4. This data supports the mechanism proposed in **Scheme 3.1**. It seems as if an acid dissociation equilibrium exists for $[Cr(\eta^3\text{-ada})_2]^-$ (K_{a1}) and that the protonated species undergoes a fast reaction at low pH. This is followed by the eventual complete dissociation of the two ada^{2-} ligands from the Cr(III) centre – slow reaction/s (2) to (4) in **Figure 3.17**).

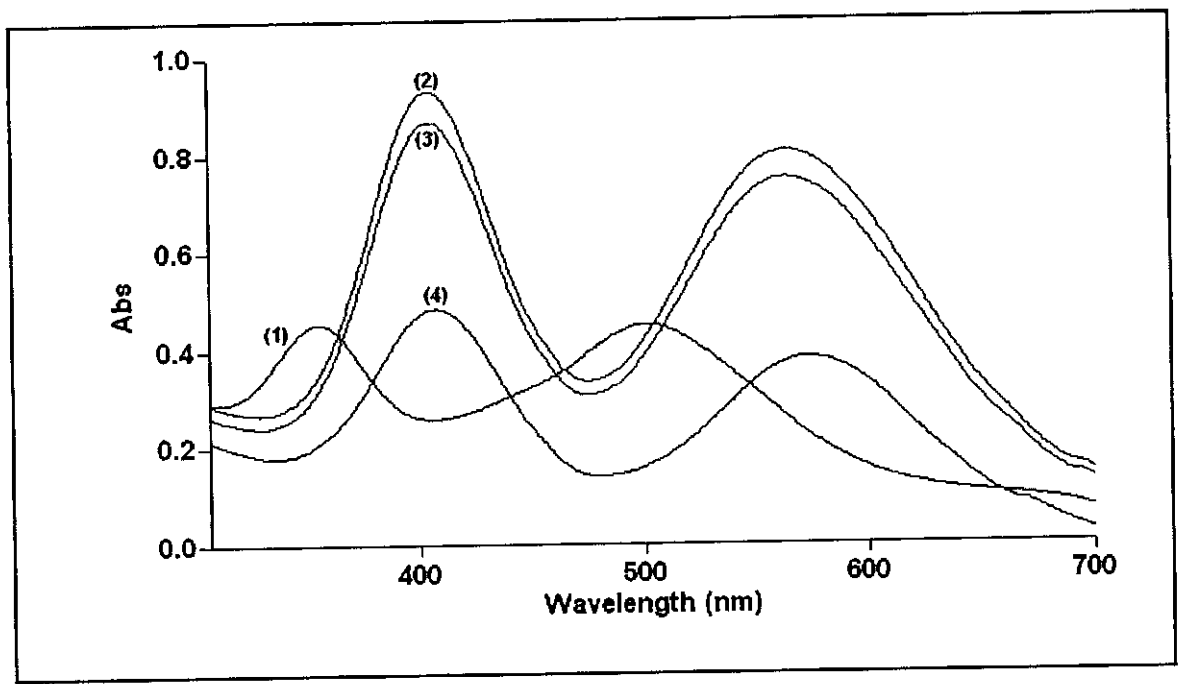

Figure 3.17: Spectral change upon acidification of a solution containing $[Cr(\eta^3\text{-ada})_2]^-$ (0.1M) at different time intervals.

(1) = $[Cr(\eta^3\text{-ada})_2]^-$ solution (pH = 6).

(2) = $[Cr(\eta^3\text{-ada})(\eta^2\text{-Hada})(H_2O)]$ solution (pH = 0.8).

(3) = $[Cr(\eta^3\text{-ada})(\eta^2\text{-Hada})(H_2O)]$ solution after 24 hours (pH = 0.8).

(4) = $[Cr(H_2O)_6]^{3+}$ solution (pH = 0.8).

3.6 Summary

The identification of the different Cr(III)-ada complexes as well as other compounds were made possible by the use of detailed IR and UV/VIS characterisation.

The use of UV/VIS spectra as characterisation proved to be helpful in the identification of the different species in solutions.

A summary of the different IR data of the different complexes is presented in **Table 3.1**. It can be seen from **Table 3.1** that the stretching frequencies of coordinated COO^- vary between 1603 and 1615 cm^{-1} and uncoordinated between 1700 and 1734 cm^{-1}. Values for $\delta(NH_2)$ range between 1587 and 1610 cm^{-1} for metal coordinated amido groups, while the values vary between 1671 and 1681 cm^{-1} for uncoordinated amido groups. It is clear from the values for $\delta(NH_2)$ that a rather large lowering of the vibrational frequency is observed when the amido group is coordinated to a metal centre in comparison to uncoordinated amido groups.

Table 3.1: Summary of the details of IR spectra of different-ada^{2-} complexes.

Compound	$\upsilon(COO^-)^a$ (cm^{-1})	$\upsilon(COOH)$ (cm^{-1})	$\delta(NH_2)$ (cm^{-1})	Reference
H_2ada	-	1700	1681	Bugella-Altamirano *et al.* (2000:2463)
$[Ni(\eta^4\text{-ada})(H_2O)_2]$	1603	-	1587	Bugella-Altamirano *et al.* (2000:2463)
$[Co(\eta^4\text{-ada})(Him)(H_2O]\cdot 1.5H_2O$	1610	-	1610	Bugella-Altamirano *et al.* (2000:2473)
$Cs[Cr(\eta^3\text{-ada})_2]\cdot 2H_2O$	1615	-	1681	This study
$[Cr(\eta^3\text{-ada})(\eta^2\text{-Hada})(H_2O)]$	1607	1734	1671	This study
$[Cr(\eta^3\text{-ada})(\eta^2\text{-Hada})(SCN)]^-$	1609	1732	1671	This study

[a] COO group coordinated to metal centre

4 X-ray crystallography

In this chapter...

This chapter focuses on the characterisation of the free acid, H_2ada and the new complex, $Cs[Cr(\eta^3\text{-ada})_2]\cdot 2H_2O$, by means of X-ray crystallography.

4.1 Introduction

There are very few examples of crystal structure determinations of metal-ada complexes available in the literature. The structural research of metal-ada chelates in solid state is a powerful identification method since it can provide information about the chelating role of the divalent anion $H_2NCOCH_2N(CH_2CO_2)^{2-}$ (ada^{2-}). It is of particular interest to investigate the way in which the primary amide of this anion could participate in metal ion chelation. All the structural determinations done on metal-ada complexes, except one, have shown ada^{2-} as a tripodal-tetradentate ligand (see Chapter 2). The exception to this is the study that was done on $[Ni(\eta^3\text{-ada})(bipy)(H_2O]\cdot 4H_2O$ (metal(II)-ion) which indicated a free N-(2-amidomethyl) group (Bugella-Altamirano *et al.*, 2000:727) resulting in a tridentately bonded ada^{2-} ligand. It is also of significance to note that no structural reports of metal(III)-ada complexes are available in the literature.

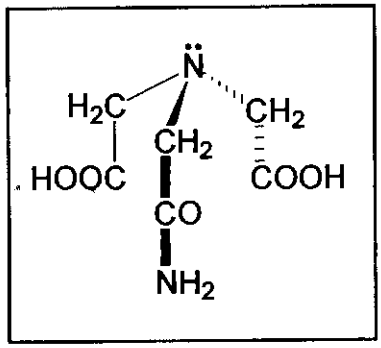

Figure 4.1: N-carbamoylmethyl-iminodiacetic acid (H_2ada).

The identification of starting complexes, intermediates and final products is vitally important for the determination of the reaction mechanism. The synthesis of $Cs[Cr(\eta^3\text{-ada})_2]\cdot 2H_2O$ and characterisation of the complex with IR and UV/VIS-spectroscopy were discussed in Chapter 3.

X-ray crystallography is an experimental technique that exploits the fact that X-rays are diffracted by crystals. X-rays have the proper wavelength (Å $\approx 1 \times 10^{-8}$ cm) to be scattered by the electron cloud of an atom of comparable size. Based on the diffraction pattern obtained from X-ray scattering off the periodic assembly of molecules or atoms in the crystal, the electron density and thus the atom arrangement within the crystal can be reconstructed. Additional phase information must be extracted either from the diffraction data or from supplementing diffraction experiments to complete the reconstruction of the molecule or crystal composition. A model is then progressively built into the experimental electron density, refined against the data and a very accurate molecular structure is obtained for the compound investigated.

This chapter deals mainly with the detailed crystal structure determination of H_2ada as the free ligand, which also turns out to be one of the final products of the kinetic study (see (III) in **Scheme 4.1**). The crystal structure determination of $Cs[Cr(\eta^3\text{-ada})_2]\cdot 2H_2O$ which was used as the starting complex for the kinetic study (see I in **Scheme 4.1**) is also discussed in this chapter.

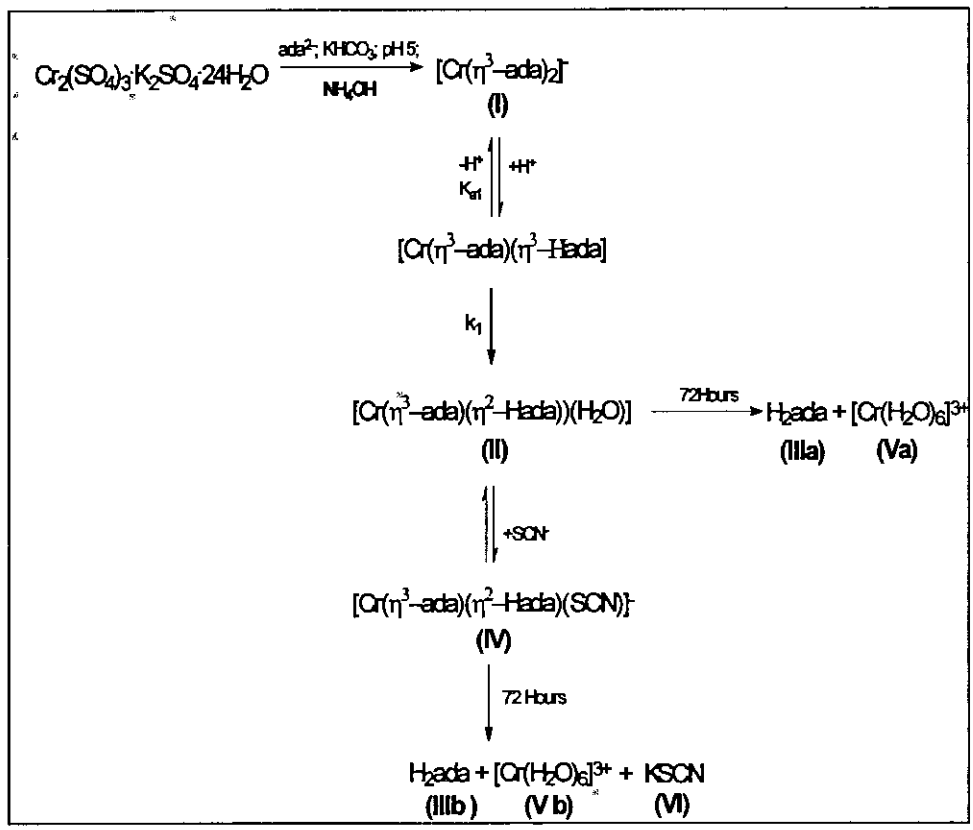

Scheme 4.1: Synthesis and reactions of $[Cr(\eta^3\text{-ada})_2]^-$.

4.2 Experimental

The synthesis and characterization of H_2ada (colourless crystals) and $Cs[(\eta^3\text{-ada})_2]\cdot 2H_2O$ (orange-pink crystals) are discussed in Chapter 3.

The density of $Cs[Cr(\eta^3\text{-ada})_2]\cdot 2H_2O$ and H_2ada were determined by flotation in iodomethane/benzene mixtures.

Intensity data were collected on a Bruker SMART 1K CCD area detector diffractometer with graphite monochromated Mo K_α radiation (50Kv, 30mA). The collection method involved ω-scans of width 0.3°. Data reduction was carried out using the program SAINT+ (Bruker, 1999a) and absorption corrections were made using the program SADABS (Sheldrick, 1996). The crystal structure was solved by direct methods using *SHELXTL* (Bruker, 1999b). Non-hydrogen atoms

were first refined isotropically followed by anisotropic refinement by full matrix least-squares calculations based on F^2 using *SHELXTL*. All other hydrogen atoms were first located in the difference map, then positioned geometrically and allowed to ride on their respective parent atoms. Diagrams and publication material were generated using SHELXTL and PLATON (Spek, 2003).

The SHELXTL (Bruker, 1999) program was used in all the calculations. Diagrams and publication material were generated using SHELXTL and Diamond (Brandenburg *et al.*, 1998). A final difference Fourier showed no sign of disorder or residual peaks.

A summary of the general crystal data and refinement parameters for H_2ada (see (III) in **Scheme 3.1**) and $Cs[(\eta^3\text{-ada})_2]\cdot 2H_2O$ (see (I) in **Scheme 3.1**) are given in **Table 4.1**.

Table 4.1: Crystal data and structure refinement for $[Cr(\eta^3\text{-ada})_2]^-$ (I) and H_2ada (III).

	(III)	(I)
Empirical formula	C6 H10 N2 O5	C12 H20 Cr Cs N4 O12
Formula weight	190.16	597.23
Temperature	293(2) K	293(2) K
Wavelength	0.71073 Å	0.71073 Å
Crystal system	Monoclinic	Monoclinic
Space group	P2(1)/n	P2(1)/n
Unit cell dimensions	a = 8.4121(14) Å	a = 9.1471(11) Å
	b = 11.3524(19) Å	b = 12.1267(14) Å
	c = 8.9947(15) Å	c = 17.475(2) Å
	α= 90°.	α= 90°.
	β= 107.597(3)°.	β= 94.516(2)°.
	γ = 90°.	γ = 90°.
Volume	818.8(2) $Å^3$	1932.4(4) $Å^3$
Z	4	4
Density (calculated)	1.543 Mg/m^3	2.053 Mg/m^3
Absorption coefficient	0.135 mm^{-1}	2.521 mm^{-1}
F(000)	400	1180
Crystal size	11.35 x 8.99 x 8.41 mm^3	0.23 x 0.22 x 0.18 mm^3
Theta range for data collection	2.91 to 28.00°.	2.05 to 25.99°.
Index ranges	-11<=h<=10,	-10<=h<=11
	-14<=k<=14,	-7<=k<=14,
	-11<=l<=4	-21<=l<=21
Reflections collected	5417	10788
Independent reflections	1961	3794 [R(int) = 0.0219]
Completeness to theta = 25.99°	99.4 %	100.0 %
Max. and min. transmission	0.3957 and 0.3088	0.6597 and 0.5948
Refinement method	Full-matrix least-squares on F2	Full-matrix least-squares on F2
Data / restraints / parameters	1961 / 0 / 130	3794 / 14 / 283
Goodness-of-fit on F2	1.041	1.026
Final R indices [I>2sigma(I)]	R1 = 0.0404, wR2 = 0.1120	R1 = 0.0256, wR2 = 0.0602
R indices (all data)	R1 = 0.0557, wR2 = 0.1196	R1 = 0.0331, wR2 = 0.0629
Largest diff. peak and hole	0.214 and -0.216 $e.Å^{-3}$	1.069 and -0.613 $e.Å^{-3}$

4.3 Crystal structure of H_2ada

The most relevant bond lengths and angles for H_2ada are reported in **Table 4.2** and **Table 4.3** respectively, while the numbering scheme of the H_2ada ligand is shown in the perspective drawing in **Figure 4.2**.

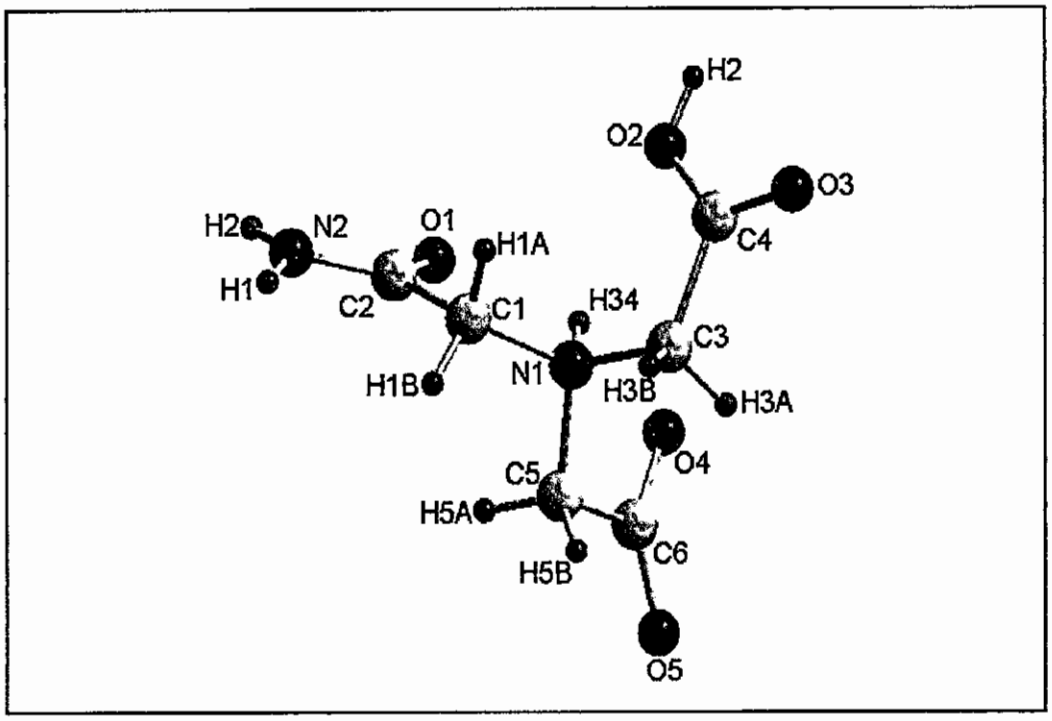

Figure 4.2: Numbering scheme of H_2ada.

Table 4.2: Selected bond lengths (Å) for H_2ada.

	(Å)		(Å)
O(2)–C(4)	1.289(2)	N(1)–C(3)	1.492(2)
O(4)–C(6)	1.275(2)	N(1)–C(5)	1.496(2)
O(3)–C(4)	1.220(2)	N(2)–C(2)	1.317(2)
O(1)–C(2)	1.226(2)	C(3)–C(4)	1.513(2)
O(5)–C(6)	1.227(2)	C(1)–C(2)	1.520(2)
N(1)–C(1)	1.491(2)	C(5)–C(6)	1.510(2)

Table 4.3: Selected bond angles (°) for the H_2ada.

	(°)		(°)
C(1)–N(1)–C(3)	112.62(1)	O(4)–C(6)–C(5)	115.80(1)
C(1)–N(1)–C(5)	112.08(1)	O(3)–C(4)–O(2)	126.74(2)
C(3)–N(1)–C(5)	112.26(1)	O(3)–C(4)–C(3)	118.87(1)
N(1)–C(3)–C(4)	112.77(1)	O(2)–C(4)–C(3)	114.39(1)
N(1)–C(1)–C(2)	107.05(1)	O(1)–C(2)–N(2)	125.01(2)
N(1)–C(5)–C(6)	112.39(1)	O(10–C(2)–C(1)	118.61(1)
O(5)–C(6)–O(4)	126.96(1)	N(2)–C(2)–C(1)	116.31(1)
O(5)–C(6)–C(5)	117.20(1)	C(1)-N(1)-H(34)	105.4(2)

The structural results indicate that the molecule exists as a dipolar zwitterion ($H_2ada^{\pm}$) in the solid state.

It is of interest to note that the N(2)-C(2) bond (1.317(2) Å of the amido group is much shorter than the N-C bonds surrounding the amino group which vary between 1.491(2) to 1.496(2) Å. This difference in bond lengths was also reported for the metal-ada complexes, $[VO(O_2)\eta^4\text{-ada}]^-$ (Sivak et al., 1995:1057), $[Cu(\eta^4\text{-ada})(Im)]$ Bugella-Altamirano *et al.* (1999:3333) and $[Ni(\eta^4\text{-ada})(H_2O)_2]$ (Bugella-Altamirano *et al.*, 2000:2463), where the N-C(amido) bond lengths varied between 1.319(3) and 1.321(3) Å and the N-C(amino) bondlengths varied between 1.477(3) and 1.508(3) Å. This variation in C-N bond length could be attributed to the fact that the N(amino) is bonded to four atoms while the N(amido) is bonded to only three atoms for ada^{2-}.

The amino nitrogen is tetrahedrally surrounded by three carbon atoms (C(1), C(3) and C(5)) as well as the H(34) hydrogen atom (see **Figure 4.3**). The tetrahedron is slightly distorted, with C-N-C angles varying from 112.08(12) to 112.62(11)° and the H-N-C angles varying between 104.9 and 109.0°.

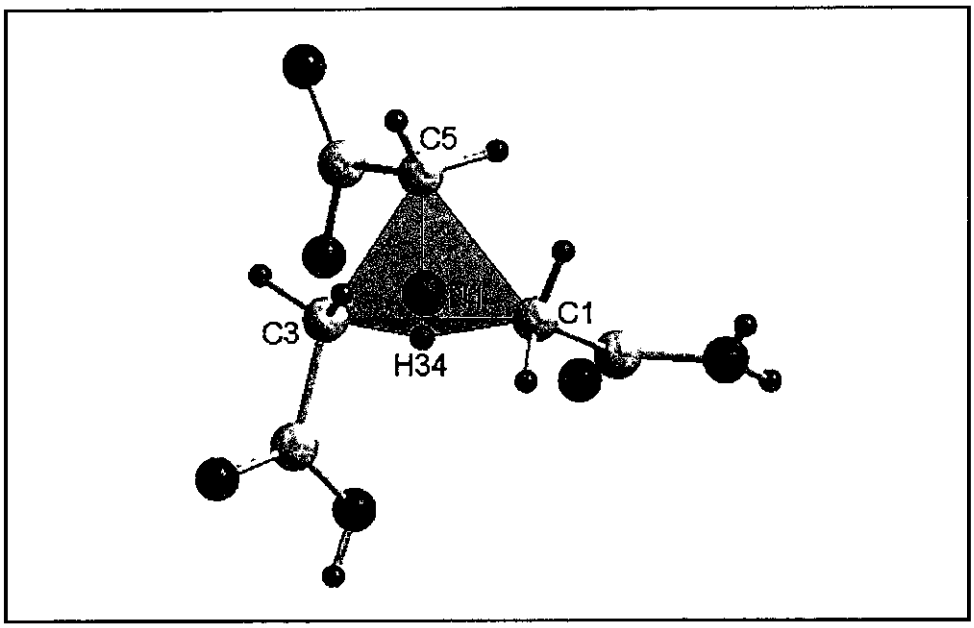

Figure 4.3: Amino nitrogen tetrahedron of H_2ada.

A hydrogen bonded network, involving N-H and O-H interactions, exists between the H_2ada molecules within the crystal. The conformation is intrastabilised by one relatively strong hydrogen bond (N(1)-H(34)···O(1)) and a second weaker hydrogen bond, N(1)-H(34)···O(4)) (see **Table 4.4** and **Figure 4.4**).

An interaction is considered to be a weak hydrogen interaction if the overall distance (D-H···A) is less than 3.2 Å and with an angle of more than 110°. Interactions with overall distance of less than 3.2 Å with a very bent angle (90-110°) should be viewed with some skepticism. In cases of doubt, angular considerations should take precedence over length considerations (*www.iucr.org*). The interaction (N(1)-H(34)···O(2) and an overall distance is 2.632(2) Å, but the angle is 104.1(2)°, it is thus unsure as to whether this interaction should be classified as a hydrogen interaction.

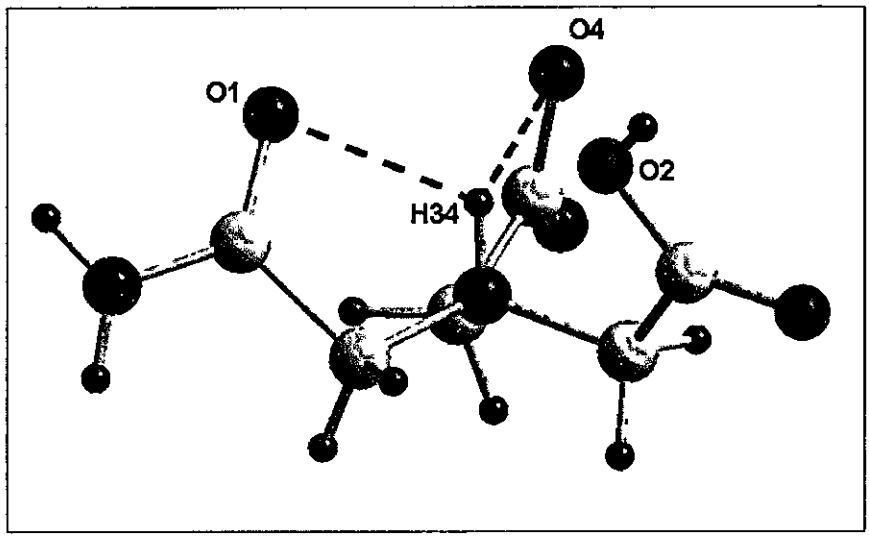

Figure 4.4: Intrastabilisation of H_2ada by means of hydrogen bonds.

An interesting structural feature is the fact that the carboxylic and carboxylate groups form pairs of adjacent dipolar zwitterions, $H_2ada^{\pm}$, that are linked by a relatively short hydrogen bond O(2)-H(2)···O(4) with overall distance of 2.486(2) Å, see **Figure 4.5**. Bugella-Altamirano *et al.* (2000:2463) found the same type of interaction as mentioned above during their crystallographic study of H_2ada with the overall distance for O(12)-H(12)···O(22) being 2.477(2) Å.

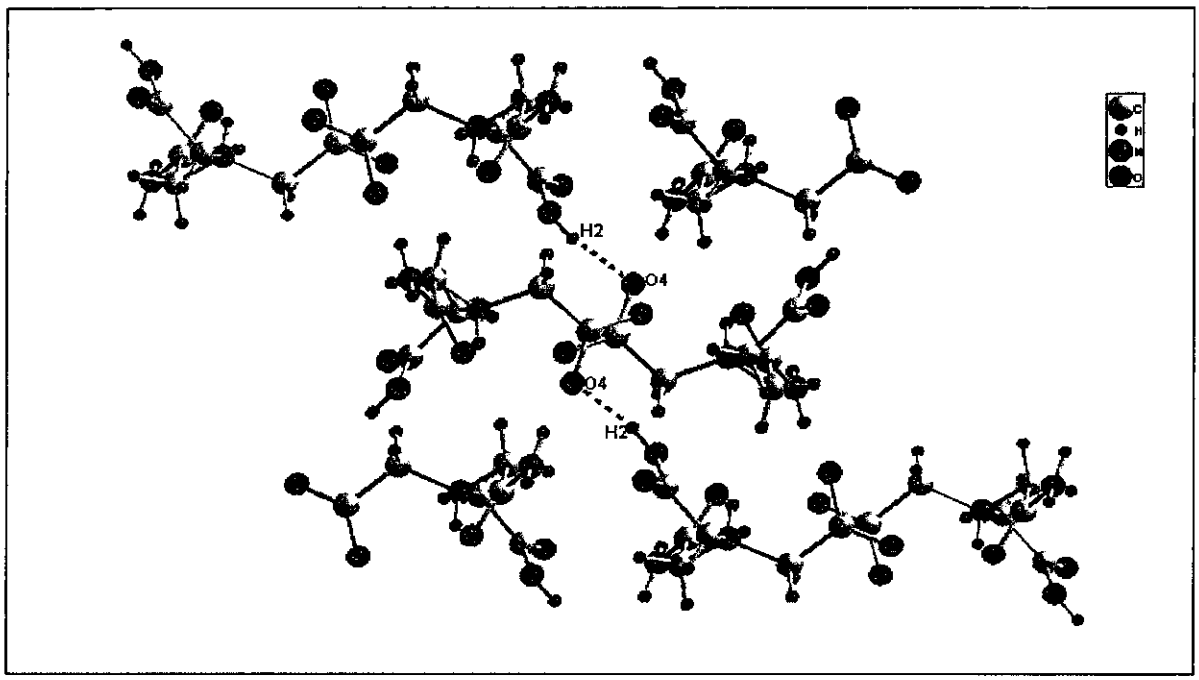

Figure 4.5: Representation of the hydrogen bond O(2)-H(2)···O(4) in H_2ada.

Table.4.4: Hydrogen-bonds (Å) for H_2ada.

D-H···A	D-H	H···A	D···A
N(1)-H(34)···O(1)	0.85(2)	2.098(2)	2.589(2)
N(1)-H(34)···O(2)	0.85(2)	2.285(2)	2.632(2)
N(1)-H(34)···O(4)	0.85(2)	2.265(2)	2.699(2)
C(5)-H(5A)···O(1)	0.97(2)	2.92(2)	3.193(2)
O(2)-H(2)···O(4)	0.819(2)	1.692(2)	2.486(2)

The rest of the bond angles and bonding distances are considered normal and correlate well with those found for H_2ada by Bugella-Altamirano *et al.* (2000:2463) (see **Table 4.5**).

Table 4.5: Average bond lengths for H_2ada.

	Average C-O bond length (Å)	Average N-C bond length (Å)	Average C-C bond length (Å)	Reference
H_2ada	1.247(2)	1.450(2)	1.513(2)	Bugella-Altamirano *et al.* (2000:2463)
H_2ada	1.247(3)	1.449(2)	1.514(3)	(this study)

A projection of H_2ada along the a axis (**Figure 4.6**) reveals that the molecules are packed in layers that stretch horizontally along the b-axis.

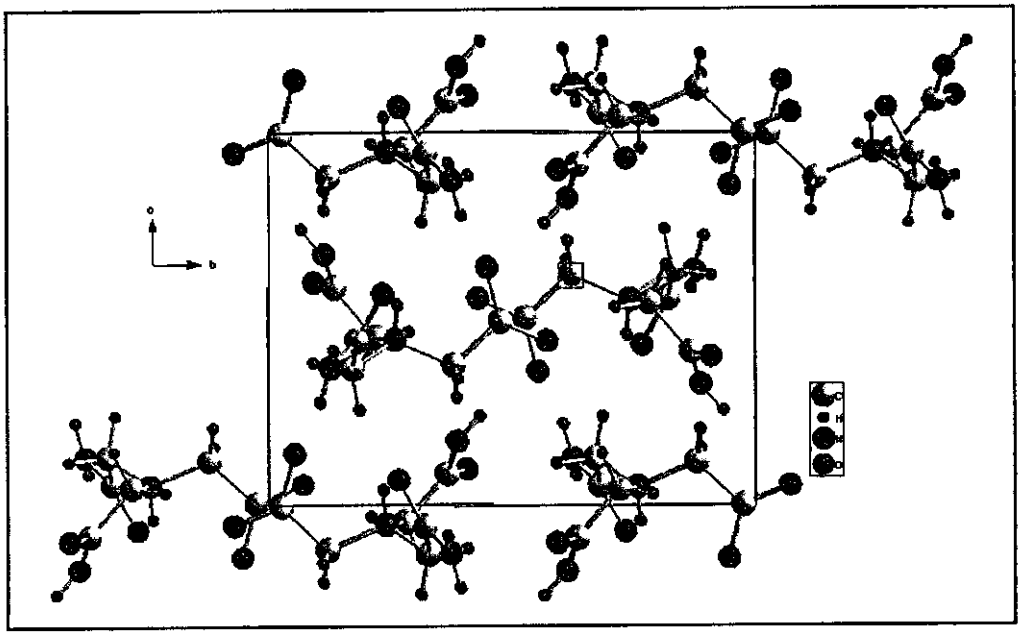

Figure 4.6: Perspective view of the unit cell of H_2ada along the a axis.

4.4 Crystal structure of $Cs[Cr(\eta^3\text{-ada})_2]\cdot 2H_2O$

The crystallographic data for $Cs[Cr(\eta^3\text{-ada})_2]\cdot 2H_2O$ obtained from this study has been published by Visser et al. (2005:1668). The numbering scheme of the $[Cr(\eta^3\text{-ada})_2]^{-2}$ anion is shown in the perspective drawing in **Figure 4.7**.

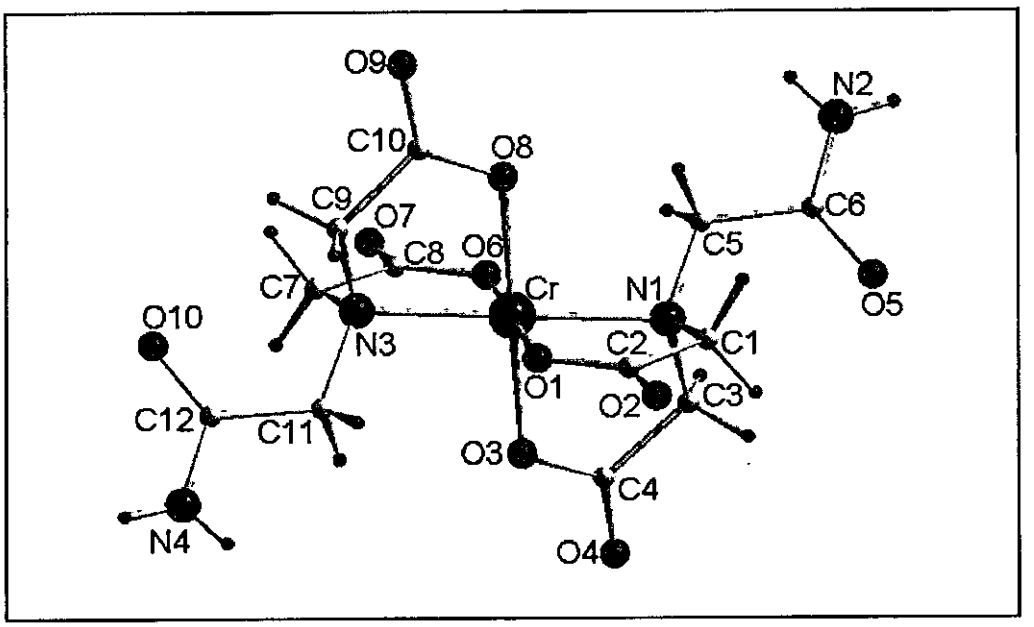

Figure 4.7: Numbering scheme for $[Cr(\eta^3\text{-ada})_2]^-$ anion.

The most relevant bond lengths and angles for the structure are reported in **Table 4.6** and **Table 4.7** respectively.

Table 4.6: Selected bond lengths (Å) for the anionic unit $[Cr(\eta^3\text{-ada})_2]^-$.

	(Å)		(Å)
Cr-O(1)	1.949(2)	N(1)-C(3)	1.492(4)
Cr-O(6)	1.952(2)	N(1)-C(1)	1.494(4)
Cr-O(3)	1.956(2)	N(2)-C(6)	1.326(2)
Cr-O(8)	1.961(2)	N(3)-C(11)	1.486(4)
Cr-N(3)	2.090(2)	N(3)-C(9)	1.492(4)
Cr-N(1)	2.096(2)	N(3)-C(7)	1.497(4)
N(1)-C(5)	1.483(4)	N(4)-C(12)	1.329(2)

Table 4.7: Selected bond angles (°) for the anionic unit $[Cr(\eta^3\text{-ada})_2]^-$.

	(°)		(°)
O(1)-Cr-O(6)	179.00(1)	N(3)-Cr-N(1)	179.31(1)
O(1)-Cr-O(3)	90.43(1)	C(5)-N(1)-C(3)	112.3(2)
O(6)-Cr-O(3)	88.57(1)	C(5)-N(1)-C(1)	112.7(2)
O(1)-Cr-O(8)	90.18(1)	C(3)-N(1)-C(1)	111.9(3)
O(6)-Cr-O(8)	90.82(1)	C(5)-N(1)-Cr	108.10(2)
O(3)-Cr-O(8)	179.21(1)	C(3)-N(1)-Cr	105.38(2)
O(1)-Cr-N(3)	95.67(9)	C(1)-N(1)-Cr	105.78(2)
O(6)-Cr-N(3)	84.36(9)	C(11)-N(3)-C(9)	111.8(2)
O(3)-Cr-N(3)	97.51(9)	C(11)-N(3)-C(7)	112.2(2)
O(8)-Cr-N(3)	82.92(9)	C(9)-N(3)-C(7)	112.5(3)
O(1)-Cr-N(1)	84.87(9)	C(11)-N(3)-Cr	108.22(2)
O(6)-Cr-N(1)	95.10(9)	C(9)-N(3)-Cr	104.76(2)
O(3)-Cr-N(1)	82.90(9)	C(7)-N(3)-Cr	106.95(2)
O(8)-Cr-N(1)	96.66(9)		

The Cr(III) centre in $Cs[Cr(\eta^3\text{-ada})_2]\cdot 2H_2O$ is surrounded by two ada^{2-} ligands. The structure determination clearly shows that ada^{2-} acts as a tridentate ligand with the N-(2-amidomethyl) group uncoordinated for both the ligands. The same mode of coordination for the ada^{2-} ligand was observed for

$[Ni(\eta^3\text{-ada})(bipy)(H_2O)]\cdot 4H_2O$ (see **Figure 2.5**), synthesised by Bugella-Altamirano *et al.* (2002:727).

Lance *et al.* (1983:492) postulated that the most likely structure for $[M(\eta^3\text{-ada})_2]^{2-}$ (M = metal(II)-ions) would be as depicted in **Figure 2.2**. These structures are based on various spectral data as well as the fact that COO^- is a better donor group compared to the amido carbonyl group. Interestingly the $[Cr(\eta^3\text{-ada})_2]^-$ structure (**Figure 4.7**) is identical to the structure proposed by Lance *et al.* even though the central metal ion is trivalent.

The chromium(III) centre is octahedrally surrounded by four carboxylate oxygen atoms (O(1), O(3), O(6) and O(8)) and two amino nitrogen atoms (N(1) and N(3)) from the two coordinated ada^{2-} ligands. The amino nitrogen atoms are *trans* with respect to each other and a centre of symmetry is observed around the Cr(III) centre.

The distortion of the Cr(III) octahedron is significant. The N-Cr-O bond angles are the most distorted from the expected 90°, with values varying between 82.90(9) and 97.51(9)°. The O-Cr-O angles vary between 88.57(10) and 90.82(10)° while the *trans* O(1)-Cr-O(6), O(3)-Cr-O(8) and N(1)-Cr-N(3) bond angles are 179.00(11), 179.21(10) and 179.31(10)° respectively. The octahedron is highlighted in **Figure 4.8**.

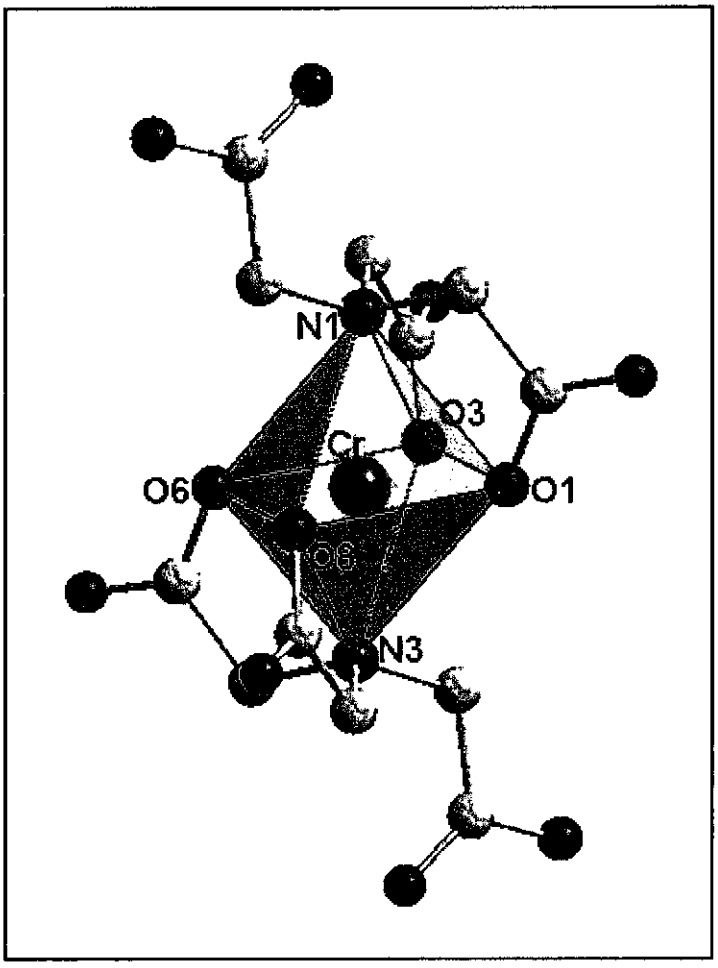

Figure 4.8: Octahedral distortion around the Cr(III) centre of the $[Cr(\eta^3\text{-ada})_2]^-$ anionic unit. The H atoms have been omitted for clarity.

The Cr(III)-N (amino) bonding distances vary between 2.090(2) and 2.096(2) Å. These values are shorter than the Ni-N(amino) bonding distance of 2.168(3) Å observed for the $[Ni(\eta^3\text{-ada})(bipy)(H_2O)]\cdot 4H_2O$ complex in which ada^{2-} acts as a tridentate ligand (Bugella-Altamirano *et al.*, 2002:727). The $Cr\text{-}O_{ada}^{2-}$ bond lengths vary from between 1.949(2) and 1.961(2) Å. These values are once again smaller than the Ni-O bonding distances observed in the $[Ni(\eta^3\text{-ada})(bipy)(H_2O)]\cdot 4H_2O$ (Bugella-Altamirano *et al.*, 2002:727) which vary between 2.040(3) and 2.042(3)Å. This difference in bond lengths could be attributed to the different ionic radii of the two metal ions. Another contributing factor could be that there are different ligands situated *trans* to the ada^{2-} ligand for the two complexes, bipy ligand for the Ni(II)-complex and a second ada^{2-} ligand for the Cr(III)-complex.

The rest of the N-C, C-C and C-O bond distances are considered normal and correlate well with those found in H_2ada (Bugella-Altamirano *et al.*, 2000:2463).

The two ada^{2-} ligands form four glycinate rings (A_1 to A_4) (see **Figure 4.9**) around the central metal ion. The strain in these rings can be described by the deviation from planarity. According to Weakliem & Hoard (1959:549) the sum of the endocyclic angles of planar acetate rings should be 538.4°. Any deviation from this implies non-planarity and thus strain of the rings. The sums of the endocyclic angles for the rings in the $Cs[Cr(\eta^3\text{-ada})_2]\cdot 2H_2O$ complex vary between 531.9 and 540.7°, a maximum deviation of *ca* 7° (see **Table 4.8**). One would expect the strain experienced by the glycinate rings to be lifted somewhat when the ligand is bonded in tridentate mode. This seems to be the case if the comparison with $Cs_2[Cr_2(\eta^4\text{-nta})_2(\mu\text{-OH})_2]\cdot 4H_2O$ is made, where deviations of up to 12° were observed in some of the acetate rings (Visser *et al.*, 1999:2795).

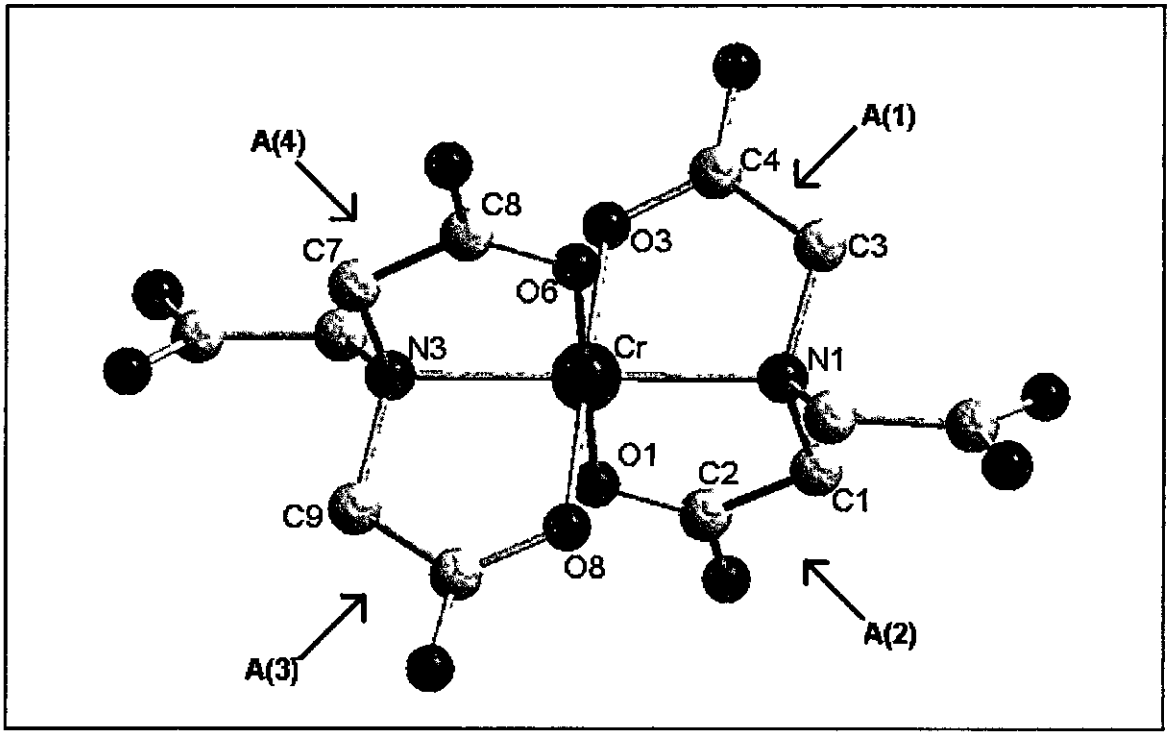

Figure 4.9: The glycinate rings (A(1) to (A(4)) of $[Cr(\eta^3\text{-ada})_2]^-$.

Table 4.8: Endocyclic angles, distances of N and Co atoms from the CCOO planes and torsion angles for the anionic unit, $[Cr(\eta^3\text{-ada})_2]^-$.

	A_1	A_2	A_3	A_4
Endocyclic angles (°)	534.19	545.35	539.66	546.11
N distance from CCOO plane	0.188(6)	-0.192(6)	-0.495(6)	-0.095(6)
Cr distance from CCOO plane	-0.354(5)	-0.060(5)	0.011(5)	0.010(5)
Torsion angles (°)				
N-Cr-O-C	-18.6(2)	2.48(3)	13.88(2)	-2.72(4)
Co-O-C-C	10.62(2)	2.66(2)	0.23(3)	-0.19(2)
N-C-C-O	8.88(2)	-8.76(2)	-21.4(3)	4.49(3)
Cr-N-C-C	-21.3(3)	9.55(3)	29.24(3)	-5.98(3)
O-Cr-N-C	20.97(2)	-6.61(2)	-23.3(2)	4.71(2)

The deviation from the ring planarity is further illustrated by the torsion angles that vary between -23.3(2) and 29.24(2)°. These values are closer to the ideal value of 0° than the torsion angles of 30.0(1) and -37.3(2)° for the glycinate rings of $[VO(O_2)(\eta^4\text{-ada})]^-$ (Sivak *et al.*, 1995:1057). It is once again clear that the ring strain is lifted to a certain degree when ada^{2-} is tridentately coordinated instead of tetradentately.

The N and Cr atoms of $Cs[Cr(\eta^3\text{-ada})_2]\cdot 2H_2O$ were calculated to be displaced on opposite sides of the CCOO plane for all rings except one, with distances from the plane varying between 0.494(6) and 0.010(5) Å (see **Table 4.9**). It can be seen from the deviations of up to 0.705 Å from the CCOO planes for the $Cs_2[Cr_2(\eta^4\text{-nta})_2(\mu\text{-OH})_2]\cdot 4H_2O$ complex (Visser *et al.*,1999:2795) that the glycinate rings of the nta^{3-} complex experience more strain than that of the ada^{2-} complex. This could once again be attributed to the fact that the nta^{3-} is tetradentately coordinated in $Cs_2[Cr_2(\eta^4\text{-nta})_2(\mu\text{-OH})_2]\cdot 4H_2O$ whereas ada^{2-} is in tridentate mode in $Cs[Cr(\eta^3\text{-ada})_2]\cdot 2H_2O$.

The primary reason for the non-planarity of such rings are attributed to angular strain about the coordinated nitrogen atoms (Weakliem & Hoard, 1959:549). They argued that each ring attempts to impose its own stereochemical requirements on the nitrogen atom, while the nitrogen is also constrained to approximately tetrahedral geometry. The resulting compromise structure contains not only angle and bond-length abnormalities, but also significant distortions of the N tetrahedra.

Table 4.9: Distances (Å) of Cr and N atoms from CCOO planes.

CCOO plane	Cr	N
C(1)-C(2)-O(1)-O(2)	-0.060(5)	-0.192(6)
C(3)-C(4)-O(3)-O(4)	-0.354(5)	0.188(6)
C(7)-C(8)-O(6)-O(7)	0.010(5)	-0.095(6)
C(9)-C(10)-O(8)-O(9)	0.011(5)	-0.495(6)

The nitrogen(amino) tetrahedra of the anionic unit are both distorted from the ideal tetrahedral geometry. The C-N-Cr angles vary between 105.38(2) and 108.2(2)°. The C-N-C angles vary between 111.8(2) and 112.7(2)°. These values correlate well with those found for other metal complexes with similar tripod-type ligands such as nta^{3-} with C-N-C angles varying between 110.9(9) and 114.2(9)° for the $Cs_2[Cr_2(\eta^4\text{-nta})_2(\mu\text{-OH})_2]\cdot 4H_2O$ complex (Visser *et al.*,1999:2795).

The nitrogen tetrahedra of the anionic unit $[Cr(\eta^3\text{-ada})_2]^-$, is shown in **Figure 4.10**.

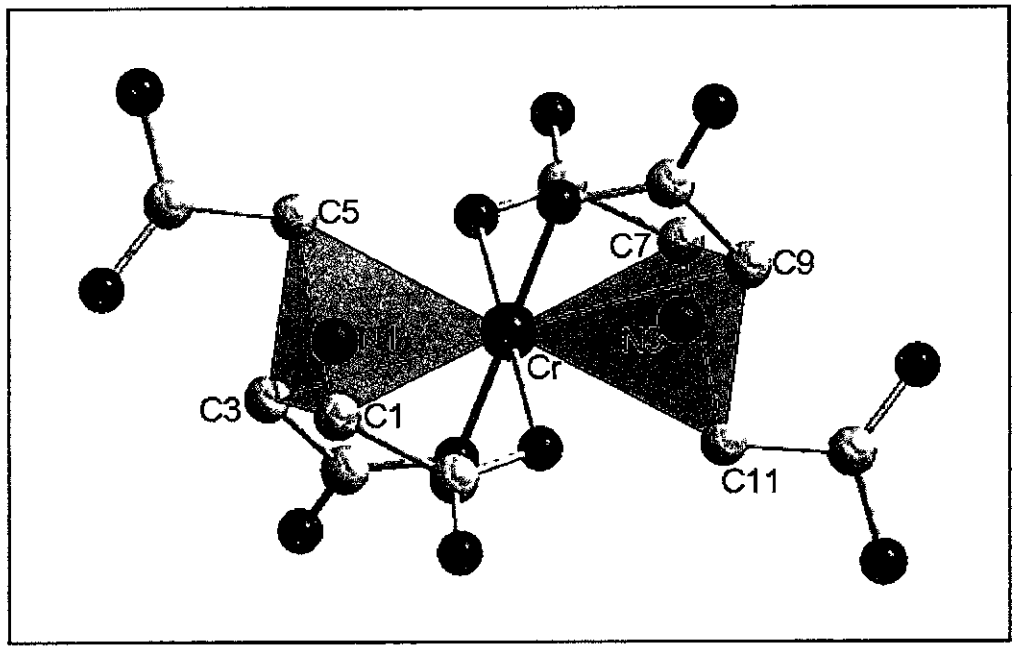

Figure 4.10: Nitrogen tetrahedra of anionic unit $[Cr(\eta^3\text{-ada})_2]^-$. The H atoms have been omitted for clarity.

The Cs^+ to oxygen interatomic distances vary between 2.988(4) and 3.398(2) Å. The Cs^+ interacts with eight oxygen atoms, two oxygens from two H_2O molecules and 6 oxygen atoms from four surrounding $[Cr(\eta^3\text{-ada})_2]^-$ anions. The geometry of this arrangement is in the form of a twisted dodecahedron, see **Figure 4.11**.

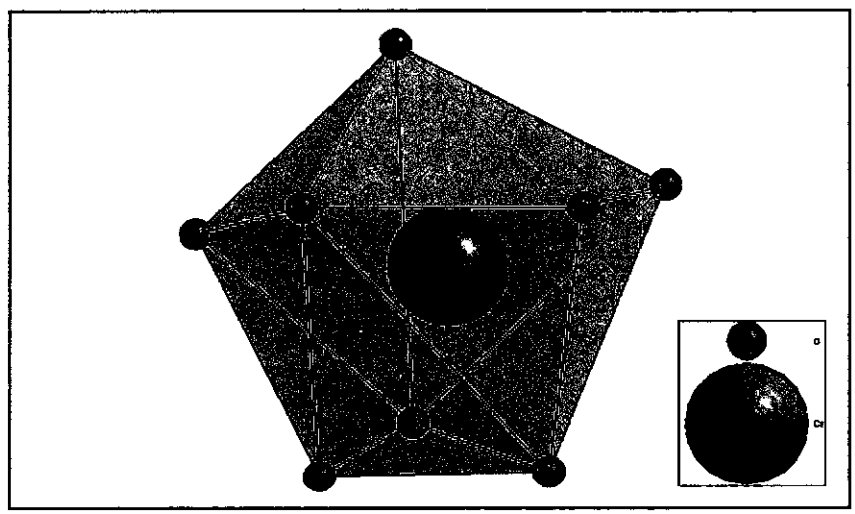

Figure 4.11: Oxygen atoms arrangement around Cs^+ in $Cs[Cr(\eta^3\text{-ada})_2]\cdot 2H_2O$.

A projection of $Cs[Cr(\eta^3\text{-ada})_2]\cdot 2H_2O$ molecules along the a axis is shown in **Figure 4.12**. The complex anions are packed in layers parallel to the a axis. The anionic units also stretch in layers parallel to the b axis with the Cs^+ cations and crystal waters filling the spaces between the layers. An interesting feature is that the anionic units are packed in layers that stretch diagonally across the a-b plane.

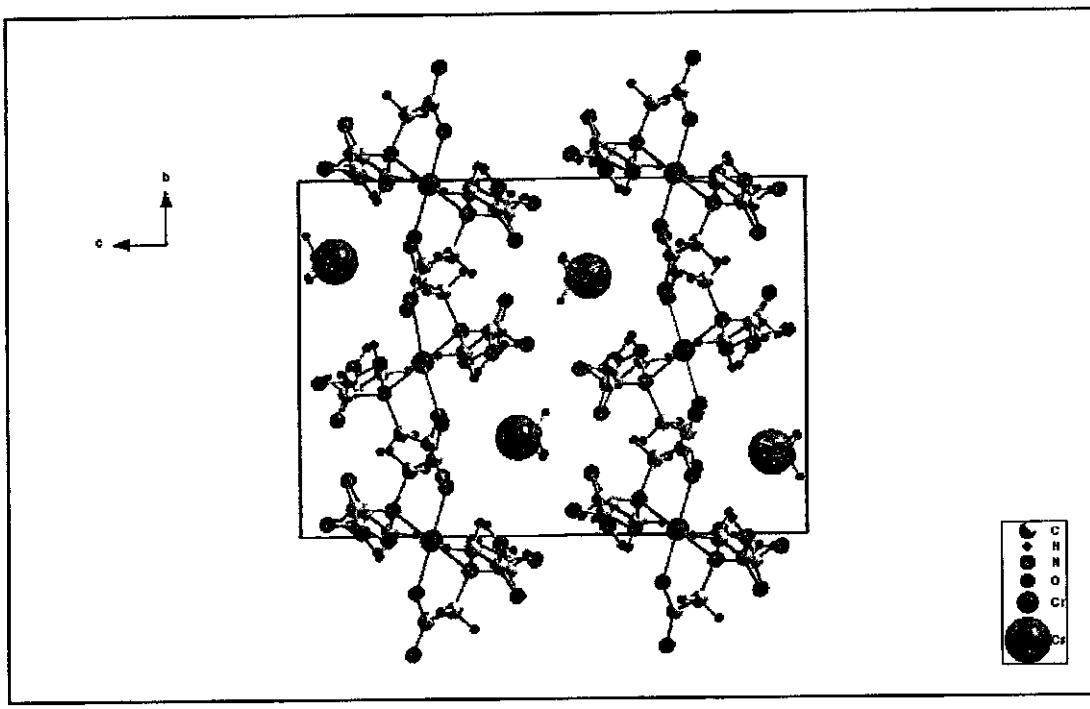

Figure 4.12: Perspective view of the unit cell of $Cs[Cr(\eta^3\text{-ada})_2]\cdot 2H_2O$ along the a axis.

4.5 Conclusion

Bugella-Altamirano and co-workers (2000:2463) were the first to report the crystal structure for H_2ada in spite of the fact that H_2ada has been commercially available for many years. In this study the H_2ada ligand is also the final product for reactions between $Cs[Cr(\eta^3\text{-ada})_2]\cdot 2H_2O$ complex and H^+ ions as well as SCN^- ions that were studied kinetically. The isolation and characterisation of this product was vitally important in the construction of the reaction mechanism as well as the reaction rates (k_1, k_2, k_{-2}) for these reactions (see Chapter 5).

The crystal packing of the H_2ada zwitterions is clearly dominated by the hydrogen bonds between the molecules, especially the relatively short hydrogen bond between O(2)-H(2)···O(4). A further contribution to the distortion of the amino nitrogen tetrahedra seems to be due to the hydrogen bonds that intrastabilise the molecule.

The $Cs[Cr(\eta^3\text{-ada})_2]\cdot 2H_2O$ complex has been isolated and characterized with X-ray crystallography for the first time. This is the first structural report of a metal(III) complex with ada^{2-} as ligand and the second in which ada^{2-} acts as a tridentate ligand.

The glycinate ring strain experienced by the $Cs[Cr(\eta^3\text{-ada})_2]\cdot 2H_2O$ complex is significantly less than the strain experienced by the $Cs_2[Cr_2(\eta^4\text{-nta})_2(\mu\text{-OH})_2]\cdot 4H_2O$ (Visser *et al.*,1999:2795) and $[VO(O_2)(\eta^4\text{-ada})]^-$ (Sivak *et al.*, 1995:1057) complexes. The ring and angular strain seems to be somewhat lifted when the ligand (ada^{2-}) is bonded in tridentate mode instead of tetradentate mode.

5 Kinetic study of the reactions of Cr(III)-ada complexes

In this chapter...

The first part of the chapter focuses on the reactions between $Cs[Cr(\eta^3\text{-}ada)_2]\cdot 2H_2O$ and H^+, while the latter part focuses on the substitution reactions of $[Cr(\eta^3\text{-}ada)(\eta^2\text{-}Hada)(H_2O)]$ with NCS^- ions.

5.1 Introduction

The synthesis and characterisation of the different Cr(III)-ada complexes in Chapter 3 clearly indicated the reactivity of this complex towards H^+ ions as well as NCS^- ions under certain conditions. This tendency to react with H^+ to form different complexes was also observed for Cr(III)- and Co(III)-nta as well as Co(III)-apda complexes (Visser *et al.*, 1994:1051, Visser *et al.*, 2002:461 and Potgieter *et al.*, 2005:1968).

Detailed kinetic studies performed on these complexes indicated that the different metal-tripod complexes exhibit different reactions, after the first protonation step. Research have shown that the initial protonation reaction for the $[Co(\eta^4\text{-}nta)(\mu\text{-}OH)]_2^{2-}$ complexes was followed by the breaking of the hydroxo bridge to form the *cis*-aqua complex (Visser *et al.* (2002:461), $[Co(\eta^4\text{-}nta)(H_2O)_2]^{2-}$ which itself showed normal protonation/deprotonation behaviour (Visser *et al.*, 1997:2851). The Co(III)-apda complex $[Co(\eta^3\text{-}Hapda)_2]^{2-}$ on the other hand, only showed the protonation/deprotonation of the uncoordinated propionate arm of the tripod ligand (Potgieter *et al.*, 2005:1968).

Another interesting result from these studies on the different metal-tripod complexes, pointed to additional interactions between H^+ ions and the electron rich carboxylic oxygens which are common to all of these kind of tripod ligands. In some cases, this interaction was followed by the partial dissociation of the tripod ligand in a slow step to form a new complex (Visser *et al.*, 1994:1051 and Visser *et al.*, 2002:461). All these complexes were relatively unstable in solutions at low pH for long periods which resulted in the complete dissociation of the tripod ligands.

The kinetic studies performed on the Cr(III)- and Co(III)-nta and Co(III)-apda (Visser *et al.*, 1994:1051, Visser *et al.*, 2002:461 and Potgieter *et al.*, 2005:1968) complexes also yielded interesting results. It was found that the tripod ligands had a labilising effect on the metal(III) complexes. It was postulated that these electron rich tripod ligands donate electron density to the metal(III) centers making them react more like the labile metal(II) ions.

The absence of any kinetic data on metal(III)-ada complexes as well as the isolation and characterisation of the various Cr(III)-ada complexes in Chapter 3, necessitated the kinetic study on this complex.

5.2 Experimental procedures

All reagents and chemicals were of analytical grade and double distilled water was used in all experiments. All pH measurements were performed on a pH 211 microprocessor pH meter, calibrated with pH 7.01 (HI7007) and pH 4.01 (HI7004) buffer solutions, all obtained form Hanna instruments. Kinetic measurements were performed on a Cary 50 (Conc.) spectrophotometer equipped with constant temperature cell holders (accuracy within 0.1°C). Scientist (Micromath, 1990) was used to fit the data. All the kinetic runs were performed under pseudo first-order conditions with the ligand in excess in each case. The reaction between $[Cr(\eta^3\text{-ada})_2]^-$ and H^+ was followed at 405 nm while

the substitution reaction with NCS^- was followed at 295 nm. The ionic strength of all the reaction solutions was kept constant by addition of $NaClO_4$. The solid lines and the figures represent computer least squares fits of data, while the experimentally determined values are represented by dots. Detailed tables of the experimental values are given in Appendix A (Section II).

5.3 Kinetic results

The UV/VIS spectra taken at 10°C for the reaction between $[Cr(\eta^3\text{-ada})_2]^-$ and H^+ ions (pH = 0.3) showed a relative fast reaction with the formation of two new absorption maxima at 405 and 564 nm (time = ± 15 minutes, with a spectrum obtained every 30 seconds). Three isosbestic points were also observed at 363, 466 and 499 nm for this reaction (see **Figure 5.1**) pointing to the formation of one product during this reaction.

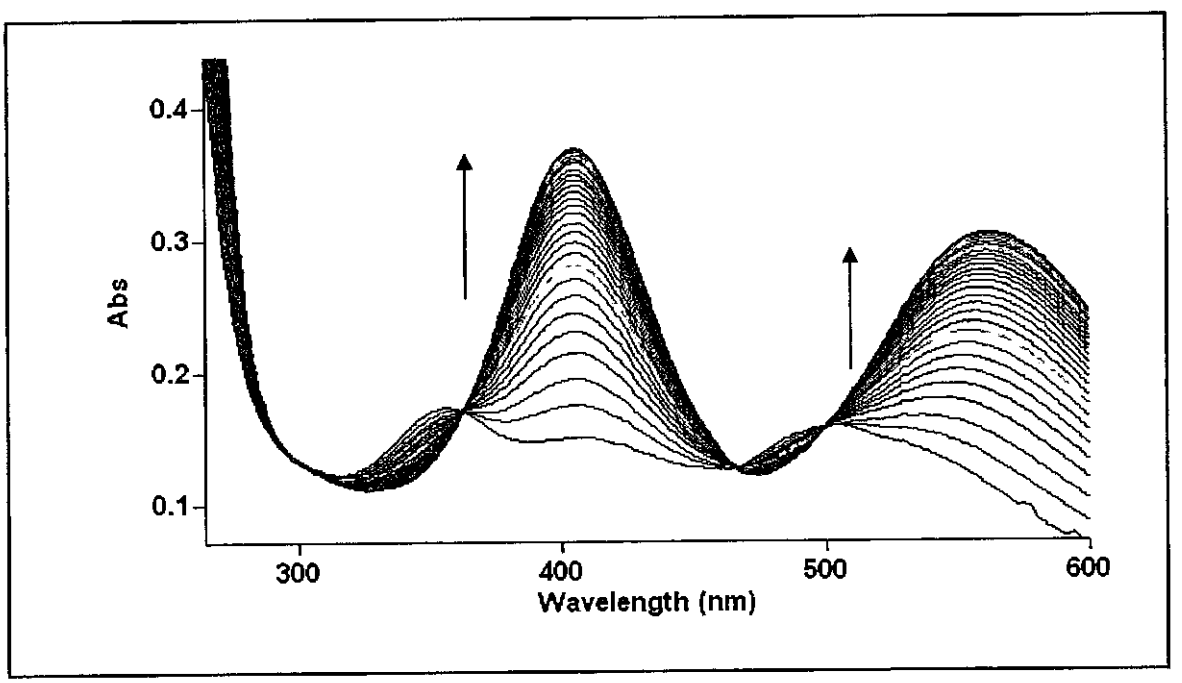

Figure 5.1: Spectral change of $Cs[Cr(\eta^3\text{-ada})_2]\cdot 2H_2O$ (2.5×10^{-3} M) upon the addition of HCl (1 M) with scans obtained every 30 seconds at 10°C (final pH = 0.3).

On closer inspection, a second, slower reaction, which resulted in a small decrease in absorption at 405 nm and the disappearance of the three isosbestic points (see **Figure 5.2**), was observed. This resulted in a slow of the absorption maxima to 406 and 566 nm. The solution was allowed to stand several days after which a precipitate formed. The UV/VIS spectrum obtained for the filtrate had absorption maxima 406 and 574 nm. This points to the formation of $[Cr(H_2O)_6]^{3+}$ (see Paragraph 3.4.4).

The precipitate obtained from the solution just mentioned, was identified as H_2ada (see Paragraph 3.4.3). This information points to the dissociation of the two ada^{2-} ligands in acidic solution.

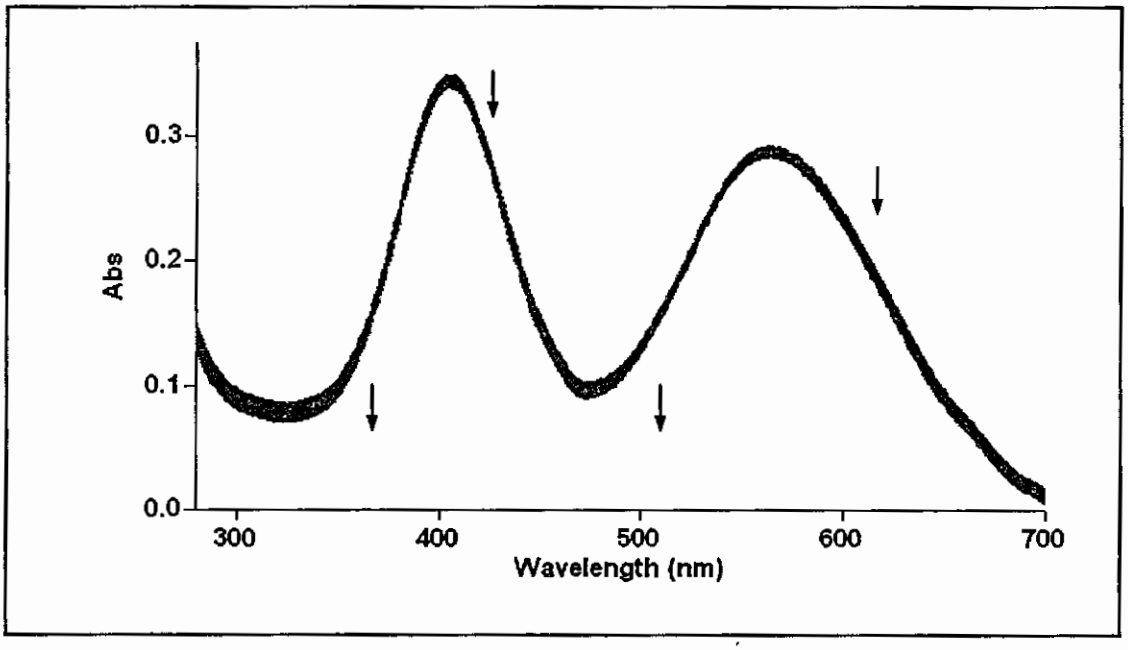

Figure 5.2: Spectral change of $Cs[Cr(\eta^3\text{-ada})_2]\cdot 2H_2O$ (2.0×10^{-3} M) upon the addition of HCl (1 M) (the second reaction) with scans obtained every 3 minutes for 24 hours at 10°C (final pH = 0.3).

In order to investigate whether there is an acid association equilibrium present before the onset of the reaction as depicted in **Figure 5.1,** acid was added to a solution containing $[Cr(\eta^3\text{-ada})_2]^-$ (resulting pH = 0.8, at low temperatures). This led to the immediate change in absorption (see **Figure 5.3** and Chapter 3,

Paragraph 3.5). As the chelate ring opening reaction follows the protonation/deprotonation equilibrium very quickly, the protonation reaction was investigated at a temperature of 5°C. The UV/VIS spectrum of a solution containing $[Cr(\eta^3\text{-ada})_2]^-$ (pH = 5.96) was recorded (see (1) in **Figure 5.3**), the pH was lowered to 0.8 (see (2) in **Figure 5.3**) and immediately re-adjusted to pH = 6 (see (3) in **Figure 5.3**).

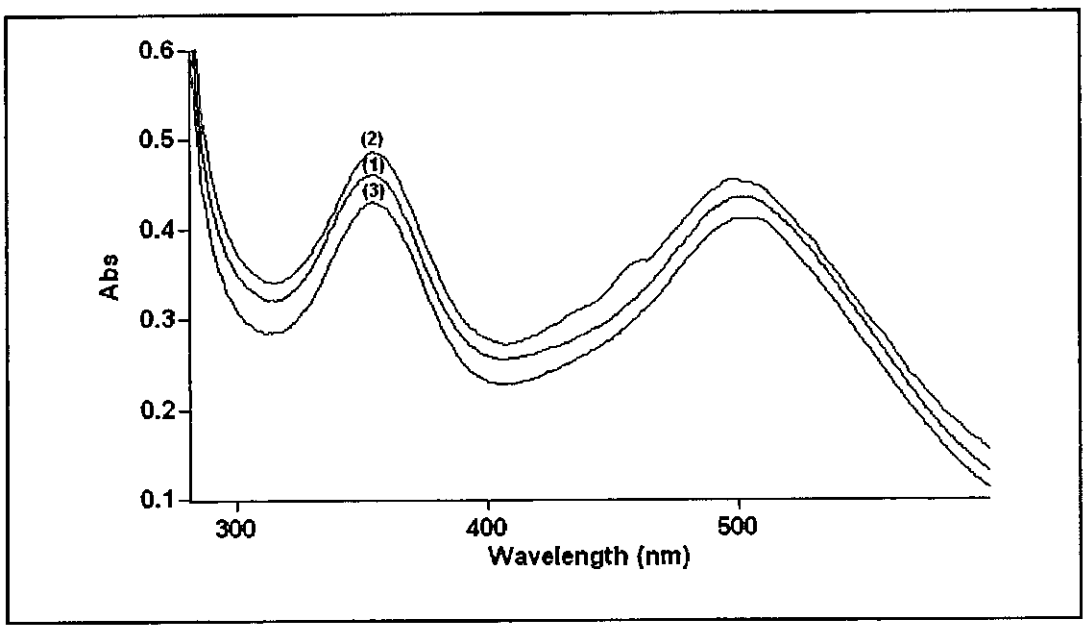

Figure 5.3: pH adjustment of $[Cr(\eta^3\text{-ada})_2]^-$ (6.0×10^{-3}M). T = 5°C, total time = 60 seconds.
(1) = $[Cr(\eta^3\text{-ada})_2]^-$ solution (pH = 6)
(2) = $[Cr(\eta^3\text{-ada})(\eta^3\text{-Hada})]$ solution (pH = 0.78)
(3) = $[Cr(\eta^3\text{-ada})_2]^-$ solution (pH = 6), after pH re-adjustment of (2)

In another experiment, a solution containing $[Cr(\eta^3\text{-ada}_2]^-$ was dissolved in H_2O, H^+ (HCl, 1.0 M) (pH = 0.8) was added and the reaction between $[Cr(\eta^3\text{-ada}_2]^-$ and H^+ was allowed to go to completion (the first reaction). A few drops of a solution containing KSCN was subsequently added to this solution which resulted in a dramatic change in spectrum with peak formation at 295 nm (**Figure 5.4**).

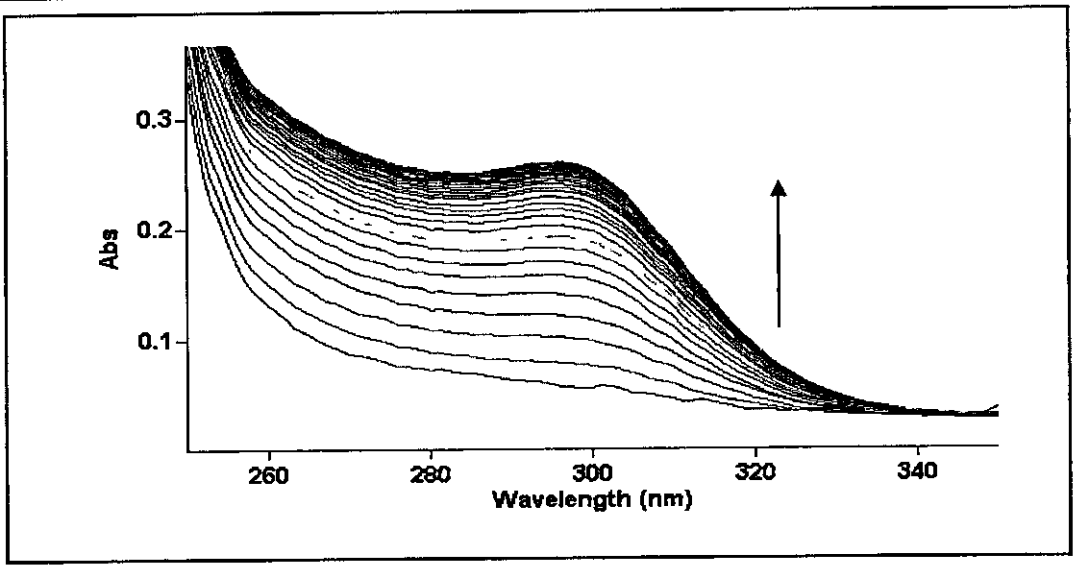

Figure 5.4: UV/VIS spectral change upon addition of a solution of NCS^- (1.0×10^{-3}) (pH = 0.8) to a solution of $Cs[Cr(\eta^3\text{-ada})_2]\cdot 2H_2O$ (5.0×10^{-4} M) (pH = 0.8). T = 25°C.

A schematic presentation of all the reactions, using these results in conjunction with the isolation of the H_2ada and $[Cr(H_2O)_6]^{3+}$ at low pH values (pH = 0.3) after 48 hours and longer (see Chapter 3), is presented in **Scheme 5.1**.

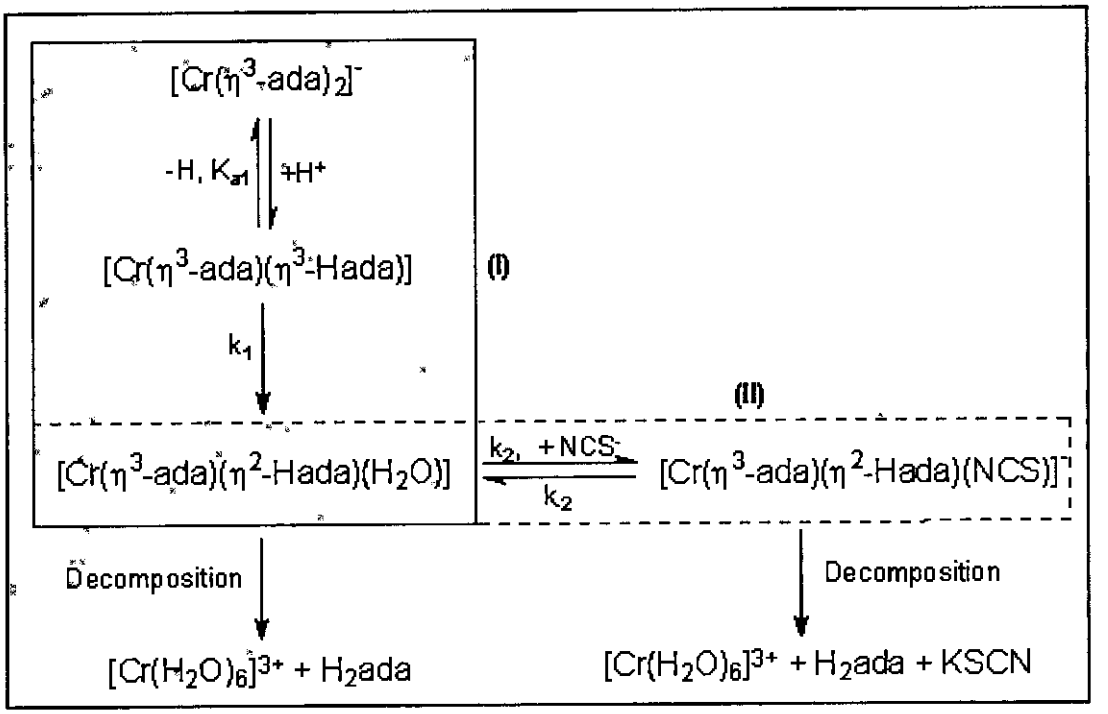

Scheme 5.1: pH dependence and reactions of $Cs[Cr(\eta^3\text{-ada})_2]\cdot 2H_2O$.

5.3.1 Reactions between $[Cr(\eta^3\text{-ada})_2]^-$ and H^+

pH dependence of $Cs[Cr(\eta^3\text{-ada})_2]\cdot 2H_2O$

The initial results obtained from this study clearly indicate the presence of different species at different pH values (see Chapter 3, Paragraph 3.5). Other important observations made from these studies, is that protonation finally activates the starting complex towards substitution reactions. It is thus postulated that the first protonation reaction is given by **Scheme 5.2**.

$$[Cr(\eta^3\text{-ada})_2]^- + H^+ \underset{K_{a1}}{\rightleftharpoons} [Cr(\eta^3\text{-ada})(\eta^3\text{-Hada})]$$

Scheme 5.2: Proposed protonation of $[Cr(\eta^3\text{-ada})_2]^-$.

It can be seen in **Figure 5.3** that the absorption difference observed upon changing the pH is very small. The fact that the pH meter also could not accurately measure the pH below 0.5, made the determination of the K_{a1} value highly inaccurate. The UV/VIS spectrum change from (2) to (3) in **Figure 5.3** however indicates that the reaction that took place is reversible. The fact that absorption maxima (2) is lower than (1) is most probably due to dilution upon addition of HCl and a solution of KOH (see Chapter 3, Paragraph 3.5). The large extinction coefficient of the product formed in the second reaction (see **Figure 5.1**) also complicated the K_{a1} determination which resulted in a continual change in absorption after acidification.

Chelate ring-opening reaction of $[Cr(\eta^3\text{-ada})(\eta^3\text{-Hada})]$

A relatively fast reaction was spectophotometrically observed (see **Figure 5.1** and Chapter 3, Paragraph 3.5) after the pH of a solution containing

$Cs[Cr(\eta^3\text{-ada})_2]\cdot 2H_2O$ was lowered to 0.8. The fact that it was possible to follow this reaction, (chelate ring-opening step) with conventional spectophotometric methods points to a reaction different from normal protonation reactions. A second reaction/s was also observed which was much slower (took at least 24 hours to complete) than the first reaction (see Chapter 3, Paragraph 3.5). After a period of three days the free acid H_2ada was isolated and the UV/VIS spectrum of the remaining violet coloured solution was identified in Paragraph 3.4.4 as containing $[Cr(H_2O)_6]^{3+}$. It was however decided to not investigate the further slow dissociation of the ada^{2-} ligands due to precipitate formation.

The possibility of substitution reactions with different ligands such as Cl^- in solution at these pH values were eliminated by the study of the reactions between $[Cr(\eta^3\text{-ada})_2]^-$ and different strong acids with coordinating and non-coordinating anions, see **Table 5.1.**

Table 5.1: Observed rate constants for the reaction between $[Cr(\eta^3\text{-ada})_2]^-$ (5.0×10^{-3} M) and different acids and anions, T = 20 °C, λ = 405nm, μ = 6.5×10^{-1} M ($NaClO_4$).

Reactant	$(10^2)k_{obs}$ (s^{-1})
0.25 M HCl	5.28(4)
0.25 M HCl + 0.4 M NaCl	5.34(3)
0.25 M $HClO_4$	5.31(2)
0.50 M HCl	9.22(3)

Keeping in mind that the ada^{2-} dissociates from the metal(III) centre in acidic solution, **Scheme 5.1** is proposed for describing the observed kinetics.

The rate law for the first reaction (see (I) in **Scheme 5.1**) is given by Equation 5.2.

$$\mathbf{R = k_1[Cr(\eta^3\text{-ada})(\eta^3\text{-Hada})]} \qquad \mathbf{(5.2)}$$

The total Cr(III) concentration, $[Cr]_{tot}$ is indicated by Equation 5.3.

$$[Cr]_{tot} = [Cr(\eta^3\text{-ada})(\eta^3\text{-Hada})(H_2O)] + [Cr(\eta^3\text{-ada})_2^-] \quad (5.3)$$

The acid dissociation constant, K_{a1} is given in Equation 5.4.

$$K_{a1} = \frac{[Cr(\eta^3\text{-ada})_2^-][H^+]}{[Cr(\eta^3\text{-ada})(\eta^3\text{-Hada})]} \quad (5.4)$$

Under pseudo first-order conditions with $[Cr]_{tot} << [H^+]$ the observed rate, k_{obs}, can be derived from Equation 5.5 (Appendix A, Section III).

$$k_{obs} = \frac{k_1}{(K_{a1}/[H^+] + 1)} \quad (5.5)$$

The results obtained in Figure 5.4 were fitted to Equation 5.5 and the values of k_1, K_{a1} at different temperatures are reported in **Table 5.3**. The activation enthalpy ($\Delta H^{\#}$) and entropy ($\Delta S^{\#}$) were calculated from these results using the Eyring Equation (see Appendix A) values are also reported in **Table 5.3**.

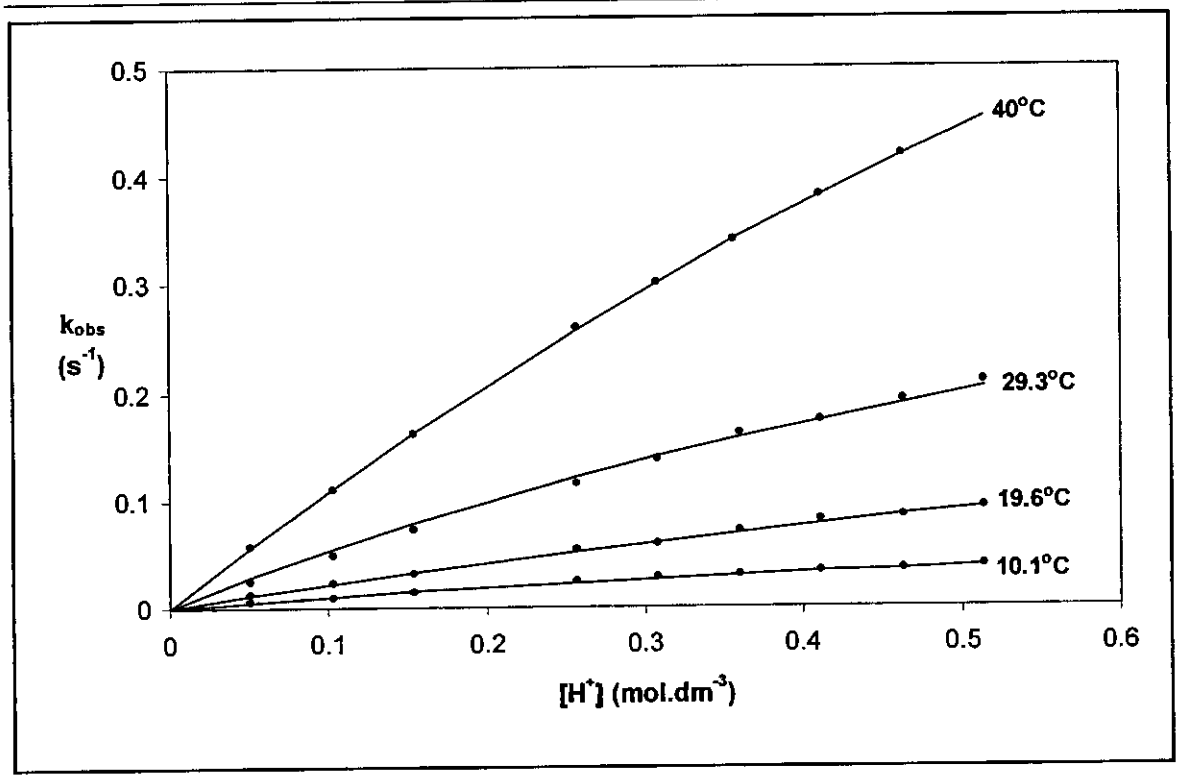

Figure 5.5: Plot of k_{obs} *vs.* $[H^+]$ at different temperatures, μ = 0.6 M ($NaClO_4$), λ = 405.0 nm, $[Cr(\eta^3\text{-ada})_2]^-$ = 5.0 x 10^{-3} M.

Substitution reaction of $[Cr(\eta^3\text{-ada})(\eta^2\text{-Hada})(H_2O)]$ with NCS^-

pH dependence

In the first part of the study of the substitution reactions between the Cr(III)-ada complex and NCS^- the reaction was followed after the completion of the chelate ring opening step which was discussed in previous paragraphs (see Chapter 3). The reaction was followed in a pH range where no precipitation occurred in order to verify whether the $[Cr(\eta^3\text{-ada})(\eta^2\text{-Hada})(H_2O)]$ was the only reacting metal complex in solution. The effect of pH on the rate of the reaction between $[Cr(\eta^3\text{-ada})(\eta^2\text{-Hada})(H_2O)]$ and NCS^- was also investigated, the observed rate constants are listed in **Table 5.2**.

Table 5.2: Observed rate constants for the reaction between $[Cr(\eta^3\text{-ada})(\eta^2\text{-Hada})(H_2O)]$ and NCS^- at different pH values, T = 25°C, λ = 295nm, μ = 5.0 x 10^{-2} M ($NaClO_4$).

pH	(10^2) k_{obs}
1.45	18.2(4)
1.07	17.5(2)
0.80	17.7(2)
0.51	17.1(3)

NCS^- dependence

The total rate law for the substitution reaction of $[Cr(\eta^3\text{-ada})(\eta^2\text{-Hada})(H_2O)]$ with NCS^- (see (II) in **Scheme 5.1**) is given by Equation 5.6.

$$\mathbf{R = k_2[Cr(\eta^3\text{-ada})(\eta^2\text{-Hada})(H_2O)][NCS^-] - k_{-2}[Cr(\eta^3\text{-ada})(\eta^2\text{-Hada})(NCS)]} \quad \mathbf{(5.6)}$$

The observed rate constant (k_{obs}) can be derived from Equation 5.6 and is given by Equation 5.7.

$$\mathbf{k_{obs} = k_2[NCS^-] + k_{-2}} \quad \mathbf{(5.7)}$$

Equation 5.7 predicts linear kinetics and the experimental results obtained in **Figure 5.6** were fitted and these results in conjunction with the activation parameters ($\Delta H^{\#}$ and $\Delta S^{\#}$) are reported in **Table 5.4**.

Plots of k_{obs} vs. $[NCS^-]$ for the substitution reaction at pH 1.0 and at 5.0, 14.7, 25.0 and 35.1°C are shown in **Figure 5.6**. The plots are linear and the k_2 and k_{-2} values were calculated, see **Table 5.4**.

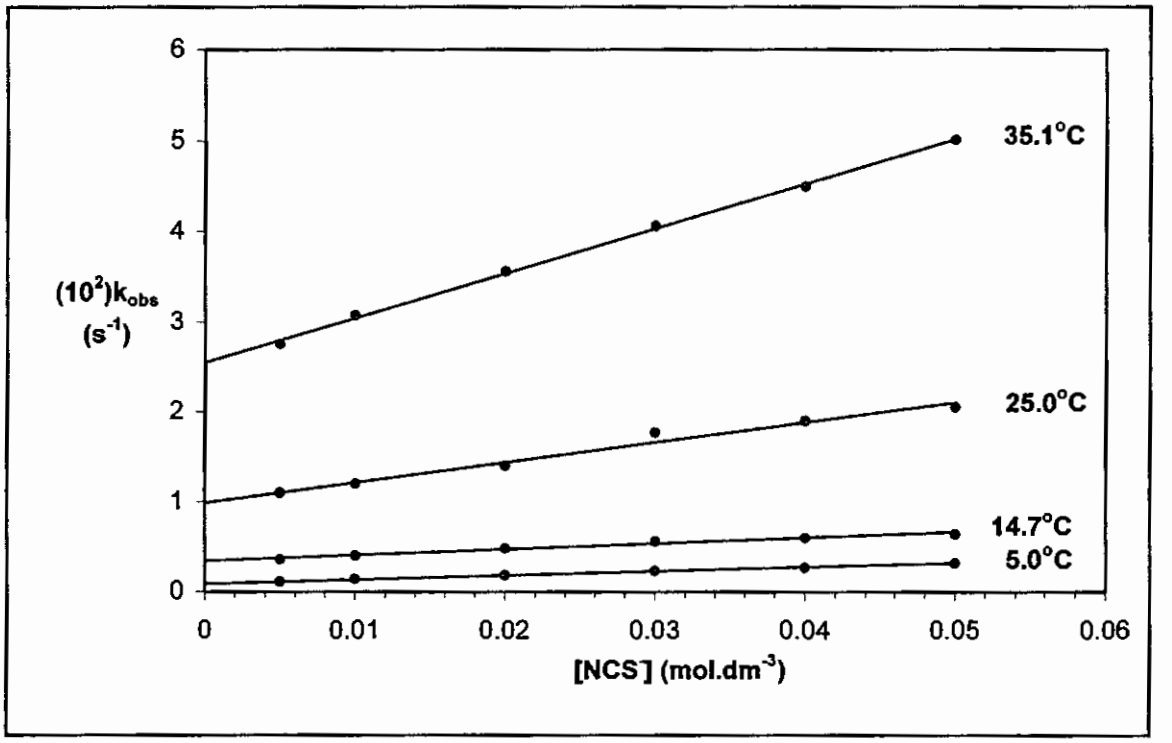

Figure 5.6: Plot of k_{obs} *vs.* [NCS^-] for the reaction between $[Cr(\eta^3\text{-ada})(\eta^2\text{-Hada})(H_2O)]$ and NCS^- at different temperatures, μ = 0.05M ($NaClO_4$), λ = 295 nm, $[Cr(\eta^3\text{-ada})_2]^+$ = 5.0×10^{-4} M.

Combination of H^+/NCS^- dependence

In order to better understand this system another experiment was undertaken in which a solution containing NCS^- at pH = 0.5 was added to a $[Cr(\eta^3\text{-ada})_2]^+$ solution. The UV/VIS spectra were obtained at a low temperature (5°C) in order to try to suppress the ring-opening reaction (see **Figure 5.7**). The observed rate constant for this reaction was calculated as 2.0(3) x 10^{-3} s^{-1}. This rate constant is the same within experimental error as the one obtained for the reaction in which the first reaction was allowed to go to completion before the NCS^- was added (2.3(2) x 10^{-3} s^{-1}).

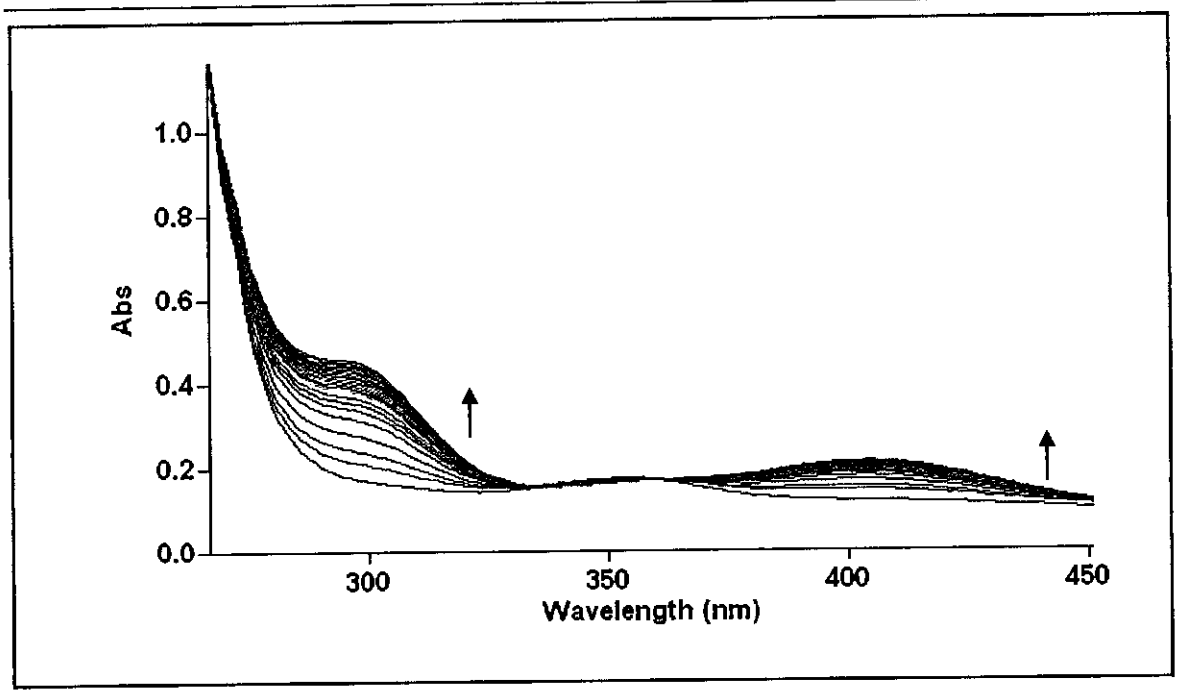

Figure 5.7: UV/VIS spectra of solution containing $[Cr(\eta^3\text{-ada})_2]^+$ (3.0×10^{-3} M) (pH = 0.8) to which a solution of NCS^- (0.03 M) was immediately added. T = 5°C, spectrum obtained every 60 seconds.

5.4 Discussion of kinetic results

A summary of the rate constants and activation parameters for all the reactions that were studied kinetically appear in **Table 5.3** and **Table 5.4**. The kinetic results obtained in this study is discussed in the following paragraphs.

Table 5.3: Summary of the rate constants and activation parameters for the reaction between $[Cr(\eta^3\text{-ada})_2]^-$ and H^+ ions.

Temp (°C)	10.1	19.6	29.3	40.0
k_1 (M^{-1} s^{-1})	0.18(3)	0.43(3)	1.08(2)	2.23(2)
K_a (M)	1.91(3)	1.89(2)	2.12(4)	1.72(2)
pK_a	-0.28	-0.27	-0.33	-0.24
$\Delta H^{\#}$ (k_1) (kJ mol^{-1})	70.0(3)			
$\Delta S^{\#}$ (k_1) (J mol^{-1} K^{-1})	-13.6(3)			

Table 5.4: Summary of the rate constants and activation parameters for the reaction between $[Cr(\eta^3\text{-ada})(\eta^2\text{-Hada})(H_2O)]$ with NCS^- ions.

Temp (°C)	5.0	14.7	25.0	35.1
$(10)k_2$ ($M^{-1}s^{-1}$)	0.45(2)	0.62(3)	2.19(2)	4.96(4)
$(10^2)K_2$ (s^{-1})	0.095(4)	0.32(3)	0.99(2)	2.54(3)
K_1 (M^{-1})[a]	47.2(2)	19.20(1)	22.03(2)	19.53(1)
$\Delta H^{\#}$ (k_2) (kJ mol^{-1})	57.44(3)			
$\Delta S^{\#}$ (k_2) (J mol^{-1})	-65.23(3)			

Overall mechanism

The isolation and characterisation of the starting complex, intermediates and the final products for all of the reactions investigated in this study, made it possible to

postulate a reaction mechanism (see **Scheme 5.1**). One intermediate that was characterised, $[Cr(\eta^3\text{-ada})(\eta^2\text{-Hada})(H_2O)]$, (see Chapter 3, Paragraph 3.4.2) points to the chelate ring-opening of the $[Cr(\eta^3\text{-ada})_2]^-$ complex in solution upon acidification. The final products of the subsequent reactions (H_2ada and $[Cr(H_2O)_6]^{3+}$) (see Chapter 3, Paragraph 3.4.3 and 3.4.4) that were isolated and characterised points to the eventual dissociation of the two ada^{2-} ligands.

The intermediate complex ($[Cr(\eta^3\text{-ada})(\eta^2\text{-Hada})(NCS)]^-$) and final products ($H_2$ada, $[Cr(H_2O)_6]^{3+}$ and KSCN) that were characterised (see Chapter 3, Paragraph 3.4.3, 3.4.4 and 3.4.5) indicate that the coordinated aqua ligand in $[Cr(\eta^3\text{-ada})(\eta^2\text{-Hada})(H_2O)]$ is substituted by NCS^- (see **Scheme 5.1** and Chapter 3, Paragraph 3.4.5).

Chelate ring-opening reaction

It can be seen from the results obtained in the study where strong acids with different weakly coordinated anions were kinetically investigated (see **Table 5.1**) that the observed rate constant remained the same within experimental error upon addition of the different acids. The rates also remained constant with a variation in Cl^- concentration. The increase in k_{obs} with increase in $[H^+]$ clearly indicate that the observed reactions and therefore the study conducted between $[Cr(\eta^3\text{-ada})_2]^-$ and H^+ ions does indeed involve only H^+ ions.

It can be seen from results in **Table 5.3** and **Figure 5.4** that the experimental data fits well with the rate laws (Equation 5.5 and Equation 5.7). The characterisation of the starting complex, intermediates as well as the final products of these reactions (see Chapter 3) also confirm this postulation and we conclude that **Scheme 5.1** and **Scheme 5.3** is a fair representation of the mechanism of the reaction between $[Cr(\eta^3\text{-ada})_2]^-$ and H^+ ions.

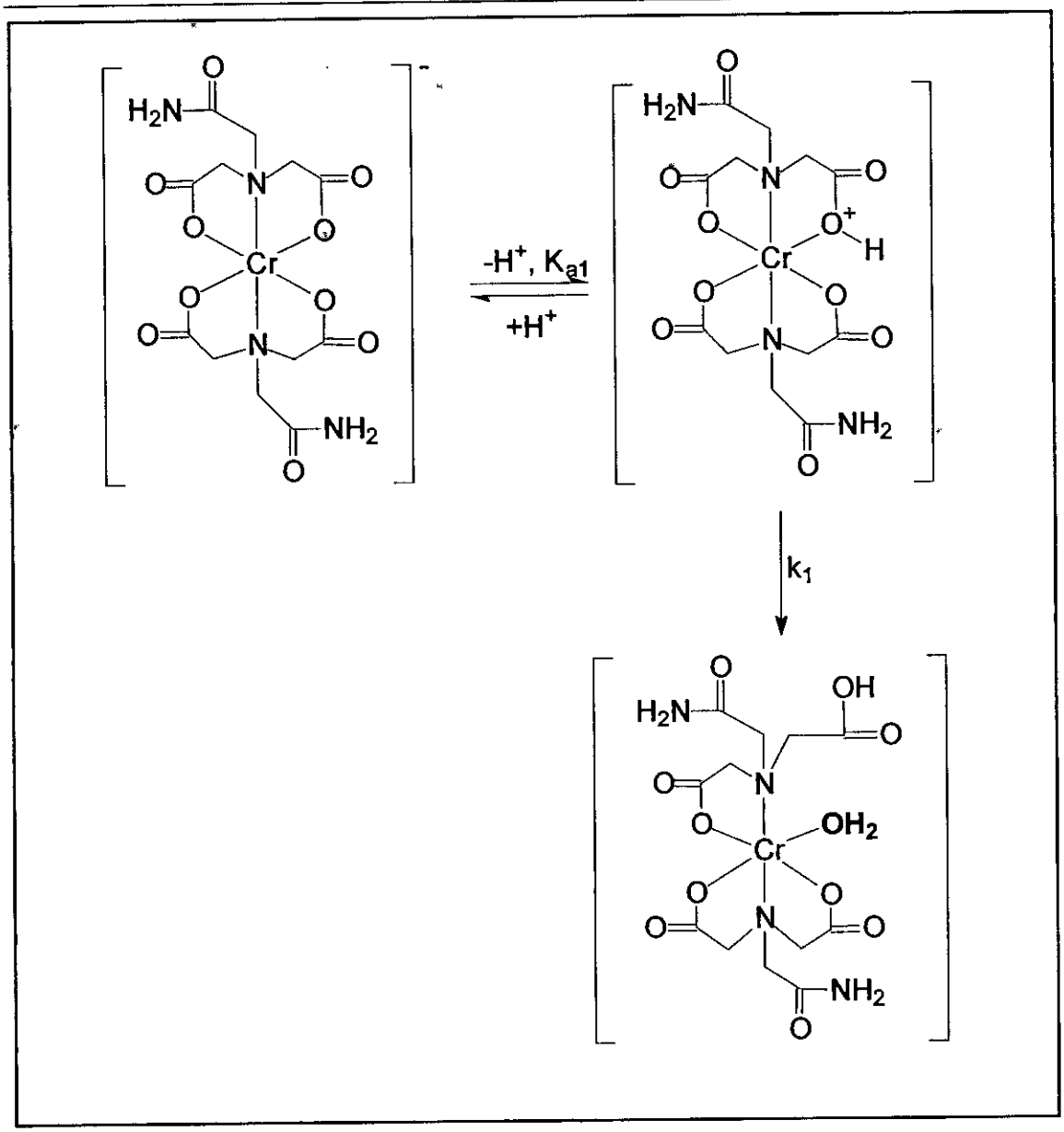

Scheme 5.3: Chelate ring-opening reaction of $[Cr(\eta^3\text{-ada})_2]^-$ upon addition of H^+ ions.

It was possible to calculate the first acid dissociation constant for $[Cr(\eta^3\text{-ada})_2]^-$ from the kinetic data. The calculated K_{a1} values are relatively constant as can be seen in **Table 5.3**. These values all indicate that the $[Cr(\eta^3\text{-ada})_2]^-$ complex is a relatively strong acid, comparing with trifluoroacetic acid which has a pK_a of -0.25 (*web.chem.ucla.edu*). A very low pK_a value like this indicates that the electron density of the carboxylate oxygens are not readily available for bond

formation with protons which are most probably due to the relative high oxidation state of the Cr ion which necessitates strong metal-oxygen bonds.

The value of k_1 (4.34(4) × 10^{-1} $M^{-1}s^{-1}$ at 19.6°C) is higher than the value calculated for a similar reaction between $[Cr(\eta^4\text{-nta})(H_2O)_2]$ and H^+ ions (k_1 = 12.7(3) × 10^{-3} $M^{-1}s^{-1}$ at 25,1°C) (Visser *et al.*, 1994:1051). As mentioned earlier ligands such as nta^{3-} and ada^{2-} have a labilising effect on metal complexes due to their electron donating ability. More electron density is donated to the chromium(III) centre in the $[Cr(\eta^3\text{-ada})_2]^-$ complex than in the $[Cr(\eta^4\text{-nta})(H_2O)_2]$ complex due to the fact that there are two electron donating ligands (ada^{2-}) in the first complex and only one (nta^{3-}) in the second.

The values for $\Delta H^{\#}$ and $\Delta S^{\#}$ for the ring-opening reaction in the reaction of $[Cr(\eta^3\text{-ada})_2]^-$ with H^+ is 70.0(3) kJ mol^{-1} and -13.6(3) J mol^{-1} K^{-1}, respectively. In contrast to the activation enthalpy ($\Delta H^{\#}$), the activation entropy ($\Delta S^{\#}$) supplies more information regarding the reaction mechanism. Positive $\Delta S^{\#}$ values are indicative of a dissociative mechanism while negative $\Delta S^{\#}$ values indicate an associative mechanism in most cases. The negative $\Delta S^{\#}$ suggests a I_a mechanism, but the fact that this value is quite low means that no definite conclusions can be made. Additional information such as high pressure kinetic studies are necessary in order to establish the intimate mechanism for this reaction.

Substitution reaction of $[Cr(\eta^3\text{-ada})(\eta^2\text{-Hada})(H_2O)]$ with NCS^-

The results obtained for the substitution reaction between $[Cr(\eta^3\text{-ada})(\eta^2\text{-Hada})(H_2O)]$ and NCS^- at different pH values are indicated in **Table 5.2**. These results point to only one reactive Cr(III)-ada species at these different pH values. Since the first reaction was allowed to go to completion, it implies that the reactive species is $[Cr(\eta^3\text{-ada})(\eta^2\text{-Hada})(H_2O)]$ as indicated in

Scheme 5.4 and that a further change in pH (at this time scale) does not change the Cr(III)-ada species to any other species.

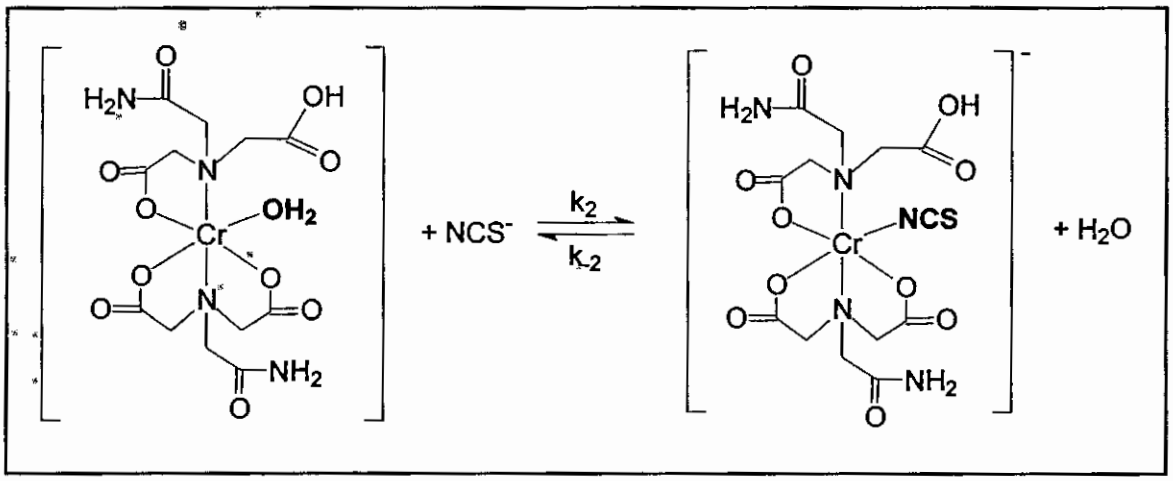

Scheme 5.4: Substitution reaction of $[Cr(\eta^3\text{-ada})(\eta^2\text{-Hada})(H_2O)]$ with NCS^-.

It is again clear From **Table 5.4** and the preceding figures that the experimental data fits well with the rate law (Equation 5.9) and we conclude that **Scheme 5.1** is a fair representation of the mechanism of the substitution reaction between $[Cr(\eta^3\text{-ada})(\eta^2\text{-Hada})(H_2O)]$ and NCS^- ions also depicted in **Scheme 5.4.**

The stability constant, K_1, of $[Cr(\eta^3\text{-ada})(\eta^2\text{-Hada})(NCS)]^-$ at 25°C was calculated as 22.03 M^{-1}. This value is almost 120 times smaller than the similar value obtained for $[Co(TPPS)(H_2O)(NCS)]^{4-}$ and 290 times smaller than the value obtained for the formation of $[Co(TmpyP)(H_2O)(NCS)]^{4+}$ (2.6(4) × 10^3 M^{-1} and 6.4(2) × 10^3 M^{-1}, respectively (Ashley & Leipoldt, 1981:2326). The increase in stability for the porphyrine complexes is probably due to the fact that the formal charge of these complexes is spread over a very large planar surface area, which does not exist for the ada^{2-} and nta^{3-} complexes.

The value of k_2 (2.19(2) × 10^{-1} $M^{-1}s^{-1}$) at 25°C is almost 40 times faster than the value calculated for the reaction of $[Cr(\eta^4\text{-nta})(H_2O)_2]$ and NCS^- ions (k_1 = 5.8(2) × 10^{-3} $M^{-1}s^{-1}$ at 24.7°C, Visser *et al.*, 1994:1051) and 10^5 times of

orders faster than the reactions of $[Cr(NH_3)_5(H_2O)]^{3+}$ with NCS^- ions ($k_1 = 4.6 \times 10^{-5}$ $M^{-1}s^{-1}$ at 25.0°C, Duffy & Early *et al.*, 1967:272) (see **Table 5.5**). Interestingly the k_2 for this study, with two ada^{2-} ligands partially bonded to the metal(III) centre, is slightly higher than the value obtained for the reaction between $[Cr(TPPS)(H_2O)_2]^{3-}$ and NCS^- ions with $k_1 = 4.67\times 10^{-3}$ $M^{-1}s^{-1}$ at 24.7°C (Ashley *et al.*, 1980:1608) (see **Table 5.5**). This indicates that the ada^{2-} ligand exerts a very high degree of labilisation on the chromium(III) complexes. This labilisation can be contributed to the fact that ada^{2-} donates electron density to the central metal ion which in turn weakens the metal-aqua bond. This also indicates that the electron donating ability of the two ada^{2-} ligands in $[Cr(\eta^3\text{-ada})(\eta^2\text{-Hada})(NCS)]^-$ is in the same order of magnitude of the porphyrine ligand. This trend was also observed for the similar Co(III)-nta complexes (Visser *et al.*, 2002:461).

Table 5.5: The rate constants for substitution reaction between the various Cr(III) complexes and NCS^-.

	Temp (°C)	k ($M^{-1}s^{-1}$)	References
$[Cr(\eta^4\text{-nta})(H_2O)_2]^-$	24.7	$5.8(2) \times 10^{-3}$	Visser *et al.* (1994:1051)
$[Cr(NH_3)_5(H_2O)]^{3+}$	25.0	4.6×10^{-5}	Duffy & Early *et al.* (1967:272)
$[Cr(TPPS)(H_2O)_2]^{3-}$	24.7	$2.6(4) \times 10^{-3}$	Ashley *et al.* (1980:1608)
$[Cr(\eta^3\text{-ada})(\eta^2\text{-Hada})(H_2O)]$	25.0	$2.2(2) \times 10^{-1}$	This study

The values for $\Delta H^{\#}$ and $\Delta S^{\#}$ for the substitution reaction of the aqua ligand (k_2) in the reaction of $[Cr(\eta^3\text{-ada})(\eta^2\text{-Hada})(H_2O)]$ with NCS^- ions are 57.4(2) kJ mol^{-1} and 65.2(3) J mol^{-1} K^{-1} respectively. The negative value for $\Delta S^{\#}$ suggests a I_a mechanism. Additional information such as high pressure kinetic studies are necessary in order to establish the intimate mechanism of substitution for Cr(III)-ada complexes.

Combination of H^+/NCS^- dependence

The rate constant for the simultaneous addition of H^+ and NCS^- ions to $[Cr(\eta^3\text{-ada})_2]^-$ is the same within experimental error as the one obtained for the same reaction in which the first reaction was allowed to go to completion before the NCS^- was added. This indicates that the NCS^- ligand does not react with the protonated species, $[Cr(\eta^3\text{-ada})(\eta^3\text{-Hada})]$, but rather with $[Cr(\eta^3\text{-ada})(\eta^2\text{-Hada})(H_2O)]$. The k_1 values at different temperatures (see **Table 5.3**) is 10 times larger than the values of k_2 at different temperatures (see **Table 5.4**) when the two reactions are separated (see Paragraph 3.4). This indicates that the concentration of the reactive species, $[Cr(\eta^3\text{-ada})(\eta^2\text{-Hada})(H_2O)]$, is constant when the substitution reaction with NCS^- ions occurs. A steady-state approximation can be assumed to be occurring during this experiment and the reaction rate is largely dependent on the NCS^- concentration. This in turn means that the total rate law is the same as the one for the substitution reaction with NCS^- ions after the first reaction was allowed to go to completion (see Equation 5.6).

5.5 Conclusion

1) N-carbamoylmethyl-iminodiacetic acid (H_2ada) is an electron rich species and is a close analogue of Nitrilotriacetic acid (H_3nta). It has been shown that this type of species, when coordinated to inert metal centers like Cr(III) will greatly enhance the reactivity of these complexes (Visser *et al.*,1994:1051). The reason for this is that the electron density is donated to the Cr(III) metal center, making it react more like the labile Cr(II) species.

2) The extra electron density on the metal centre gives it more of a Cr(II), d^4 character.

6 Critical evaluation

In this chapter...

The successes of this study and the future research possibilities are discussed in this chapter.

All the initial aims of this study have been met to a large extent. The synthesis and characterisation of $Cs[Cr(\eta^3\text{-ada})_2]\cdot 2H_2O$ by means of IR, UV/VIS and X-ray crystallography has given much needed information on metal(III)-ada complexes. The various Cr(III)-ada complexes that have been isolated and characterised (Chapter 3 and 4) can successfully be used as biological model complexes in future studies.

The synthesis of $Cs[Cr(\eta^3\text{-ada})_2]\cdot 2H_2O$ is the first metal(III)-ada complex and only the second in which ada^{2-} acts as a tridentate ligand. It is also the first known structure which has two ada^{2-} ligands bonded to a metal centre.

The strain experienced by the glycinato rings of tridentate bonded ada^{2-} has been investigated. Comparisons with other studies have been attempted for the first time.

Due to the uncoordinated $CONH_2$ groups in the $[Cr(\eta^3\text{-ada})_2]^-$ complex, the ability of this complex to act as a ligand in other complexes will also be investigated in future studies.

The study of the pH dependence of $[Cr(\eta^3\text{-ada})_2]^-$ was successful and the acid dissociation reaction constant was determined. The study of the ring-opening reaction of $[Cr(\eta^3\text{-ada})_2]^-$ upon addition of H^+ at different temperatures was successful in that a possible reaction mechanism could be postulated.

The study of the substitution reactions between $[Cr(\eta^3\text{-ada})(\eta^2\text{-Hada})(H_2O)]$ and thiocyanide ions at different temperatures was successfully undertaken.

High pressure kinetic studies will provide more information on the intimate reaction mechanism for the ring-opening and substitution reactions in future studies.

Appendix A: Supplementary data

Section I Crystal data

Crystal data for $Cs[Cr(\eta^3\text{-ada})_2]\cdot 2H_2O$

Table A.1: Atomic coordinates (x 104) and equivalent isotropic displacement parameters (Å2x 103) for 2m_hv2_a. U(eq) is defined as one third of the trace of the orthogonalized Uij tensor.

Atom	x	y	z	U(eq)
Cr	4993(1)	125(1)	2576(1)	18(1)
Cs	1933(1)	2264(1)	705(1)	35(1)
N(1)	3736(3)	977(2)	3336(1)	18(1)
N(2)	39(3)	264(3)	3930(2)	37(1)
N(3)	6224(3)	-736(2)	1814(1)	18(1)
N(4)	9925(3)	-115(3)	1206(2)	35(1)
O(1)	6524(2)	155(2)	3417(1)	33(1)
O(2)	7059(2)	690(2)	4623(1)	35(1)
O(3)	5525(2)	1615(2)	2273(1)	31(1)
O(4)	4724(3)	3342(2)	2202(2)	37(1)
O(5)	1490(3)	1723(2)	4262(2)	38(1)
O(6)	3472(2)	119(2)	1728(1)	29(1)
O(7)	2929(3)	-357(2)	516(1)	43(1)
O(8)	4431(2)	-1365(2)	2877(1)	28(1)
O(9)	4989(3)	-3143(2)	2793(1)	33(1)
O(10)	8461(3)	-1585(2)	942(1)	34(1)
C(1)	4635(3)	994(3)	4088(2)	30(1)
C(2)	6202(3)	591(3)	4049(2)	24(1)
C(3)	3530(4)	2105(3)	3004(2)	28(1)
C(4)	4672(3)	2402(3)	2457(2)	24(1)
C(5)	2328(3)	382(3)	3374(2)	28(1)
C(6)	1246(3)	864(3)	3904(2)	25(1)

Table A.1 Continued

C(7)	5326(4)	-778(3)	1061(2)	32(1)
C(8)	3790(3)	-314(3)	1092(2)	26(1)
C(9)	6455(4)	-1849(3)	2166(2)	29(1)
C(10)	5204(3)	-2166(3)	2643(2)	23(1)
C(11)	7632(3)	-141(3)	1758(2)	26(1)
C(12)	8706(3)	-697(3)	1258(2)	23(1)
O(11)	5160(4)	2351(4)	574(2)	89(1)
O(12)	-1450(4)	2138(2)	372(3)	101(2)
Cr	4993(1)	125(1)	2576(1)	18(1)
Cs	1933(1)	2264(1)	705(1)	35(1)
N(1)	3736(3)	977(2)	3336(1)	18(1)
N(2)	39(3)	264(3)	3930(2)	37(1)
N(3)	6224(3)	-736(2)	1814(1)	18(1)

Table A.2: Bond angles (°) for $Cs[Cr(\eta^3\text{-ada})_2]\cdot 2H_2O$

Bond	Angle (°)	Bond	Angle (°)
O(1)- Cr- O(6)	179.00(11)	C(1)-N(1)-Cr	105.78(17)
O(1)-Cr-O(3)	90.43(11)	C(6)-N(2)-H(2A)	122(3)
O(6)-Cr-O(3)	88.57(10)	C(6)-N(2)-H(2B)	118(3)
O(1)-Cr-O(8)	90.18(11)	H(2A)-N(2)-H(2B)	120(3)
O(6)-Cr-O(8)	90.82(10)	C(11)-N(3)-C(9)	111.8(2)
O(3)-Cr-O(8)	179.21(10)	C(11)-N(3)-C(7)	112.2(2)
O(1)-Cr-N(3)	95.67(9)	C(9)-N(3)-C(7)	112.5(3)
O(1)-Cr-N(3)	84.36(9)	C(11)-N(3)-Cr	108.22(18)
O(6)-Cr-N(3)	97.51(9)	C(9)-N(3)-Cr	104.76(17)
O(3)-Cr-N(3)	82.92(9)	C(7)-N(3)-Cr	106.95(18)
O(8)-Cr-N(3)	84.87(9)	C(12)-N(4)-Cs#5	153.9(2)
O(1)-Cr-N(1)	95.10(9)	C(12)-N(4)-H(4A)	122(3)
O(6)-Cr-N(1)	82.90(9)	Cs#5-N(4)-H(4A)	74(3)
O(3)-Cr-N(1)	96.66(9)	C(12)-N(4)-H(4B)	117(3)
O(8)-Cr-N(1)	179.31(10)	Cs#5-N(4)-H(4B)	57(3)
N(3)-Cr-N(1)	88.90(8)	H(4A)-N(4)-H(4B)	120(3)
O(11)-Cs-O(10)#1	164.82(11)	C(2)-O(1)-Cr	117.3(2)
O(11)-Cs-O(12)	76.30(10)	C(2)-O(2)-Cs#6	121.3(2)
O(10)#1-Cs-O(12)	80.90(10)	C(4)-O(3)-Cr	116.61(19)

Table A.2 Continued

O(11)-Cs-O(2)#2	69.10(6)	C(4)-O(4)-Cs	83.45(19)
O(10)#1-Cs-O(2)#2	90.54(7)	C(8)-O(6)-Cr	117.6(2)
O(12)-Cs-O(2)#2	118.31(8)	C(8)-O(6)-Cs	88.30(18)
O(11)-Cs-O(8)#3	146.68(6)	Cr-O(6)-Cs	129.63(10)
O(10)#1-Cs-O(8)#3	74.70(9)	C(8)-O(7)-Cs	92.3(2)
O(12)-Cs-O(8)#3	95.06(6)	C(10)-O(8)-Cr	116.58(19)
O(2)#2-Cs-O(8)#3	131.12(8)	C(10)-O(8)-Cs#7	96.20(17)
O(11)-Cs-O(9)#3	133.74(6)	Cr-O(8)-Cs#7	141.82(10)
O(10)#1-Cs-O(9)#3	63.73(9)	C(10)-O(9)-Cs#7	97.46(19)
O(12)-Cs-O(9)#3	130.18(6)	C(12)-O(10)-Cs#1	133.0(2)
O(2)#2-Cs-O(9)#3	39.27(5)	N(1)-C(1)-C(2)	114.3(2)
O(8)#3-Cs-O(9)#3	75.27(10)	N(1)-C(1)-H(1A)	108.7
O(11)-Cs-O(7)	69.81(6)	C(2)-C(1)-H(1A)	108.7
O(10)#1-Cs-O(7)	102.14(7)	N(1)-C(1)-H(1B)	108.7
O(12)-Cs-O(7)	132.37(6)	C(2)-C(1)-H(1B)	108.7
O(2)#2-Cs-O(7)	132.54(6)	H(1A)-C(1)-H(1B)	107.6
O(8)#3-Cs-O(7)	179.00(11)	O(2)-C(2)-O(1)	124.7(3)
O(9)#3-Cs-O(7)	95.89(6)	O(2)-C(2)-C(1)	118.4(3)
O(11)-Cs-O(6)	72.29(9)	O(1)-C(2)-C(1)	116.9(3)
O(10)#1-Cs-O(6)	108.02(6)	O(1)-C(2)-Cs#6	151.2(2)
O(12)-Cs-O(6)	115.19(7)	C(1)-C(2)-Cs#6	81.98(17)
O(2)#2-Cs-O(6)	153.13(6)	N(1)-C(3)-C(4)	113.0(2)
O(8)#3-Cs-O(6)	98.97(5)	N(1)-C(3)-H(3A)	109.0
O(9)#3-Cs-O(6)	72.10(5)	C(4)-C(3)-H(3A)	109.0
O(7)-Cs-O(6)	38.39(5)	N(1)-C(3)-H(3B)	109.0
O(11)-Cs-N(4)#4	125.43(10)	C(4)-C(3)-H(3B)	109.0
O(10)#1-Cs-N(4)#4	89.32(7)	H(3A)-C(3)-H(3B)	107.8
O(12)-Cs-N(4)#4	58.75(7)	O(4)-C(4)-O(3)	123.8(3)
O(2)#2-Cs-N(4)#4	146.56(7)	O(4)-C(4)-C(3)	119.9(3)
O(8)#3-Cs-N(4)#4	89.47(6)	O(3)-C(4)-C(3)	116.3(3)
O(9)#3-Cs-N(4)#4	50.83(6)	O(4)-C(4)-Cs	77.88(19)
O(7)-Cs-N(4)#4	53.29(6)	O(3)-C(4)-Cs	98.06(19)
O(6)-Cs-N(4)#4	56.73(7)	N(1)-C(5)-C(6)	93.11(19)
O(11)-Cs-C(8)	65.74(10)	N(1)-C(5)-H(5A)	116.7(3)
O(10)#1-Cs-C(8)	87.76(7)	C(6)-C(5)-H(5A)	108.1

Table A.2 Continued

O(12)-Cs-C(8)	116.15(7)	N(1)-C(5)-H(5B)	108.1
O(2)#2-Cs-C(8)	139.81(7)	C(6)-C(5)-H(5B)	108.1
O(8)#3-Cs-C(8)	119.78(6)	H(5A)-C(5)-H(5B)	108.1
O(9)#3-Cs-C(8)	89.65(6)	O(5)-C(6)-N(2)	107.3
O(7)-Cs-C(8)	19.96(6)	O(5)-C(6)-C(5)	124.5(3)
O(6)-Cs-C(8)	20.90(6)	N(2)-C(6)-C(5)	122.3(3)
N(4)#4-Cs-C(8)	59.69(7)	N(3)-C(7)-C(8)	113.2(3)
O(11)-Cs-C(10)#3	130.16(9)	N(3)-C(7)-H(7A)	113.7(3)
O(10)#1-Cs-C(10)#3	140.94(7)	C(8)-C(7)-H(7A)	108.8
O(12)-C-C(10)#3	64.71(10)	N(3)-C(7)-H(7B)	108.8
O(2)#2-Cs-C(10)#3	111.90(7)	C(8)-C(7)-H(7B)	108.8
O(8)#3-Cs-C(10)#3	20.38(6)	H(7A)-C(7)-H(7B)	108.8
O(9)#3-Cs-C(10)#3	19.40(6)	O(7)-C(8)-O(6)	107.7
O(7)-Cs-C(10)#3	115.05(7)	O(7)-C(8)-C(7)	123.5(3)
O(6)-Cs-C(10)#3	87.40(6)	O(6)-C(8)-C(7)	119.4(3)
N(4)#4-Cs-C(10)#3	69.09(7)	O(7)-C(8)-Cs	117.1(3)
C(8)-Cs-C(10)#3	106.75(7)	O(6)-C(8)-Cs	67.72(19)
O(11)-Cs-O(4)	54.31(8)	C(7)-C(8)-Cs	70.80(17)
O(10)#1-Cs-O(4)	142.49(6)	N(3)-C(9)-C(10)	137.7(2)
O(12)-Cs-O(4)	139.66(9)	N(3)-C(9)-H(9A)	111.6(2)
O(2)#2-Cs-O(4)	95.17(5)	C(10)-C(9)-H(9A)	109.3
O(8)#3-Cs-O(4)	65.04(5)	N(3)-C(9)-H(9B)	109.3
O(9)#3-Cs-O(4)	82.74(6)	C(10)-C(9)-H(9B)	109.3
O(7)-Cs-O(4)	103.05(5)	H(9A)-C(9)-H(9B)	109.3
O(6)-Cs-O(4)	70.64(5)	O(9)-C(10)-O(8)	108.0
N(4)#4-Cs-O(4)	116.55(6)	O(9)-C(10)-C(9)	123.8(3)
C(8)-Cs-O(4)	83.48(6)	O(8)-C(10)-C(9)	116.1(3)
C(10)#3-Cs-O(4)	76.20(6)	O(9)-C(10)-Cs#7	63.13(17)
O(11)-Cs-H(11C)	13.8	O(8)-C(10)-Cs#7	63.43(15)
O(10)#1-Cs-H(11C)	102.7	C(9)-C(10)-Cs#7	161.7(2)
O(12)-Cs-H(11C)	175.5	N(3)-C(11)-C(12)	115.1(3)
O(2)#2-Cs-H(11C)	85.0	N(3)-C(11)-H(11A)	108.5
O(8)#3-Cs-H(11C)	105.0	C(12)-C(11)-H(11A)	108.5
O(9)#3-Cs-H(11C)	118.9	N(3)-C(11)-H(11B)	108.5
O(7)-Cs-H(11C)	81.4	C(12)-C(11)-H(11B)	108.5

Table A.2 Continued

O(6)-Cs-H(11C)	69.3	H(11A)-C(11)-H(11B)	107.5
N(4)#4-Cs-H(11C)	125.7	O(10)-C(12)-N(4)	124.2(3)
C(8)-Cs-H(11C)	68.0	O(10)-C(12)-C(11)	123.1(3)
C(10)#3-Cs-H(11C)	116.4	N(4)-C(12)-C(11)	112.7(3)
O(4)-Cs-H(11C)	40.5	Cs-O(11)-H(11C)	113.9
C(5)-N(1)-C(3)	112.3(2)	Cs-O(11)-H(11D)	120.2
C(5)-N(1)-C(1)	112.7(2)	H(11C)-O(11)-H(11D)	100.2
C(3)-N(1)-C(1)	111.9(3)	Cs-O(12)-H(12A)	123.5
C(5)-N(1)-Cr	108.10(18)	Cs-O(12)-H(12B)	122.8
C(3)-N(1)-Cr	105.38(17)	H(12A)-O(12)-H(12B)	102.8

Symmetry transformations used to generate equivalent atoms:

$1^{\#}$ -x,-y,-z

$2^{\#}$ -x+1,-y+2,-z+1

$3^{\#}$ -x+1,-y+1,-z+2

Table A.3: Bond lengths (Å) for $Cs[Cr(\eta^3\text{-ada})_2]\cdot 2H_2O$.

Bond	Length (Å)	Bond	Length (Å)
Cr-O(1)	1.949(2)	O(3)-C(4)	1.289(4)
Cr-O(6)	1.952(2)	O(4)-C(4)	1.226(4)
Cr-O(3)	1.956(2)	O(5)-C(6)	1.227(4)
Cr-O(8)	1.961(2)	O(6)-C(8)	1.283(4)
Cr-N(3)	2.090(2)	O(7)-C(8)	1.228(4)
Cr-N(1)	2.096(2)	O(8)-C(10)	1.288(4)
Cs-O(11)	2.980(4)	O(8)-Cs#7	3.308(2)
Cs-O(10)#1	2.988(2)	O(9)-C(10)	1.232(4)
Cs-O(12)	3.107(4)	O(9)-Cs#7	3.308(2)
Cs-O(2)#2	3.128(2)	O(10)-C(12)	1.223(4)
Cs-O(8)#3	3.308(2)	O(10)-Cs#1	2.988(2)
Cs-O(9)#3	3.308(2)	C(1)-C(2)	1.521(4)
Cs-O(7)	3.330(3)	C(1)-H(1A)	0.9700
Cs-O(6)	3.398(2)	C(1)-H(1B)	0.9700
Cs-N(4)#4	3.566(3)	C(2)-Cs#6	3.910(3)
Cs-C(8)	3.596(3)	C(3)-C(4)	1.515(4)
Cs-C(10)#3	3.677(3)	C(3)-H(3A)	0.9700
Cs-O(4)	3.743(3)	C(3)-H(3B)	0.9700

Table A.3 Continued

Cs-H(11C)	3.4450	C(5)-C(6)	1.523(4)
N(1)-C(5)	1.483(4)	C(5)-H(5A)	0.9700
N(1)-C(3)	1.492(4)	C(5)-H(5B)	0.9700
N(1)-C(1)	1.494(4)	C(7)-C(8)	1.519(4)
N(2)-C(6)	1.327(4)	C(7)-H(7A)	0.9700
N(2)-H(2A)	0.818(19)	C(7)-H(7B)	0.9700
N(2)-H(2B)	0.819(19)	C(9)-C(10)	1.517(4)
N(3)-C(11)	1.486(4)	C(9)-H(9A)	0.9700
N(3)-C(9)	1.492(4)	C(9)-H(9B)	0.9700
N(3)-C(7)	1.497(4)	C(10)-Cs#7	3.677(3)
N(4)-C(12)	1.329(4)	C(11)-C(12)	1.523(4)
N(4)-Cs#5	3.566(3)	C(11)-H(11A)	0.9700
N(4)-H(4A)	0.818(19)	C(11)-H(11B)	0.9700
N(4)-H(4B)	0.817(19)	O(11)-H(11C)	0.9004
O(1)-C(2)	1.279(4)	O(11)-H(11D)	0.9246
O(2)-C(2)	1.229(4)	O(12)-H(12A)	0.9048
O(2)-Cs#6	3.128(2)	O(12)-H(12B)	0.9161

Table A.4: Anisotropic displacement parameters ($Å^2 \times 10^3$) for $Cs[Cr(\eta^3\text{-ada})_2]\cdot 2H_2O$.

Atom	U_{11}	U_{22}	U_{33}	U_{23}	U_{13}	U_{12}
Cr	16(1)	18(1)	19(1)	-3(1)	4(1)	0(1)
Cs	45(1)	33(1)	27(1)	2(1)	6(1)	3(1)
N(1)	16(1)	18(1)	21(1)	-1(1)	3(1)	1(1)
N(2)	25(2)	44(2)	44(2)	-11(2)	16(1)	-6(1)
N(3)	16(1)	19(1)	21(1)	-2(1)	4(1)	0(1)
N(4)	27(2)	33(2)	49(2)	-8(1)	21(1)	-4(1)
O(1)	22(1)	52(2)	26(1)	-14(1)	1(1)	7(1)
O(2)	28(1)	49(2)	27(1)	-6(1)	-4(1)	5(1)
O(3)	33(1)	23(1)	41(1)	-1(1)	18(1)	-1(1)
O(4)	43(2)	25(1)	45(2)	14(1)	12(1)	4(1)
O(5)	34(1)	36(2)	46(2)	-16(1)	15(1)	-2(1)
O(6)	22(1)	43(1)	24(1)	-7(1)	1(1)	8(1)
O(7)	30(1)	70(2)	28(1)	-12(1)	-7(1)	12(1)
O(8)	27(1)	24(1)	36(1)	3(1)	16(1)	3(1)

Table A.4 Continued

O(9)	34(1)	21(1)	44(1)	7(1)	11(1)	-1(1)
O(10)	32(1)	32(1)	38(1)	-13(1)	10(1)	-2(1)
C(1)	26(2)	46(2)	19(2)	-5(2)	2(1)	8(2)
C(2)	22(2)	25(2)	24(2)	1(1)	1(1)	-1(1)
C(3)	31(2)	20(2)	34(2)	3(1)	10(1)	7(1)
C(4)	22(2)	26(2)	24(2)	0(1)	-2(1)	-1(1)
C(5)	20(2)	25(2)	39(2)	-8(1)	9(1)	-5(1)
C(6)	22(2)	27(2)	26(2)	0(1)	4(1)	4(1)
C(7)	25(2)	47(2)	24(2)	-10(2)	-1(1)	7(2)
C(8)	23(2)	29(2)	25(2)	-1(1)	2(1)	1(1)
C(9)	27(2)	21(2)	41(2)	3(1)	13(1)	4(1)
C(10)	22(2)	24(2)	23(2)	1(1)	1(1)	-1(1)
C(11)	21(2)	24(2)	34(2)	-8(1)	11(1)	-4(1)
C(12)	22(2)	27(2)	21(2)	1(1)	6(1)	3(1)
O(11)	67(2)	149(4)	53(2)	-9(2)	18(2)	-26(2)
O(12)	58(2)	110(3)	131(4)	59(3)	-16(2)	-11(2)

Table A.5: Hydrogen coordinates (x 10^4) and isotropic displacement parameters ($Å^2$ x 10^3) for $Cs[Cr(\eta^3\text{-ada})_2]\cdot 2H_2O$.

Atom	x	y	z	U(eq)
H(2A)	-640(30)	450(30)	4180(20)	44
H(2B)	-40(40)	-290(20)	3660(20)	44
H(4A)	10600(30)	-340(30)	970(20)	42
H(4B)	10040(40)	420(20)	1490(20)	42
H(1A)	4158	537	4449	36
H(1B)	4660	1742	4284	36
H(3A)	3571	2639	3419	34
H(3B)	2564	2152	2734	34
H(5A)	2546	-369	3537	33
H(5B)	1847	347	2860	33
H(7A)	5254	-1539	890	39
H(7B)	5828	-367	684	39
H(9A)	7367	-1852	2490	35

Table A.5 Continued

H(9B)	6537	-2392	1764	35
H(11A)	8105	-55	2271	31
H(11B)	7418	591	1556	31
H(11C)	5675	2599	999	134
H(11D)	5541	2792	207	134
H(12A)	-1920	1550	149	151
H(12B)	-2002	2720	182	151

Table A.6: Hydrogen bonds for $Cs[Cr(\eta^3\text{-ada})_2].2H_2O$ (Å and °).

D-H...A	d(D-H) (Å)	d(H...A) (Å)	d(D...A) (Å)	<(DHA) (°)
O(12)-H(12B)...O(5)#2	0.92	2.14	2.940(4)	145.1
O(12)-H(12A)...O(7)#8	0.90	2.03	2.928(4)	170.7
O(11)-H(11D)...O(5)#9	0.92	2.01	2.904(4)	161.6
O(11)-H(11C)...O(3)	0.90	2.54	3.093(4)	120.3
O(11)-H(11C)...O(4)	0.90	2.50	3.142(4)	128.2
N(4)-H(4B)...O(9)#10	0.817(19)	2.15(2)	2.960(4)	172(4)
N(4)-H(4A)...O(7)#5	0.818(19)	2.33(2)	3.100(4)	157(3)
N(2)-H(2B)...O(4)#7	0.819(19)	2.28(2)	3.076(4)	165(4)
N(2)-H(2A)...O(2)#4	0.818(19)	2.32(2)	3.111(4)	164(3)

Symmetry transformations used to generate equivalent atoms:

1# -x,-y,-z

2# -x+1,-y+2,-z+1

3# -x+1,-y+1,-z+2

4# x,y-1,z

5# -x+1,-y,-z+1

6# -x+1,-y+1,-z+1

7# -x,-y,-z+1

8# -x,-y+1,-z

Crystal data for H_2ada

Table A.7: Atomic coordinates (x 10^4) and equivalent isotropic displacement parameters (A^2 x 10^3) for ada^{2-}. U(eq) is defined as one third of the trace of the orthogonalized Uij tensor.

Atom	X	Y	Z	U(eq)
O(2)	7004(1)	3873(1)	1736(1)	38(1)
O(4)	7696(2)	533(1)	1396(1)	39(1)
O(3)	4222(2)	4080(1)	976(2)	45(1)
O(1)	10287(2)	2670(1)	693(1)	45(1)
O(5)	6510(2)	-708(1)	-560(2)	44(1)
N(1)	7096(2)	2422(1)	-517(2)	26(1)
N(2)	10708(2)	3744(2)	-1264(2)	47(1)
C(3)	5419(2)	2806(1)	-461(2)	31(1)
C(1)	7893(2)	3302(1)	-1298(2)	29(1)
C(5)	7060(2)	1217(1)	-1199(2)	35(1)
C(6)	7065(2)	257(1)	-36(2)	30(1)
C(4)	5514(2)	3666(1)	848(2)	31(1)
C(2)	9767(2)	3200(1)	-547(2)	32(1)

Table A.8: Bond angles (°) for H_2ada.

Bond	Angle (°)	Bond	Angle (°)
C(4)-O(2)-H(2	109.5	N(1)-C(1)-H(1A)	110.3
C(1)-N(1)-C(3)	112.62(11)	C(2)-C(1)-H(1A)	110.3
C(1)-N(1)-C(5)	112.08(12)	N(1)-C(1)-H(1B)	110.3
C(3)-N(1)-C(5)	112.26(12)	C(2)-C(1)-H(1B)	110.3
C(1)-N(1)-H(34)	105.2(12)	H(1A)-C(1)-H(1B)	108.6
C(3)-N(1)-H(34)	109.3(13)	N(1)-C(5)-C(6)	112.39(12)
C(5)-N(1)-H(34)	104.8(12)	N(1)-C(5)-H(5A)	109.1
C(2)-N(2)-H(1)	117.1(15)	C(6)-C(5)-H(5A)	109.1
C(2)-N(2)-H(2)	114.5(17)	N(1)-C(5)-H(5B)	109.1
H(1)-N(2)-H(2)	126(2)	C(6)-C(5)-H(5B)	109.1
N(1)-C(3)-C(4)	112.77(12)	H(5A)-C(5)-H(5B)	107.9
N(1)-C(3)-H(3A)	109.0	O(5)-C(6)-O(4)	126.96(14)
C(4)-C(3)-H(3A)	109.0	O(5)-C(6)-C(5)	117.20(14)
N(1)-C(3)-H(3B)	109.0	O(4)-C(6)-C(5)	115.80(13)

Table A.8 Continued

H(3A)-C(3)-H(3B)	107.8	O(3)-C(4)-C(3)	118.87(14)
N(1)-C(1)-C(2)	107.05(12)	O(2)-C(4)-C(3)	114.39(13)
O(1)-C(2)-N(2)	125.01(16)	N(2)-C(2)-C(1)	116.31(14)
O(1)-C(2)-C(1)	118.61(14)		

Table A.9: Bond lengths (Å) for H_2ada.

Bond	Length (Å)	Bond	Length (Å)
O(2)-C(4)	1.2885(19)	N(2)-H(1)	0.85(2)
O(2)-H(2)	0.8200(2)	N(2)-H(2)	0.85(3)
O(4)-C(6)	1.2748(18)	C(3)-C(4)	1.513(2)
O(3)-C(4)	1.220(2)	C(3)-H(3A)	0.9700(2)
O(1)-C(2)	1.2259(19)	C(3)-H(3B)	0.9700(2)
O(5)-C(6)	1.2271(19)	C(1)-C(2)	1.520(2)
N(1)-C(1)	1.4914(18)	C(1)-H(1A)	0.9700(2)
N(1)-C(3)	1.492(2)	C(1)-H(1B)	0.9700(2)
N(1)-C(5)	1.4955(19)	C(5)-C(6)	1.510(2)
N(1)-H(34)	0.85(2)	C(5)-H(5A)	0.9700(2)
N(2)-C(2)	1.317(2)	C(5)-H(5B)	0.9700(2)

Table A.10: Anisotropic displacement parameters (A^2 x 10^3) for ada^{2-}. The anisotropic displacement factor exponent takes the form: -2 pi^2 [h^2 a*^2 U11 + ... + 2 h k a* b* U12].

Atom	U11	U22	U33	U23	U13	U12
O(2)	36(1)	43(1)	34(1)	-14(1)	6(1)	1(1)
O(4)	53(1)	35(1)	27(1)	5(1)	7(1)	-4(1)
O(3)	36(1)	50(1)	55(1)	-7(1)	19(1)	2(1)
O(1)	36(1)	63(1)	30(1)	10(1)	0(1)	1(1)
O(5)	62(1)	30(1)	41(1)	-4(1)	19(1)	-9(1)
N(1)	31(1)	25(1)	20(1)	1(1)	5(1)	-2(1)
N(2)	32(1)	64(1)	46(1)	10(1)	13(1)	-5(1)
C(3)	28(1)	32(1)	31(1)	-2(1)	7(1)	-5(1)
C(1)	30(1)	29(1)	25(1)	5(1)	6(1)	-4(1)
C(5)	54(1)	26(1)	26(1)	-2(1)	13(1)	-2(1)
C(6)	33(1)	27(1)	30(1)	2(1)	12(1)	2(1)
C(4)	32(1)	28(1)	32(1)	2(1)	11(1)	-2(1)
C(2)	32(1)	35(1)	26(1)	-3(1)	6(1)	-1(1)

Table A.11: Hydrogen bonds for H_2ada (Å and °).

D-H···A	D-H	H···A	D···A
N(1)-H(34)···O(1)	0.85(2)	2.098(19)	2.5892(18)
N(1)-H(34)···O(2)	0.85(2)	2.285(18)	2.6316
N(1)-H(34)···O(4)	0.85(2)	2.265(18)	2.6999
C(3)-H(3A)···O(5)	0.97	3.55	4.100
C(5)-H(5A)···O(1)	0.97	2.92	3.193
O(2)-H(2)···O(5)	0.819	1.692	2.486

Section II Kinetic data

The tables in this section give the observed first-order rate constant for the reactions described in Chapter 5. Where applicable, the figure number representing a specific data set is included in brackets after the Table number.

Table A.12: (Figure 5.5) Plot of k_{obs} (λ = 405 nm) *vs.* $[H^+]$ for $Cs[Cr(\eta^3\text{-ada})_2]\cdot 2H_2O$ (5.0×10^{-3} M), μ = 0.6 M ($NaClO_4$).

$[H^+]$ (mol.dm^{-3})	(10^2) k_{obs} (s^{-1})			
	10.1 °C	**19.6 °C**	**29.3 °C**	**40.0 °C**
0.05	0.45	1.18	2.43	5.62
0.10	0.93	2.29	4.84	11.04
0.15	1.40	3.08	7.27	16.2
0.26	2.34	5.33	11.6	25.98
0.31	2.71	5.85	13.79	30.1
0.36	2.92	7.05	16.2	34.1
0.41	3.21	8.05	17.36	38.1
0.46	3.44	8.35	19.24	41.65
0.51	3.78	9.22	21.01	

Table A.13: (Figure 5.4) Plot of k_{obs} *vs.* $[NCS^-]$ for first reaction (k_1 step, Scheme 5.5) at different temperatures, μ = 0.05 M ($NaClO_4$), λ = 293 nm, $[Cr(\eta^3\text{-ada})_2]^-$ = 5.0×10^{-4} M.

$[NCS^-]$ (mol.dm^{-3})	(10^3) k_{obs} (s^{-1})			
	5.0 °C	**14.7 °C**	**25.0 °C**	**35.1 °C**
0.005	1.18(2)	3.65(7)	11.12(1)	27.5(5)
0.010	1.41(3)	4.08(1)	12.01(4)	30.8(1)
0.020	1.85(1)	4.88(2)	14.06(2)	35.6(2)
0.030	2.33(1)	5.65(3)	17.70(1)	40.6(2)
0.040	2.75(2)	6.02(2)	19.10(1)	45.0(3)
0.050	3.20(2)	6.41(1)	20.60(1)	50.1(1)

Section III Theoretical aspects of kinetics

Pseudo-first-order reactions (mono-variation)

The rate of a reaction is defined by the change in concentration of any of the reacting species per time unit. For the reaction

$$A + B \xrightarrow{k} C \qquad \textbf{(A.1)}$$

the rate can be expressed in terms of the disappearance of A or B or in terms of the formation of C, as shown in Equation A.2.

$$\text{Rate} = \frac{-d[A]}{dt} = \frac{-d[B]}{dt} = \frac{d[C]}{dt} \qquad \textbf{(A.2)}$$

Equation A.3 is representative of a typical rate law for Reaction A.1, if the rate of the reaction is only dependent on the concentrations of A and B.

$$\text{Rate} = k[A]^a[B]^b \qquad \textbf{(A.3)}$$

In Equation A.3, k represents the rate constant whilst a and b represents the order of the reaction with respect to the concentrations of A and B. The total order of the reaction is given by the sum of a and b. If a reaction proceeds by more than one step, the order of the reaction is determined by the reactions that precede the rate-determining step.

It is often impossible to determine the order of the reaction with respect to the different reactants in one kinetic experiment. The problem can be solved to a large extent by the method of mono-variation (isolation). This type of experiment

is conducted where [A] << [B], which causes [B] to be constant during the whole reaction. The rate of this reaction is presented in Equation A.4.

$$\text{Rate} = k_{obs}[A]^a \quad \textbf{(A.4)}$$

In Equation A.4, k_{obs} is the observed rate constant with

$$k_{obs} = k[B]^b \quad \textbf{(A.5)}$$

It often happens that a = 1, which means that the kinetics of Reaction A.1 simplifies to that of a first order reaction where k_{obs} is the pseudo-first-order rate constant.

In practice k_{obs} is determined at different concentrations of [B]. If the reaction were first-order with respect to [B], a plot of k_{obs} versus [B] would, according to Equation A.5, produce a straight line though the origin. The slope of the graph then gives the second-order rate constant.

If the straight line does not pass through the origin of the graph it indicates that there is a second reaction independent of [B]. The rate of the reaction is then given by Equation A.6.

$$\text{Rate} = k_1[A][B] + k_2[A] \quad \textbf{(A.6)}$$

From Equation A.5 and the above discussion, the pseudo-first-order reaction constant is given by Equation A.6.

$$k_{obs} = k_1[B] + k_2 \quad \textbf{(A.7)}$$

A plot of k_{obs} vs. [B] would produce a straight line with slope k_1 and a section of k_2.

Eyring equation

$$\ln(k/T) = \ln(k_b/h) + (\Delta S^{\#}/R) - (\Delta H^{\#}/RT) \quad \textbf{(A.8)}$$

In Equation A.8, T = Temperature in Kelvin, k_b = Boltzman's constant, h = Planck's constant and R = universal gas constant. The activation parameters $\Delta H^{\#}$ and $\Delta S^{\#}$ can be obtained experimentally from a plot of **ln(k/T)** vs. **(1/T)**. The activation enthalpy, $\Delta H^{\#}$, is calculated from the slope **$\{-\Delta H^{\#}/R\}$** of the graph while the activation entropy, $\Delta S^{\#}$, is calculated from the section **$\{\ln(k_b/h) + (\Delta S^{\#}/R)\}$** of the graph.

Appendix B: Hazardous Chemicals

Ammonium Hydroxide



Physical state; Appearance:

Very volatile, colourless solution of ammonia in water, with pungent odour.

Chemical dangers:

Reacts with many heavy metals and their salts forming explosive compounds. Attacks many metals forming flammable/explosive gas. The solution in water is a strong base, it reacts violently with acids.

Routes of exposure:

The substance can be absorbed into the body by inhalation of its vapour or aerosol and by ingestion.

Inhalation risk:

A harmful contamination of the air can be reached very quickly on evaporation of this substance at 20 °C.

Effects of short-term exposure:

The substance is corrosive to the eyes, the skin and the respiratory tract. Corrosive on ingestion as well. Inhalation of high concentrations of vapour may cause laryngeal oedema, inflammation of the respiratory tract, and pneumonia. The effects may be delayed.

Effects of long-term exposure:

Lungs may be affected by repeated or prolonged exposure to the vapour or aerosol.

Chromium(III)potassium sulphate dodecahydrate

Physical state; Appearance:

Dark violet odourless solid.

Physical dangers:

Irritating to eyes and skin.

Chemical dangers:

Excessive heating is to be avoided as well as the use of strong oxidising agents.

Routes of exposure:

The substance can be absorbed into the body by inhalation of its vapour, by ingestion as well as contact with skin.

Effects of short-term exposure:

Upon inhalation irritation of the mucous membranes, coughing and dyspnoea could occur. After skin contact irritations can occur. The substance irritates the eyes and could cause conjunctivitis. Irritation of the mucous membranes in the mouth, pharynx, oesophagus and gastrointestinal tract may be caused after ingestion.

Effects of long-term or repeated exposure:

Tendency of poor wound healing after long term exposure could occur.

Ethanol

Physical state; Appearance:

Colourless liquid, with characteristic odour.

Physical dangers:

The vapour mixes well with air and explosive mixtures are easily formed.

Chemical dangers:

Reacts slowly with calcium hypochlorite, silver oxide and ammonia, causing fire and explosion hazard. Reacts violently with strong oxidants such as nitric acid, silver nitrate, mercuric nitrate or magnesium perchlorate, causing fire and explosion hazard.

Routes of exposure:

The substance can be absorbed into the body by inhalation of its vapour and by ingestion. Inhalation risk. A harmful contamination of the air will be reached rather slowly on evaporation of this substance at 20 °C.

Effects of short-term exposure:

The substance irritates the eyes. Inhalation of high concentration of vapour may cause irritation of the eyes and respiratory tract. The substance may cause effects on the central nervous system.

Effects of long-term or repeated exposure:

The liquid affects the skin. The substance may have effects on the upper respiratory tract and central nervous system, resulting in irritation, headache, fatigue and lack of concentration.

Hydrochloric Acid

Physical state; Appearance:

Colourless liquid, with pungent odour.

Physical dangers:

Corrosive acid.

Chemical dangers:

The solution in water is a strong acid, it reacts violently with bases and is corrosive. Reacts violently with oxidants forming toxic gas. Attacks many metals in the presence of water, forming combustible gas.

Routes of exposure:

The substance can be absorbed into the body by inhalation.

Inhalation risk:

A harmful concentration of this gas in the air will be reached very quickly on loss of containment.

Effects of short-term exposure:

Rapid evaporation of the liquid may cause frostbite. The substance is corrosive to the eyes, the skin and the respiratory tract. Inhalation of high concentrations of the gas may cause pneumonitis and lung oedema, resulting in reactive airways dysfunction syndrome (RADS). The effects may be delayed. Medical observation is indicated.

Effects of long-term or repeated exposure:

The substance may have effects on the lungs, resulting in chronic bronchitis. The substance may have effects on the teeth, resulting in erosion.

N-2-Carbamoylmethyl-iminodiacetic acid (H_2ada)

Physical state; Appearance:

White crystalline solid.

Environmental hazard:

Very polluting substance.

Effects of short-term exposure:

No hazardous effects have been found.

Perchloric acid



Physical state; Appearance:

Colourless liquid, with pungent odour.

Chemical dangers:

May explode on heating. The substance decomposes on heating producing toxic and corrosive fumes. The substance is a strong oxidant and reacts violently with combustible and reducing materials, organic materials and strong bases, causing fire and explosion hazard. Attacks many metals forming flammable/explosive gas. The acid is unstable if the concentration is over 72 %; may explode by shock or concussion when dry or drying. Mixtures with combustible material (such as paper) may ignite spontaneously at room temperature.

Routes of exposure:

The substance can be absorbed into the body by inhalation and by ingestion.

Inhalation risk:

No indication can be given about the rate in which a harmful concentration in the air is reached on evaporation of this substance at 20 °C.

Effects of short-term exposure:

Corrosive. The vapour is very corrosive to the eyes, the skin and the respiratory tract. Inhalation of vapour or mist may cause lung oedema. The effects may be delayed. Medical observation is indicated.

Potassium Bicarbonate

Physical state; Appearance:

White powder or granules.

Routes of exposure:

The substance can be absorbed into the body by inhalation of its aerosol and by ingestion.

Inhalation risk:

May cause respiratory tract irritation.

Effects of short-term exposure:

Irritation.

Potassium thiocyanate

Physical state; Appearance:

Odourless and colourless solid.

Chemical dangers:

Contact with acid liberates a very toxic gas.

Routes of exposure:

Harmful by inhalation, in contact with skin and if swallowed.

.

Effects of short-term exposure:

Upon inhalation irritation of the mucous membranes, coughing and dyspnoea could occur. After uptake of large quantities agitation, spasms and ataxia could occur.

Effects of long-term or repeated exposure:

Changes in the blood picture.

Sodium perchlorate

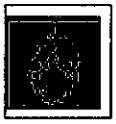

Physical state; Appearance:

Odourless, colourless crystals.

Chemical dangers:

Explosive when mixed with combustible material.

Routes of exposure:

Harmful when swallowed.

Effects of short-term exposure:

After swallowing a possible symptom could be muscular weakness. Slight irritations could occur when in contact with eyes and skin. Inhalation of dust may cause irritation symptoms in the respiratory tract.

Bibliography

ASHLEY, K.R., LEIPLODT, J.G. and JOSHI, V.K., *1980. Inorg. Chem., 19:1608.*

ASHLEY, R.A. & LEIPOLDT, J.G., *1981. Inorg. Chem., 20:2326.*

BRANDENBURG, K. & BERNDT, M., 1998. *Visual Crystal Structure Information System, Version 2.1, Germany.*

BEST, S.P., ARMSTRONG, R.S., BEATTIE, J.K., *1980. Inorg. Chem., 19:1958.*

BHATTACHARYYA, S.K. & BANJEREE, R., *1997. Polyhedron, 16:849.*

BOCARSLY, J.R., CHIANG, M.Y., BRYANT, L. and BARTON, J.K., *1990. Inorg. Chem., 29:4898.*

BRUKER (1999), *SAINT+. Version 6.02 (includes XPREP and SADABS). Bruker AXS INC., Madison, Wisconsin, USA.*

BRUKER (1999), *SHELXTL.* Version 5.1 (includes XS, XL, XP, XSHELL). Bruker AXS INC., Madison, Wisconsin, USA.

BUGELLA-ALTAMIRANO, E., GONZÁLEZ-PÉREZ, J.M., CHOQUESILLO-LAZARTE, D., CARBALLO, R., CASTIÑEIRAS, A. and NICLÓS-GUTIÉRREZ, J., *2002. Inorg. Chem. Com., 5:727.*

BUGELLA-ALTAMIRANO, E., GONZÁLEZ-PÉREZ, J.M., SICILIA-ZAFRA, A.G., NICLÓS-GUTIÉRREZ, J. and CASTIÑEIRAS, A., *1999. Polyhedron, 18:3333.*

BUGELLA-ALTAMIRANO, E., GONZÁLEZ-PÉREZ, J.M., SICILIA-ZAFRA, A.G., NICLÓS-GUTIÉRREZ, J. and CASTIÑEIRAS, A., *2000. Polyhedron, 19:2463.*

BUGELLA-ALTAMIRANO, E., GONZÁLEZ-PÉREZ, J.M., SICILIA-ZAFRA, A.G., NICLÓS-GUTIÉRREZ, J. and CASTIÑEIRAS, A., *2000. Polyhedron, 19:2473.*

CHATTERJEE, C. and STEPHEN, M., 2002. *Polyhedron, 20:2917*

COOPER, J.A., BLACKWELL, L.F. and BUCKLEY, P.D., *1984. Inorg. Chim. Acta, 92:23.*

COTTON, F.A. & WILKINSON, G. *Advanced Inorganic Chemistry, A Comprehensive Text. New York: John Wiley and Sons.*

DASSARMA, S. & DASSARMA, B., *1979. Inorg. Chem.,18:3618.*

DEMAINE, M.M. & HUNT, J.B., *1971. Inorg. Chem., 10:2106.*

DUFFY, N.V. & EARLY, J.E., *1967. J. Am. Chem. Soc.,89:272.*

EL-AWADAY, A.A. & HUGUS, Z.Z., *1971. Inorg. Chem., 10:1415.*

ELLIS, D., SCOTT, K.L. and WHARTON, R.K., *1972. Inorg. Chem., 11:2565.*

FALLAB, S., *1967. Angew. Chem. (Int. Ed.), 6:496.*

GARNETT, P.J. & WATTS, D.W., *1947. Inorg. Chim. Acta, 8:307.*

GORDAN, P.F. &GREGORY, P., *1983. Organic chemistry in colour. Berlin: Springer-Verlag.*

GRANT, D.M. & HAMM, R.E., *1958. J. Am. Chem. Soc., 80:4166.*

HALLORAN, L.J., CAPUTO, R.E., WILLET, R.D. and LEGG, J.I., *1975. Inorg. Chem., 14:1762.*

HARTFORD, W.H., *1979. (In Grayson, m., ed. Kirk-Othmer Encyclopedia of Chemical Technology. New York: John Wiley & Sons. p. 82-120.)*

HAULIN, Z. & XU, Z., *1990. Polyhedron, 9:137.*

HAY, R.W., *1984. Coord. Chem. Rev., 57:1.*

HAYLOCK, S.J., BUCKLEY, P.D. & BLACKWELL, L.F., *1983. J. Inorg. Biochem., 19:105.*

HELIS, H.M., DE MEESTER, P. and HODGSON, D.J., *1977. J. Am. Chem. Soc., 99:3309.*

HOFFMAN, A.B. & TAUBE, H., *1968. Inorg. Chem., 7:903.*

Jahn, H.A. & Teller, E., 1937, *Proc. Roy. Soc., A 161:220*

JITSUKAWA ,K., MORIOKA, T., MASUDA, H., OGOSHI, H. and EINAGA, H., *1994. Inorg. Chim. Acta, 216:249.*

KOINE, N., BIANCHINI, J. and LEGG, I., *1986. Inorg. Chem., 25:2835.*

LANCE, E.A. and NAKON, R., *1981. Inorg. Chim. Acta. 55:L1.*

LANCE, E.A., RHODES, C.W. and NAKON, R., *1983. Anal. Biochem., 133:492.*

LEE HIN-FAT & HIGGINSON, W.C.E., *1971. J. Chem. Soc., A:2589.*

LEIPOLDT, J.G. & MEYER, H., *1987. Polyhedron, 6:1631.*

LINHARDT, V.M. & SIEBERT, H., *1969. Z. Anorg. Allg. Chem., 364:24.*

MELOON, D.R. & HARRIS, G.M., *1977. Inorg. Chem., 16:434.*

MOORE, P., *1984. (In Twigg, M.V., ed. Mechanisms of Inorganic and Organometallic Reactions, Volume 2. New York: Plenum Press).*

NAGAO, R., FUMIYUKI, M. and SAITO, Y., *1972. Acta Cryst., B28:1852.*

NAKAMOTO, K., *1963. Infrared Spectra of Inorganic and Coordination Compounds. New York: John Wiley & Sons.*

OGINO, H., WATANBE, T. and TANAKA, N., *1975. Inorg. Chem., 14:2093.*

PARR, P.P., RHODES, C., and NAKON, R., *1983. Inorg. Chim. Acta., 80:L11.*

POTGIETER, H.J.W, VISSER, H.G., PURCELL, W., *2005. Polyhedron., 24:1968.*

PURCELL, F.P. & KOTZ, J.C., *1985. Inorganic Chemistry, Japan: W.B. Saunders Company. p. 710.*

RADANOVIC, D.J.,*1984. Coord. Chem. Rev., 54:159*

SANTOS, T.M., DE JESUS, J.P. and O'BRIEN, P., *1992. Polyhedron, 11:1687.*

SCHWARZENBACH, G., ANDEREGG, G., SCHNEIDER, W. and SENN, H., *1955. Helv. Chim. Acta., 38:1147.*

SCIENTIST FOR WINDOWS, *1990. Least Square Parameter Estimation, Version 4.00, Micromath.*

SHELDRICK, G.M., (1996), *SADABS. Version 2.03. University of Gottingen, Germany.*

SIVAK, M., TYRSELOVA, J. and PAVELCIK, F., *1995. Polyhedron, 15:1057.*

SMITH, G.S. & HOARD, J.L., *1959. J. Am. Chem. Soc., 81:556.*

SPEK, A.L., *1990. Acta. Cryst. A46:c34.*

SPEK, A.L. *1998. PLATON, A Multipurpose Crystallographic Tool, Utrecht University, Utrecht, The Netherlands.*

SRDANOV, G., HERAK, R., RADANOVIC, D.L.& VESSELINOVIC, D.S., *1980. Inorg. Chim. Acta, 38:37.*

SUDMEIER, J.L. & OCCUPATI, *1968. Inorg. Chem., 7:2524.*

SULFAB, Y., TAYLOR, R.S. and SYKES, A.G., *1976. Inorg. Chem., 15:2388.*

SYKES, A.G. & WEIL, J.A., *1970. (In. Edwards, J.O. ed. Inorganic Reaction Mechanisms, Volume 13. New York: John Wiley and Sons).*

TERRIL, J.B. & REILLY, C.N., *1966. Inorg. Chem., 5:1988.*

THACKER, M.A. & HIGGINSON, W.C.E., *1975. J. Chem. Soc. Dalton Trans., p. 704.*

TOEPFER, E.W., MERTZ, W., POLANSKY, M.M., ROGINSKY, E.E., and WOLF, W.R., *1977. J. Agric. Food Chem., 25:162.*

TOFTLUND, H. & SPRINGBORG, J., *1976. J. Chem. Soc. Chem. Comm., p. 1017.*

UEHARA, A., KYUNO, E. & TSUCHIYA, R., *1968. Bull. Chem. Soc. Japan., 40:2317.*

VISSER, H.G., LEIPLODT, J.G., PURCELL, W. and MOSTERT, D., *1994. Polyhedron, 13:1051.*

VISSER, H.G., PURCELL, W. and BASSON, S.S., *1999. Polyhedron, 18:2795.*

VISSER, H.G., PURCELL, W. and BASSON, S.S., *2001. Polyhedron, 20:185.*

VISSER, H.G., PURCELL, W. and BASSON, S.S., *2002. Trans. Metal Chem., 27:461.*

VISSER, H.G., PURCELL, W. and BASSON, S.S., *2003. Trans. Metal Chem., 28:235.*

VISSER, H.G., PURCELL, W., BASSON, S.S. and CLAASEN, Q., *1997. Polyhedron, 16:2851.*

VISSER, H.G., PURCELL, W., CLOETE, N., and MULLER, A., *2005. Acta.Cryst., E61:1668.*

VOGEL, A.I., *1989. Vogel's Textbook of Quantitative Chemical Analysis, Fifth Edition. Essex: Longman. P.317.*

WEAKLIEM, H.A. & HOARD, J.L., *1959. J. Am. Chem. Soc., 81:549.*

web.chem.ucla.edu/~harding/30/30H_s01/30H_s01_modeling_02_key.pdf (downloaded 2005-11-03).

WESTBROOK, J.H., 1979. *Chromium and chromium alloys. (In GRAYSON, M., ed. Kirk-Othmer Encyclopedia of Chemical Technology. New York: John Wiley &Sons. p. 54-82.)*

WEYH, J.A., NEWLUN, A.K., BAKER, T.J. and SHIOYAMA, T.K., *1973. Inorg. Chem., 12:2374.*

WOLCOTT, D. & HUNT, J.B., *1968. Inorg. Chem., 7:755.*

www.iucr.org (downloaded 2005-10-19).

Abstract

N-Carbamoylmethyl-iminodiacetic acid (H_2ada) is widely used in biological buffers of pH 6.0 - 7.4 and is also a well known chelating agent that acts as a tetradentate ligand under most circumstances. The first known structure determination with coordinated ada^{2-} was reported by Sivak and co-workers (1995:1057) during a study in which they characterised $[VO(O_2)(\eta^4\text{-ada})]^-$. Only one complex, $[Ni(\eta^3\text{-ada})(bipy)(H_2O]\cdot 4H_2O$, has been reported in the literature in which ada^{2-} is coordinated as a tridentate ligand (Bugella-Altamirano *et al.*, 2000:727).

The synthesis of $Cs[Cr(\eta^3\text{-ada})_2]\cdot 2H_2O$ was confirmed by means of IR, UV/VIS spectroscopy and X-ray crystallography. The $Cs[Cr(\eta^3\text{-ada})_2]\cdot 2H_2O$ complex is the first metal(III)-ada complex and only the second metal-ada complex with ada^{2-} coordinated in tridentate mode.

The IR vibrational frequencies obtained for $Cs[(\eta^3\text{-ada})_2]\cdot 2H_2O$ are indicative of COO^- groups coordinated to the Cr(IIII) metal centre and of uncoordinated glycinamido groups. The crystal structure determination confirmed the IR data by clearly showing that all the COO^- groups are coordinated to the Cr(III) centre and that both amido groups remained uncoordinated. The intermediates and the final products of the kinetic studies performed in this study, were also successfully isolated and characterised by means of IR, UV/VIS spectrums and X-ray crystallography. (see **Scheme 1**).

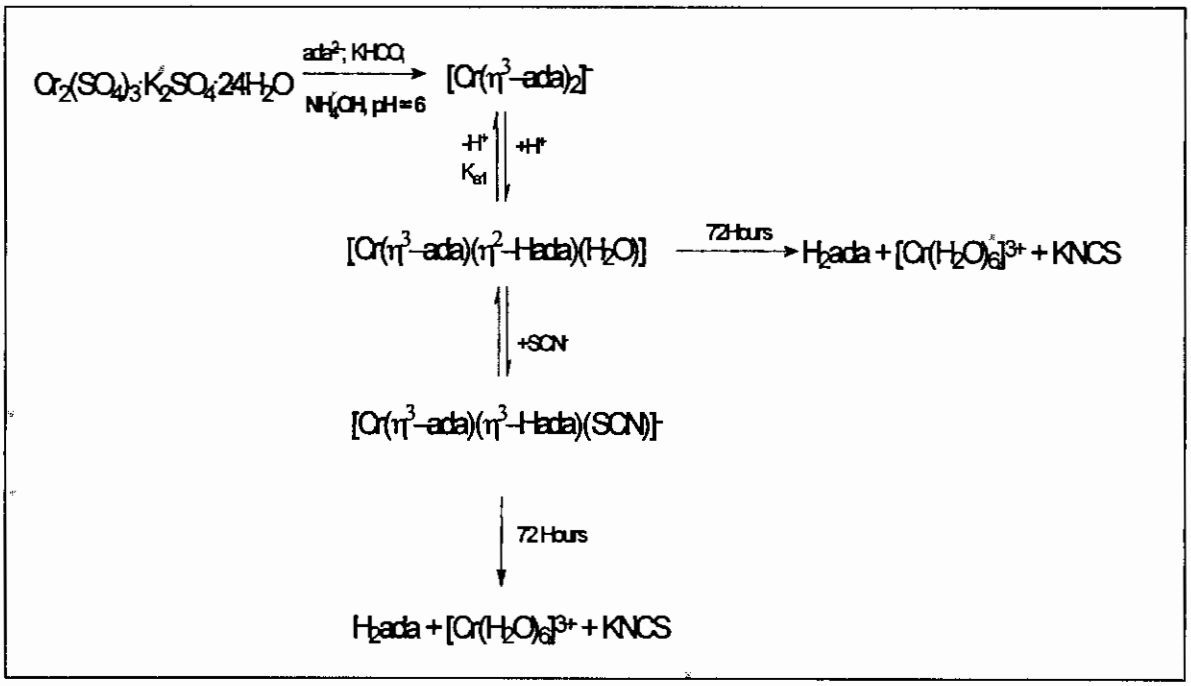

Scheme 1: Complexes and reactions of chromium(III)-ada.

The interest in the characterization of metal-ada complexes have increased in the last few years, but kinetic studies on metal-ada complexes are yet to be published. The first UV/VIS and kinetic investigation on a metal-ada complex was performed in this study.

The UV/VIS investigation revealed that the protonation of the $[Cr(\eta^3\text{-ada})_2]^-$ complex leads to the breaking of a Cr-O(carboxylate) bond and the subsequent coordination of an aqua ligand to the Cr(III) centre, forming the $[Cr(\eta^3\text{-ada})(\eta^2\text{-Hada})(H_2O)]$ intermediate. This first reaction of the stepwise dissociation of the two ada^{2-} ligands from $[Cr(\eta^3\text{-ada})_2]^-$ was investigated ($k_1 = 4.34(4) \times 10^{-1}\ M^{-1}s^{-1}$ at 19.6°C).

The substitution reaction between $[Cr(\eta^3\text{-ada})(\eta^2\text{-Hada})(H_2O)]$ and NCS^- was also studied. At pH = 0.8 NCS^- ions substituted the aqua ligand ($2.2 \times 10^{-1}\ M^{-1}s^{-1}$ at 25°C) before the ada^{2-} ligands dissociated from the Cr(III)-ada complex over a period of three days.

The above mentioned reactions that were kinetically investigated in this study all have relatively fast reaction rates. This is indicative of the labilisation of the Cr(III) complex by the electron rich ada^{2-} ligands, in which the electron density is donated to the normally inert Cr(III) centre making it react more like the labile Cr(II) species.

The various Cr(III)-ada complexes that were isolated and characterised can successfully be used as biological model complexes in future studies. These complexes could for example be used to simulate the bonding of metal ion to functional groups of wool fibre or might have uses as models in pharmacology.

Keywords: chromium(III), N-carbamoylmethyl-iminodiacetic acid, chelate ring-opening, substitution reactions, X-ray crystallography.

Opsomming

N-Karbamoïelmetiel-iminodiasynsuur (H_2ada) word gebruik in biologiese buffers van pH 6.0-7.4 en is ook welbekend as 'n chelerings agent wat as 'n tetradentate ligand optree in die meeste omstandighede. Die eerste bekende struktuur-bepaling met gekoordineerde ada^{2-} was gerapporteer deur Sivak en medewerkers (1995:1057) gedurende 'n studie waarin hulle $[VO(O_2)(\eta^4\text{-ada})]^-$ gekarakteriseer het. Slegs een kompleks, $[Ni(\eta^3\text{-ada})(bipy)(H_2O]\cdot 4H_2O$, waarin ada^{2-} gekoordineer is as 'n tridentate ligand, is in die literatuur gerapporteer.

Die sintese van $Cs[Cr(\eta^3\text{-ada})_2]\cdot 2H_2O$ was bevestig deur die gebruik van IR, UV/VIS spektroskopie en X-straal kristallografie. The $Cs[Cr(\eta^3\text{-ada})_2]\cdot 2H_2O$ kompleks is die eerste metal(III)-ada kompleks en ook die tweede metal-ada kompleks met ada^{2-} wat tridentaat gekoordineer is.

Die IR vibrasie frekwensies wat vir $Cs[Cr(\eta^3\text{-ada})_2]\cdot 2H_2O$ verkry is het aangedui dat die COO^- groepe gekoördineer is aan die metaal sentrum en dat die glisienamido groepe ongekoördineer gebly het. Die kristalstruktuur bepaling het die IR data bevestig, deur aan te dui dat al die COO^- gekoördineerd is aan die Cr(III) senter en dat albei amido groepe ongekoördineerd gebly het. Die intermediêre en die eindprodukte van die kinetiese studies, was ook suksesvol geïsoleer en gekarakteriseer deur gebruik van IR, UV/VIS spektroskopie en X-straal kristallografie (sien **Skema 1**).

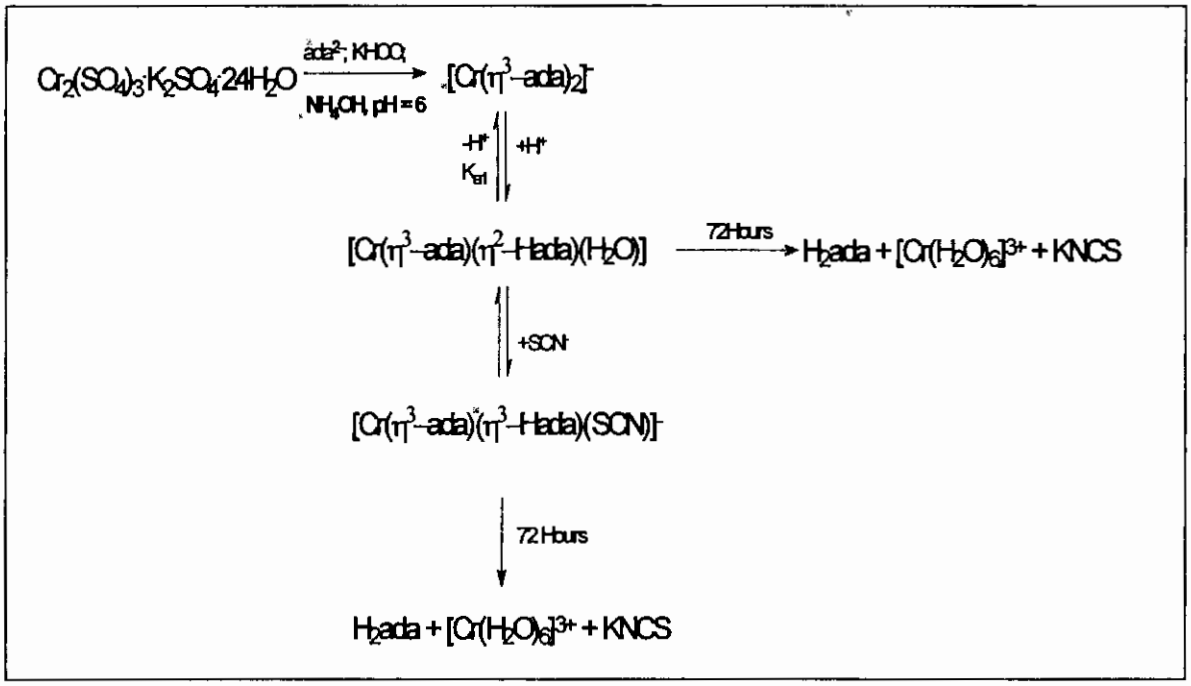

Skema 1: Komplekse en reaksies van chroom(III)-ada.

Die belangstelling in die karakterisering van metal-ada komplekse het onlangs toegeneem, maar geen kinetiese studies is nog gepubliseer nie. Die eerste UV/VIS en kinetiese bestudering van 'n metal-ada kompleks was uitgevoer in hierdie studie.

Die UV/VIS studie het aangedui dat die protonering van die $[Cr(\eta^3\text{-ada})_2]^-$ kompleks lei tot die breking van 'n Cr-O(karboksilaat) binding en die opvolgende koordinering van 'n akwa ligand aan die Cr(III) senter, met die vorming van die $[Cr(\eta^3\text{-ada})(\eta^2\text{-Hada})(H_2O)]$ intermediêr. Hierdie stapsgewyse dissosiasie van die twee ada^{2-} ligande van $[Cr(\eta^3\text{-ada})_2]^-$ is ondersoek ($k_1 = 4.34(4) \times 10^{-1}\ M^{-1}s^{-1}$ at 19.6°C).

Die substitusiereaksies tussen $[Cr(\eta^3\text{-ada})(\eta^2\text{-Hada})(H_2O)]$ en NCS^- was ook bestudeer. Die akwa ligand word by pH = 0.8 deur NCS^- ione gesubstitueer ($2.2(2) \times 10^{-1}\ M^{-1}s^{-1}$ by 25°C) waarna die ada^{2-} ligande gedissosieer het van die Cr(III)-ada kompleks oor 'n tydperk van drie dae.

Opsomming

Die bogenoemde reaksies wat kineties gevolg was in hierdie studie is relatief vinnig. Dit dui aan dat labilisering van die Cr(III) kompleks deur die elektronryk ada^{2-} ligande plaasvind waarin die elektrondigtheid gedoneer word aan die Cr(III) senter wat normaalweg inert is om soos die meer labiele Cr(II) spesie op te tree.

Die verskeie Cr(III)-ada komplekse wat geïsoleer en gekarakteriseer is in hierdie studie kan suksesvol as biologiese modelkomplekse gebruik word in toekomstige studies. Hierdie komplekse kan byvoorbeeld gebruik word om die binding van 'n metaal aan 'n funksionele groep van wol na te boots of kan gebruik word as modelkomplekse in farmakologie.

Sleutelwoorde: chroom(III), N-karbamoielmetiel-iminodiasynsuur, chelaat ring-oopmaking, substitusie reaksies, X-straal kristallografie.